The postcranial skeleton of the gliding reptile Coelurosauravus elivensis Piveteau, 1926 (Diapsida, Weigeltisauridae) from the late Permian Of Madagascar

Valentin Buffa, Eberhard Frey, J.-Sébastien Steyer, Michel Laurin

The postcranial skeleton of the gliding reptile *Coelurosauravus elivensis* Piveteau, 1926 (Diapsida, Weigeltisauridae) from the late Permian of Madagascar

Journal:	*Journal of Vertebrate Paleontology*
Manuscript ID	JVP-2022-0005.R1
Manuscript Type:	Article
Date Submitted by the Author:	n/a
Complete List of Authors:	Buffa, Valentin; Muséum National d'Histoire Naturelle, Origines et Évolution Frey, Eberhard; Staatliches Museum für Naturkunde Karlsruhe, Geosciences Steyer, Jean-Sébastien; Museum National d'Histoire Naturelle Laurin, Michel; CNRS, URM 7207;
Key Words:	Coelurosauravus, Postcranium, Weigeltisauridae, Permian, Gliding reptiles, Arboreality

The postcranial skeleton of the gliding reptile *Coelurosauravus elivensis* Piveteau, 1926 (Diapsida, Weigeltisauridae) from the late Permian of Madagascar

VALENTIN BUFFA,*[,1] EBERHARD FREY,[2] J.-SÉBASTIEN STEYER,[1] and MICHEL LAURIN[1]

[1]Centre de Recherche en Paléontologie – Paris, UMR 7207 CNRS-MNHN-SU, Muséum national d'Histoire naturelle, CP38, 8 rue Buffon, 75005 Paris, France, valentin.buffa@edu.mnhn.fr;

[2]Sonnenbergstraße 27, 75180 Pforheim, Germany;

* Corresponding author

ABSTRACT—The postcranial skeleton of the gliding neodiapsid reptile *Coelurosauravus elivensis* (Lower Sakamena Formation, late? Permian, southwestern Madagascar) is re-described in detail based on all previously referred specimens. The exquisite preservation of the material provides three-dimensional details of the individual bones, which are missing in the Laurasian weigeltisaurid material. A new skeletal reconstruction of *C. elivensis* is proposed including the first reconstruction of a weigeltisaurid reptile in lateral view. The re-examination of the material highlights interspecific differences in the postcranium of weigeltisaurids, in particular in the trunk and patagial spars. These animals have long been considered as arboreal and gliding reptiles. However, new information on the postcranium of *C. elivensis* reveals strong similarities with both extant and extinct quadrupeds specialized for a clinging arboreal lifestyle. Additionally, the presence of an additional phalanx in the fifth digit of the manus is now attested for all weigeltisaurids where this region is preserved. We suggest that this morphology could have allowed weigeltisaurids to grasp their patagium as observed in the extant gliding agamid *Draco*. Weigeltisaurids are thus the earliest known gliding vertebrates and some of the first tetrapods with an obligatory arboreal lifestyle, but also represent the only known vertebrates with a hyperphalangy aligned with a gliding apparatus.

INTRODUCTION

Despite their sparse late Paleozoic fossil record, early diapsids show a surprisingly large morphological disparity (Sues, 2019). Several terrestrial, semi-aquatic and arboreal taxa had indeed appeared by the end of the Permian (Carroll, 1975, 1978, 1981; Gow, 1975; Currie, 1981a). Among those, the late Permian Weigeltisauridae are the earliest known gliding tetrapods (Carroll, 1978; Evans, 1982; Bulanov and Sennikov, 2015a–c; Buffa et al., 2021), and their study is paramount to understand the evolution of gliding flight in amniotes.

Weigeltisauridae include several taxa known from Laurasia and Gondwana (Bulanov and Sennikov, 2015a–c): *Weigeltisaurus jaekeli* (Weigelt, 1930) (Lopingian, Germany and England); *Coelurosauravus elivensis* Piveteau, 1926 (Capitanian–Lopingian?, Madagascar); *Glaurung schneideri* Bulanov and Sennikov, 2015c (Lopingian, Germany); *Rautiania alexandri* Bulanov and Sennikov, 2006 (Capitanian–Lopingian?, Russia); and *Rautiania minichi* Bulanov and Sennikov, 2006 (Capitanian–Lopingian?, Russia). *Wapitisaurus problematicus* Brinkman, 1988 (Early Triassic, Canada) was described as a weigeltisaurid, but its cranial morphology does not conform to recent descriptions, notably in lacking a large temporal fenestra (TMP 86.153.14, VB, pers. obs.; Brinkman, 1988). Following recent studies (Bulanov and Sennikov, 2010; Buffa et al., 2021), we will thus not consider this taxon as a weigeltisaurid, pending the systematic revision of the sole, poorly known specimen.

Weigeltisaurids have been considered pterosaurs (Weigelt, 1930:626), dinosaur relatives (Boule, 1910; Piveteau, 1926), rhynchocephalians (Weigelt, 1930), early ("pelycosaur-grade") synapsids (Kuhn, 1939) or stem-saurians (Huene, 1956; Carroll, 1978; Evans and Haubold, 1987; Laurin, 1991). Today, all recent phylogenetical analyses recover weigeltisaurids as stem-saurians (e.g. Ezcurra et al., 2014; Schoch and Sues, 2018; Pritchard

and Sues, 2019; Sobral et al., 2020; Griffiths et al., 2021), possibly closely related to drepanosauromorphs (Merck, 2003; Senter, 2004; Pritchard et al., 2021) or 'paliguanids' (Müller, 2004).

The anatomy of weigeltisaurids is unique with respect to their arboreal and aerial lifestyle. While the cranium has recently received a lot of attention (Bulanov and Sennikov, 2006, 2010, 2015a–c; Schaumberg et al., 2007; Buffa et al., 2021; Pritchard et al., 2021), their postcranium remains poorly understood (Frey et al., 1997; Schaumberg et al., 2007; Bulanov and Sennikov, 2010; Pritchard et al., 2021). The present study aims to describe novel postcranial details of *Coelurosauravus* from the Lopingian? of Madagascar, which has not been revised recently (Carroll, 1978; Evans, 1982; Evans and Haubold, 1987).

Institutional Abbreviations

GM, Geiseltalmuseum, Martin-Luther-Universität, Halle, Germany; **MNHN**, Muséum national d'Histoire naturelle, Paris, France; **SMNK**, Staatliches Museum für Naturkunde Karlsruhe, Karlsruhe, Germany; **SSWG**, Sektion Geologie, Ernst-Moritz-Arndt Universität, Griefswald, Germany; **TMP**, Tyrell Museum of Paleontology, Drumheller, Canada; **TWCMS**, Sunderland Museum, Tyne and Wear County Museums, Sunderland, England.

MATERIAL AND METHODS

Material

We examined all specimens previously referred to *Coelurosauravus elivensis* (Carroll, 1978; Bulanov and Sennikov, 2015a; Buffa et al., 2021). For comparison, we also examined

original specimens or high-fidelity epoxy resin casts previously referred to *Weigeltisaurus*. The complete list of the studied material is provided in Table 1.

Geological Background

All known specimens of *Coelurosauravus elivensis* come from the upper beds of the Lower Sakamena Formation (southwestern Madagascar), which is commonly considered of Wuchiapingian age (e.g. Piveteau, 1926; Currie, 1981a; Hankel, 1994; Lucas, 2017). However, recent reinvestigations (Smith, 2020) and a possible Capitanian age for the Russian taxa (Sennikov and Golubev, 2017) suggest that the age of the Lower Sakamena Formation is poorly constrained and could extend from late Guadalupian to late Lopingian (possibly Capitanian to Changhsingian). All specimens are preserved in fine-grained nodular concretions. The remains are mostly preserved as external molds, showing skeletal imprints largely in connection. Most bones have been eroded and possibly further removed by etching or using acid so that only their external molds are preserved. A more comprehensive review of the first excavations led by J.-M. Colcanap in southwestern Madagascar during the early 20th century is underway by VB.

Taxonomic Remarks

Buffa et al. (2021) provide an overview of current challenges and uncertainties in weigeltisaurid taxonomy. We follow their taxonomic framework (Table 1), summarized as follows: (1) The more recent MNHN.F.MAP inventory numbers for the MNHN specimens (including *Coelurosauravus elivensis*). (2) *Weigeltisaurus jaekeli* is exclusively used for the holotype specimen. (3) All other Western European specimens are referred to by their collection numbers, housing institution or locality reference. (4) All specimens from Eastern

Europe are referred to as *Rautiania* sp. except for type specimens following Bulanov and Sennikov (2010).

According to this framework, SMNK-PAL 2882 is referred to as 'the Ellrich specimen' (Table 1) in contrast to Pritchard et al.'s (2021) recent referral of this specimen to *Weigeltisaurus jaekeli*. This should not be taken as a disagreement with Pritchard et al.'s (2021) reexamination of this specimen, but as the result of a more cautious consideration of the species *W. jaekeli* itself. As stated by Buffa et al. (2021), this standpoint highlights the need for reexamination of this species' diagnosis in light of other Western European specimens, especially since such a revision may result in *W. jaekeli* being recovered as a junior synonym of *Gracilisaurus ottoi* (see Haubold and Shaumberg, 1985).

Reflectance Transformation Imaging (RTI)

By computing a single 'interactive specimen', on which the illumination can be reoriented, RTI can help identify individual bones on jumbled specimens (Hammer et al., 2002). We use this method to compensate for the nature of preservation of the specimens using the same custom-made portable light dome as Buffa et al. (2021, an updated version of that used by Béthoux et al., 2016; Cui et al., 2018). Sets of 54 photographs under different LED sources were compiled using the RTIBuilder software. The resulting RTI files provided in Supplemental Data (Figs. S1–S3) can be opened using the software RTIViewer (both software packages are freely available at www.culturalheritageimaging.org).

SYSTEMATIC PALEONTOLOGY

NEODIAPSIDA Benton, 1985 sensu Reisz, Modesto and Scott, 2011a

WEIGELTISAURIDAE Kuhn, 1939

COELUROSAURAVUS ELIVENSIS Piveteau, 1926

v*1926 *Coelurosauravus elivensis* (gen. nov, sp. nov.); Piveteau, 1926:173–177, pl. 17.1, 17.3.

v1977 "Institut de Paléontologie, Paris, no. 1908-5-2"; Carroll, 1977:385, fig. 14.

v1978 *Coelurosauravus elivensis* Piveteau, 1926; Carroll, 1978:144–149, figs. 1–4.

v1978 *Daedalosaurus madagascariensis* (gen. nov., sp. nov.); Carroll, 1978:149–159, figs. 5–7.

v1982 *Coelurosauravus elivensis* Piveteau, 1926; Evans, 1982:111–116, figs. 14–19.

v1987 *Coelurosauravus elivnensis* Piveteau, 1926; Evans and Haubold, 1987:275–302, figs. 3–5, 12–17, 21.

v2015 *Coelurosauravus elivensis* Piveteau, 1926; Bulanov and Sennikov, 2015a:413–423, figs. 1, 2, pl. 5.

v2021 *Coelurosauravus elivensis* Piveteau, 1926; Buffa et al., 2021:1–25, figs. 1, 3–8.

Lectotype—External mold of the dorsal surface of a partially preserved skeleton, MNHN.F.MAP325a (Piveteau, 1926:pl. 17.1; Carroll, 1978:fig. 2; Evans, 1982:fig. 16B; Evans and Haubold, 1987:figs. 3B, 13C, 16B, 16D, 17; Bulanov and Sennikov, 2015a:pl. 5.1b; Buffa et al., 2021:figs. 1, 3). See Buffa et al. (2021) for discussion of the type material.

Paralectotype—External mold of the ventral surface of a partially preserved skeleton, MNHN.F.MAP317a, b, preserved on two slabs (part and counterpart) (Piveteau, 1926:pl.

17.3; Carroll, 1978:fig. 3; Evans, 1982:figs. 15, 16A; Evans and Haubold, 1987:figs. 3A, 13A, 13B; Bulanov and Sennikov, 2015a:pl. 5.2; Buffa et al., 2021:figs. 4, 8A).

Referred Material—External mold of a sub-complete skeleton, MNHN.F.MAP327a, b, preserved on two slabs (part and counterpart) (Carroll, 1978:figs. 5–7; Evans, 1982:figs. 14, 17, 18; Evans and Haubold, 1987: figs. 4, 5, 12, 14, 15A, 21; Buffa et al., 2021: figs. 5, 6A, 7, 8B, 8C).

Type Horizon—Top of the lower Sakamena Formation, late? Permian (?Capitanian–Lopingian).

Type Locality—Sakamena River, upstream region, exact location unknown, southwestern Madagascar.

Emended Diagnosis—Maxillary teeth with symmetrical apices; anterior maxillary teeth significantly larger than mid-/posterior teeth; anterior and dorsal jugal processes subequal (shared with *Rautiania*); ornamented dorsal jugal process; parietal posttemporal process not tapering in width (shared with *Glaurung*); ornamental tubercles on parietal posttemporal process (shared with *Glaurung*); patagial spars regularly positioned throughout the wing (modified from Buffa et al., 2021).

Remarks—*Coelurosauravus* possesses 23 presacral vertebrae, including five cervicals and 18 dorsals. This contrasts with the 21 presacral vertebrae including eight cervicals and 13 dorsals of the Ellrich specimen. However, as no other weigeltisaurid specimen preserves a complete presacral vertebral column, we refrain from polarizing this character state in weigeltisaurids and provisionally exclude it from the diagnosis of *Coelurosauravus*, pending the discovery of additional weigeltisaurid specimens preserving this feature.

OSTEOLOGICAL REDESCRIPTION

The material of *Coelurosauravus* permits an almost complete examination of the postcranial skeleton. In the lectotype, the individual bone imprints (hereafter 'bones' for simplicity) are badly preserved due to late diagenetic compression and disarticulation, but the specimen comprises most of the skeletal elements between the skull and mid-length of the tail (Figs. 1, 2). The paralectotype specimens show well-preserved individual bones still mostly in connection between the skull and last presacral, but the sacral and caudal vertebrae are missing, as are both hindlimbs (Figs. 3, 4). Lastly, MNHN.F.MAP327a, b is the best preserved and one of the most complete weigeltisaurid specimens to date. The main slab preserves most of the skeleton, with the individual lying on its left side although the trunk region is mostly covered by the patagial spars (Figs. 5, 6). The counter slab preserves a large portion of the mid-posterior tail with the vertebrae lying in connection (Fig. 7).

Buffa et al. (2021) previously noted the ontogenetic maturity of all *Coelurosauravus* specimens based on size-independent criteria (recently reviewed in Griffin et al., 2021). This is in contrast to the view of Bulanov and Sennikov (2015a:422), who considered all specimens as 'juveniles.' As noted by Buffa et al. (2021), the postcranium shows closed neurocentral sutures, fused scapula and coracoid and well-ossified long bones, carpals and tarsals (see below). All of these characters are commonly used as indicators of morphological maturity in extinct reptiles, such as the coeval stem-saurians from the late Permian of Madagascar (Currie, 1981a; Currie and Carroll, 1984; Caldwell, 1995). The postcranium thus conforms with the evaluation of Buffa et al. (2021) of the ontogenetic maturity of all *Coelurosauravus* specimens.

Vertebral Column

All *Coelurosauravus* specimens preserve portions of the vertebral column, with the vertebrae lying mostly in connection. The presacral series is best preserved in the paralectotypes (Figs. 3, 4), and is less well preserved in the lectotype (Figs. 1, 2) and MNHN.F.MAP327a (Figs. 5, 6). The latter specimen also preserves partial sacral vertebrae. The caudal vertebrae are best preserved in MNHN.F.MAP327a, b (Figs. 5–7). The anterior portion of the tail is also preserved in the lectotype (Figs. 1, 2). For all specimens, the presacrals will be numbered cranial to caudal, starting with the atlas (presacral 1).

As is visible on the slightly displaced presacral and caudal vertebrae of MNHN.F.MAP327a (Figs. 5, 6, 8A, 8B), the vertebrae are all deeply amphicoelous, possibly notochordal as is typical in stem-saurians (Carroll, 1975, 1981; Gow, 1975; Currie, 1980, 1981a) including other weigeltisaurids (Evans, 1982). In most archosauromorphs, the notochordal canal is closed (Gow, 1975; Nesbitt et al., 2015; Pritchard et al., 2015). The centra of all vertebrae are long and low (between two or three times as long as high; Fig. 8). In contrast, the centra of other early diapsids are only slightly longer than high (Carroll, 1975, 1981; Gow, 1975; Currie, 1980, 1981a). The neural arches of *Coelurosauravus* are slender with the zygapophyses close to the median line, as is typical in neodiapsids but in contrast to the swollen morphology typical of early eureptiles and araeoscelidians (Sumida, 1990; Sumida and Modesto, 2001). None of the vertebrae show the mammillary processes present in araeoscelidians (Vaughn, 1955), *Hovasaurus* (Currie, 1981a) and some early archosauromorphs (Gow, 1975; Gottmann-Quesada and Sander, 2009).

Several vertebrae of *Coelurosauravus* bear sharp laminae extending between anatomical landmarks such as the rib facets or zygapophyses. The description of these structures follows the nomenclature of Wilson (1999).

Presacral Count—The anterior-most two vertebrae preserved on MNHN.F.MAP327a lie anterior to the pectoral girdle on MNHN.F.MAP327a (Figs. 5, 6, 8A, 8B). Owing to the slight anterior displacement of the vertebrae and lateral rotation of the pectoral girdle, we identify the first preserved vertebrae as the last cervical, and the second one as the first dorsal. In addition, these vertebrae show a transition from a ventrally turned and pointed transverse process to a horizontal and blunt one (Figs. 8A, 8B). This transition occurs between presacrals 5 and 6 in the complete presacral column of MNHN.F.MAP317a (Figs. 3, 4). A similar transition is also seen on the lectotype (Figs. 1, 2). According to our interpretation, *Coelurosauravus* thus possesses five cervical vertebrae. Lastly, we suggest that MNHN.F.MAP317a, b preserves the entire presacral series (Figs. 3, 4), indicating that *Coelurosauravus* has 18 dorsal vertebrae. This conforms well to the distance between pectoral and pelvic girdles in MNHN.F.MAP327a (see dorsal vertebrae below). Thus, including the five cervicals and 18 dorsals, the presacral vertebral column of *Coelurosauravus* consists of 23 presacral vertebrae.

In contrast, eight cervicals and thirteen dorsals were reported in the Ellrich specimen (Frey et al., 1997; Müller et al., 2010; Pritchard et al., 2021). Similarly, Schaumberg (1976, 1986) reports at least six or seven cervicals in the Wolfsberg specimen. Thus, there appears to be hitherto unreported variability in the number of presacral vertebrae in weigeltisaurids.

The total presacral count of weigeltisaurids is low compared with other stem-saurians: 28 to 29 in *Araeoscelis*, 26 in *Petrolacosaurus*, 25 in *Hovasaurus* and likely in *Thadeosaurus*, at least 24 in *Youngina*, and 24 in *Claudiosaurus* (Carroll, 1981; Currie, 1981a; Reisz, 1981; Currie and Carroll, 1984; Reisz et al., 1984; Smith and Evans, 1996). Müller et al. (2010) suggested that the plesiomorphic state for diapsids was 26 presacrals including 6 cervicals and 20 dorsals. The presacral count is similarly high in drepanosauromorphs: 31 in *Megalancosaurus*, 24 in *Vallesaurus* and at least 27 in *Drepanosaurus* (Renesto et al., 2010).

Atlas-Axis Complex—Most of the bones of the atlas-axis complex are preserved in ventral view in MNHN.F.MAP317a (Figs. 3, 4, 8C, 8D). The bones are slightly disarticulated but lie roughly in their anatomical position relative to the skull and post-axial cervicals. According to our interpretation, the preserved elements consist of the atlantal centrum, intercentrum and paired neural arches, the axis, and the axial intercentrum (Figs. 8C–8E). It is unclear whether or not there was a proatlas.

Bulanov and Sennikov (2015a) interpreted a circular element close to the braincase of MNHN.F.MAP317a as the occipital condyle, formed entirely by the basioccipital. However, as this does not conform to the better-preserved basioccipital of MNHN.F.MAP327a (Buffa et al., 2021), we identify this element as an atlantal vertebral centrum in posteroventral view based on its position relative to the braincase and neck of the animal (Figs. 8C, 8D). The dorsal margin of the bone is hidden under the right atlantal neural arch. The ventral margin of the atlantal centrum is rounded, suggesting that it is sub-circular in outline. The bone was not fused with the axial intercentrum, as in some early amniotes *Acerosodontosaurus*, *Hovasaurus* and most early archosauromorphs (Gow, 1972, 1975; Currie, 1980, 1981a; Sumida et al., 1992; Dilkes, 1998; deBraga, 2003; Campione and Reisz, 2011; Miedema et al., 2020) but unlike some allokotosaurian archosauromorphs and most lepidosauromorphs (Hoffstetter and Gasc, 1969; Nesbitt et al., 2015; O'Brien et al., 2018).

The posterior margin of the atlantal centrum is mostly occupied by a large, circular notochordal pit. Such a pit is also present in captorhinids (Peabody, 1952; Sumida, 1990) and varanopids (Campione and Reisz, 2011). This was certainly also the case in most stem-saurians with a notochordal atlantal centrum (Vaughn, 1955; Carroll, 1981; Reisz, 1981), although the posterior surface of the atlantal centrum is rarely described. The atlantal centrum of *Coelurosauravus* is short and ring-like in anterior or posterior view, as is typical in early amniotes (Romer, 1956; Sumida, 1990; Sumida et al., 1992).

The contralateral atlantal neural arches are unfused. The right neural arch is almost complete and visible in posterior view, whereas the left is broken and only its neural spine is visible (Figs. 8C, 8D). We were unable to identify the neurocentral suture between the appressed atlantal centrum and right neural arch, although it might have been present in the unpreserved anterior portions of the bones. The atlantal neural arch is composed of a ventral process that articulated with the anterior portion of the atlantal centrum, as in most early amniotes (Romer, 1956; Sumida et al., 1992), and of a slender posterior process projecting posterodorsally that articulated with the axis. The posterior process is narrow and bears the neural spine as well as a small but distinct postzygapophysis (Figs. 8C–8E). There is no trace of an atlantal rib or of a corresponding articular facet on the atlantal neural arch, suggesting that this rib was absent in *Coelurosauravus*, as is the case in *Claudiosaurus* and *Hovasaurus* (Carroll, 1981; Currie, 1981a), but in contrast to the condition in early reptiles (Reisz, 1981; Sumida, 1990).

In MNHN.F.MAP317a, a short, slightly posteriorly concave plate overlies the atlantal centrum (Figs. 8C, 8D). This element likely does not represent the median process of the neural arch because it lacks the robust articular facet for the atlas described for all early amniotes (Currie, 1980; Reisz, 1981; Sumida et al., 1992; Campione and Reisz, 2011). This plate may represent a distinct element, possibly a displaced proatlas.

The atlantal intercentrum lies just posterior to the atlantal centrum and is visible in ventral view (Figs. 8C, 8D). It is about half the length of the axis and the succeeding vertebrae, but is two times longer than the atlantlal centrum. The bone tapers slightly posteriorly so that its anterior surface is slightly wider than its posterior one, which is further emphasized by a ventrolateral constriction at midlength (Figs. 8C, 8D). The ventral surface of the bone is beveled anteriorly and posteriorly, forming a X-shaped arrangement of ridges, giving the intercentrum a wide V-shaped outline in lateral view (Fig. 8E). The beveled

anteroventral surface is smoothly convex, merging with the anterior surface of the bone. The posteroventral surface is steeply beveled and represents the contact surface for the anterodorsal portion of axial intercentrum. Owing to the shape and size of the atlantal intercentrum, we suggest that it contacted the atlantal centrum dorsally and articulated with the axial intercentrum posteriorly (Figs. 8E). The bone thus excluded the atlantal centrum from the ventral margin of the cervical column, as in some early amniotes where the atlantal centrum and axial intercentrum are distinct (Gow, 1972; Sumida et al., 1992; deBraga, 2003; Campione and Reisz, 2011), araeoscelidians (Vaughn, 1955, Reisz, 1981) and early neodiapsids (Currie, 1980, 1981a).

The axis is almost identical to the succeeding cervical vertebrae, described below (Fig. 8). Its centrum is amphicoelous, long and low, about three times as long as high. Its ventral margin is horizontal in lateral view and lacks a midventral ridge or keel. This ridge is present in most early diapsids (Vaughn, 1955; Currie, 1981a; Currie and Carroll, 1984). Both anterior and posterior margins are angled anterodorsally, as in araeoscelidians (e.g. Reisz, 1981).

The neural arch of the axis bears a pair of transverse processes, two pairs of zygapophyses, and the neural spine. The transverse processes are triangular in dorsal aspect. They extend laterally at right angle to the neural arch before angling ventrally. They are prolonged posteriorly by a low posterior centrodiapophyseal lamina. Such a lamina is also present in *Petrolacosaurus* (Reisz, 1981). As suggested by the poorly preserved remains of the axial rib (Figs. 8C, 8D), the diapophysis must have been positioned on the lateral apex of the transverse process, whereas the parapophysis was likely positioned near the anterior margin of the centrum.

The zygapophyses extend anteriorly and posteriorly at right angle from the neural arch, delimiting the vertebral foramen on either side. The prezygapophyses bear dorsolaterally facing articular facets for the postzygapophyses of the atlantal neural arch. In contrast, the

prezygapophyses of the succeeding vertebrae are oriented anterodorsally and bear dorsomedially facing articular facets (Fig. 8). The neural arch is subtly excavated between the zygapophyses at the base of the neural spine, although not to the degree of the third cervical (see below). The neural spine is approximately 1.5 times the height of the centrum and roughly rectangular in lateral aspect. In contrast to the anterodorsally expanded axial neural spine of araeoscelidians and tanystropheids (Vaughn, 1955; Reisz, 1981; Nosotti, 2007: Miedema et al., 2020), its dorsal margin is anteroventrally angled, most markedly in its anterior portion, where it is angled ca. 30° to the horizontal. The posterior margin of the neural spine is subtly concave in lateral view and is thickened ventrally, where it merges with the neural arch (Figs. 8C–8E).

The axial intercentrum is small compared to the atlantal one and is visible in ventrolateral view. What is preserved suggests that it was crescentic and articulated with the beveled posteroventral surface of the atlantal intercentrum.

Post-axial Cervical Vertebrae—As discussed above, *Coelurosaruavus* has three post-axial cervical vertebrae, all of which are preserved in MNHN.F.MAP317a, b (Figs. 3, 4). Only the posterior-most cervical is preserved in MNHN.F.MAP327a (Figs. 8A, 8B). The outline of at least three poorly preserved cervicals is preserved in the lectotype (Figs. 1, 2).

As is best visible in MNHN.F.MAP317a, b, the post-axial cervicals are all similar to the axis (Fig. 8F). The centra gradually increase in length along the series. They are all slightly longer than those of the anterior-most dorsals but around 1.3 times shorter than the mid-posterior dorsals (Table 2), as is the case in the Ellrich specimen (Pritchard et al., 2021). Similarly, elongate cervical centra occur in araeoscelidians (Reisz, 1981; Reisz et al., 1984), drepanosauromorphs (Renesto et al., 2010) and several early archosauromorphs (Gow, 1975; Gottmann-Quesada and Sander, 2009; Nesbitt et al., 2015; Pritchard et al., 2015). The centra only show a slight ventrolateral constriction and lack the midventral ridge or keel typically

present in early reptiles (Vaughn, 1955; Currie, 1980, 1981a; Reisz, 1981). The anterior and posterior margins of each cervical centrum are slightly angled anterodorsally (ca. 15° to the vertical), as described for the axis. A similar angulation was reported in araeoscelidians. The cervicals of *Coelurosauravus* thus differ strongly from those of drepanosauromorphs, their putative sister group (Pritchard et al., 2021), which have heterocoelous centra, anteriorly displaced neural arches, and posteroventrally projecting hypapophyses (Renesto and Fraser, 2003; Renesto et al., 2010).

All centra are closely appressed, lacking the beveling typical of intercentral articulations, which appear absent in all specimens. Cervical intercentra are present in almost all stem-saurian diapsids (Vaughn, 1955; Carroll, 1981; Currie, 1981a; Reisz, 1981), although they are absent in drepanosauromorphs (Renesto et al., 2010) and several early archosauromorphs (Nosotti, 2007; Gottmann-Quesada and Sander, 2009; Nesbitt et al., 2015).

As is seen in MNHN.F.MAP317a, b, the transverse processes are triangular in dorsal aspect, pointing posterolaterally. In contrast to those of the axis, they are straight and not turned ventrally (Fig. 8F). The posterior centrodiapophyseal lamina is more subtle on the third cervical than on the axis (Fig. 8F) and is absent in the posteriorly following cervicals. As in the axis, the diapophysis occupied the lateral extremity of the transverse process whereas the parapophysis was positioned near the anterior margin of the centrum.

The neural arch of the third cervical of MNHN.F.MAP317a, b bears a shallow excavation between the zygapophyses lateral to the base of the neural spine (Fig. 8F). In the axis and the other post-axial cervicals, this excavation is much shallower (Figs. 3, 4, 8). Similar excavations were reported in araeoscelidians (Vaughn, 1955; Reisz, 1984) and some archosauromorphs (Nesbitt et al., 2015). The neural spines of the post-axial cervicals are all rectangular in lateral aspect and gradually increase in anteroposterior length throughout the column with the posterior-most being roughly the size of the axial neural spine. They are

relatively low, around 1.5 times the height of the centum, in contrast to the very low cervical neural spines of araeoscelidians (Vaughn, 1955), and the triangular neural spines of the *Weigeltisaurus* holotype (Evans and Haubold, 1987; Bulanov and Sennikov, 2015b). As seen in MNHN.F.MAP317a, b, the neural spine of the third cervical vertebra is strongly inclined ventrally (ca. 25° to the horizontal), as in the axis (Fig. 8F). A similar inclination is present in the anterior-most post-axial cervicals of several archosauromorphs (Gottmann-Quesada and Sander, 2009; Nesbitt et al., 2015). The posterior cervical neural spines have a more horizontal dorsal margin (Figs. 3, 4, 8A, 8B, 8F).

The cervical vertebrae of all *Coelurosauravus* specimens are associated with short ribs, in contrast to the prominent long and slender cervical ribs typical of archosauromorphs (Gow, 1975; Nesbitt et al., 2015), and the absence of ribs in the drepanosauromorphs *Megalancosaurus* and *Vallesaurus* (Renesto et al., 2010). The ribs of the third cervical of MNHN.F.MAP317a, b are the only ones preserved in their anatomical position and are oriented parasagittally (Fig. 8F). The ribs of the following cervicals are all preserved in a more posteroventral orientation, but do not appear to lie in connection with the respective vertebrae (Figs. 3, 4). Thus, the orientation of the cervical ribs remains unclear in *Coelurosauravus*. None of the articular ends of the cervical ribs are sufficiently preserved to identify them as holo- or dichocephalous or to reliably assess the presence of an accessory process. This process was reported in araeoscelidians, *Claudiosaurus* and archosauromorphs (Carroll, 1981; Reisz, 1981; Benton, 1985).

Dorsal Vertebrae—As mentioned above, we reconstruct *Coelurosauravus* with 18 dorsal vertebrae, all of which are preserved in connection in the paralectotypes (Figs. 3, 4). The dorsal series is partially preserved and separated in two portions in the lectotype (Figs. 1, 2), and most of the vertebrae are covered by the patagial spars on MNHN.F.MAP327a so that

only the extremities of some transverse processes of the mid-posterior dorsals are visible (Figs. 5, 6).

As measured on the best-preserved vertebral column of the paralectotypes, the dorsal vertebrae show incipient regionalization (Table 2). The centra of dorsals one to eight (the anterior half of the dorsal column) are all slightly shorter (ca. 0.9 times) than the post-axial cervicals. They vary in length, dorsal four being the longest of this series, and dorsal six the shortest. Dorsals 10 to 16 are the longest presacral vertebrae, with a maximum central length attained for dorsals 11 to 13 (Table 2). The posterior-most two centra show a rapid decrease in length, which is also visible in the lectotype (Fig. 3). This rapid length reduction in the two posterior-most presacrals is typical in early amniotes (e.g. Reisz et al., 2011b), and further supports a count of 18 dorsal vertebrae, which yields a total of 23 presacrals in *Coelurosauravus*.

As seen in the paralectotypes, the dorsal centra all have strongly concave ventral margins in lateral view, contrary to the straighter ventral margins of the cervical centra (Fig. 8). There is no trace of a midventral ridge or keel on any dorsal vertebra, as in other weigeltisaurids (Pritchard et al., 2021) and *Claudiosaurus* (Carroll, 1981), but in contrast to most early diapsids (Vaughn, 1955; Carroll, 1975, 1981; Currie, 1980, 1981a). The anterior and posterior surfaces of the centra are vertical throughout the dorsal column contrary to the anterodorsally inclined surfaces of the cervicals. Subcentral foramina seem mostly absent, but might be represented by a small pit on dorsal 21 (Fig. 8J). Subcentral foramina are evident in most dorsals of other early neodiapsids from Madagascar (Currie, 1980, 1981a; Carroll, 1981).

As for the cervical series, the dorsal centra of MNHN.F.MAP317a, b are closely appressed and lack any articular facet for intercentra, suggesting that intercentra were absent. Dorsal intercentra are present in all other early diapsids, but are absent in

drepanosauromorphs (Renesto et al., 2010) and in several archosauromorphs (Nosotti, 2007; Gottmann-Quesada and Sander, 2009; Nesbitt et al., 2015).

As noted above, the transverse processes are rectangular, contrary to the triangular ones of the cervicals. As seen on the paralectotypes, the diapophysis is located on the transverse process, while the parapophysis is invariably present on the anterodorsal corner of the centrum (Figs. 8G–8K). The transverse processes of *Coelurosauravus* extend lateral to the neural arch, as in other weigeltisaurids (Evans, 1982), although not to the level of some early archosauromorphs (Gow, 1975; Gottmann-Quesada and Sander, 2009; Nesbitt et al., 2015). In contrast, the transverse processes of other neodiapsids barely extend lateral to the neural arch and are hardly visible in dorsal view (Currie, 1980, 1981a; Carroll, 1981).

As best seen in MNHN.F.MAP327a, the transverse processes of the first two dorsals end bluntly in an anteroposteriorly oriented facet bearing the diapophysis (Figs. 8A, 8B). On both vertebrae, the transverse processes are reinforced by low paradiapophyseal laminae extending anteroventrally from the diapophysis to the parapophysis, and posterior centrodiapophyseal laminae, as in the anterior cervicals. The second dorsal also shows a low prezygodiapophyseal lamina extending anterodorsally from the diapophysis (Figs. 8A, 8B). These laminae are also present on the first two dorsals of the paralectotypes, although partially obscured by rib fragments (Fig. 8G). As is seen in the paralectotypes and MNHN.F.MAP327a, the transverse processes of dorsals three to eight are much shorter anteroposteriorly. The prezygodiapophyseal, paradiapophyseal and posterior centrodiapophyseal laminae are invariably present and sharper than in the first dorsals (Figs. 8G, 8H). The posterior dorsals are not as well preserved, but the laminae are clearly less marked. As is seen in dorsal 10 (Fig. 8I), the paradiapophyseal lamina is absent whereas the prezygodiapophyseal lamina remains. This is also the case in the successive vertebrae (Figs.

8J, 8K). The posterior centrodiapophyseal lamina is absent in dorsal 10 (Fig. 8I) but present in the posterior dorsals (Figs. 8J, 8K).

All of these laminae are absent in coeval neodiaspsids such as *Hovasaurus* (Currie, 1981a) and *Thadeosaurus* (MNHN.F.MAP360a, b, VB, pers. obs.), although *Acerosodontosaurus* shows sharp prezygodiapophyseal laminae in its dorsal vertebrae (MNHN.F.MAP359, VB, pers. obs.). Posterior centrodiapophyseal laminae are also present in *Petrolacosaurus* (Reisz, 1981). These laminae are, however, prevalent in early archosauromorphs (Ezcurra et al., 2014).

We were unable to detect significant variations in the orientation of the zygapophyses, but as most are obscured by rib fragments on the paralectotypes, a substantial variability in their orientation cannot be excluded. We found no trace of excavation of neural arches at the base of the neural spine of any dorsal vertebra (Fig. 8), contrary to the situation in araeoscelidians (Vaughn, 1955) and several early archosauromorphs (Nesbitt et al., 2015; Spiekman, 2018), where excavations at the base of the neural spine are present at least in the anterior dorsals.

There is, however, substantial variability in the size and shape of the neural spines (Fig. 8). The first dorsals bear low (subequal to the centrum height), rectangular neural spines with a slight increase in length along their dorsal terminus, forming concave anterior and posterior margins (Figs. 8A, 8B, 8G). The succeeding vertebrae show slightly dorsally tapering neural spines in lateral aspect with a slightly (ca. 30°) anteroventrally angled anterior margin (Fig. 8H). As seen in MNHN.F.MAP317b, the neural spines of the succeeding longer vertebrae are mostly unpreserved and their dimensions remain unknown (Figs. 8I–8K). Overall, the neural spines of *Coelurosauravus* are all subequal or longer than high in lateral view, as in *Claudiosaurus*, *Kenyasaurus* and *Saurosternon*, but in contrast to the higher-than-long spines of *Acerosodontosaurus*, *Hovasaurus*, *Thadeosaurus* and *Youngina* (Currie, 1981a,

1981b) or drepanosauromorphs (Renesto et al., 2010). They lack a transverse expansion at their dorsal terminus, as described for *Hovasaurus* (Currie, 1981a). We found no trace of the additional intervertebral articulations described by Currie (1981b) for 'younginiforms', nor of the zygosphenial joint of *Saurosternon* and some saurians (Hoffstetter and Gasc, 1969; Carroll, 1975).

Most of the dorsal ribs are incompletely preserved on the *Coelurosauravus* specimens. As is best seen on the paralectotypes (Figs. 3, 4), the more anterior dorsal ribs are slender and only slightly longer than the cervical ribs. They are strongly dichocephalous and L-shaped, with the capitulum extending at roughly a right angle to the main axis of the rib (Fig. 8H). This conforms to the position of the corresponding costal facets on the vertebrae. The ribs gradually increase in size in the more posterior vertebrae, reaching a maximum size in the mid-dorsal region (dorsals 10–16; Figs. 3, 4), but remain dichocephalous. The rib of dorsal 10 is most likely incomplete and thus does not correspond to the associated costal facets (Fig. 8I). The ribs of the posterior dorsals are poorly preserved in all specimens. What is preserved suggests that they rapidly decrease in size, becoming subequal to the anterior dorsal ribs and more strongly curved. They appear to be holocephalous, although their preservation precludes a definite statement. In contrast to drepanosauromorphs (Renesto et al., 2010) and some archosauromorphs (Spielmann et al., 2008; Nesbitt et al., 2015), none of the dorsal ribs are fused with the neural arches.

Sacral Vertebrae—The sacral vertebrae are only partially visible in right lateral aspect in MNHN.F.MAP327a because they are overlain by the iliac blade (Figs. 9A, 9B). One vertebra bears a laterally extended rib that is visible near the middle of the dorsal margin of the iliac blade and is therefore confidently identified as a sacral due to its position. The preceding vertebra is partially hidden below the anterodorsal margin of the iliac blade, but bears an expanded rib as well, which is partially visible anterior to the iliac blade (Figs. 9A,

9B). Lastly, owing to the length of the iliac blade and its slight postmortem rotation ventrally relative to the vertebral column, we consider the vertebra close to the posterior portion of the iliac blade as a sacral vertebra as well (Fig. 9). Its rib cannot be identified because the vertebra is obscured by patagial spars and the iliac blade. According to our interpretation, there are three sacral vertebrae in *Coelurosauravus*. In contrast, Carroll (1978:fig. 6) only identified the posterior-most two sacrals of MNHN.F.MAP327a. However, three sacrals were also reported in *Rautiania* (Bulanov and Sennikov, 2010), and this number was thus likely typical for weigeltisaurids. Only two sacrals were previously reported in the Eppelton specimen (Evans, 1982), but the preservation of this specimen precludes a definite statement (TWCMS B5937.1, VB, pers. obs.) *Megalancosaurus* also possesses three sacrals, although only two are reported for other drepanosauromorphs (Renesto et al., 2010). In contrast, all known stem-saurians, and most Permo–Triassic saurians possess two sacral vertebrae (Gow, 1975; Reisz, 1981; Nesbitt et al., 2015). Owing to the length of the iliac blade and the position of the sacral neural spines, the sacral vertebrae appear to have been some of the shortest in the column.

The sacral ribs are too poorly preserved to yield anatomical details. Based on the length of the iliac blade it is likely that the ribs of the sacrals from anterior to posterior were oriented posterolaterally, laterally and anterolaterally respectively, as is the case in *Rautiania* (Bulanov and Sennikov, 2010).

Caudal Vertebrae—MNHN.F.MAP327a preserves the 29 immediately postsacral caudal vertebrae, with caudals 11 to 29 being also preserved in the counterpart (MNHN.F.MAP327b, Figs. 5–7). A string of at least nine anterior caudal vertebrae is also preserved in the lectotype (Figs. 1, 2). As seen in MNHN.F.MAP327a, b, the anterior-most three caudals are only two-thirds as long as the succeeding ones (Table 3, Figs. 9C, 9D). Caudals 4 to 8 show a rapid increase in centrum length, whereas the successive caudals show no further significant variation in length.

The centra of the anterior-most three caudals of MNHN.F.MAP327a show a strong ventrolateral constriction (Figs. 9C, 9D). Their ventral margins are slightly concave in lateral view and bear a ventromedian ridge. Their neural arches are similar to those of the presacrals, but the neural spines are not preserved in any of the specimens. The transverse process of the anterior-most caudal is poorly preserved, but the following two show longitudinally expanded transverse processes (Figs. 9C, 9D). The diapophysis and parapophysis are indeed convergent and linked by a paradiapophyseal lamina, forming a L-shaped articular surface with the main axis oriented horizontally. This is reminiscent of the morphology of the sacral and first caudal vertebrae of the Eppelton specimen (Evans, 1982), and suggests the presence of caudal ribs, although they are not visible on MNHN.F.MAP327a. The first three caudals of the lectotype are poorly preserved but conform to the morphology of MNHN.F.MAP327a (Figs. 1, 2).

The successive caudals show a trend of simplification along the vertebral column. The more anterior caudals show a strong ventrolateral constriction, which gradually recedes and is absent in the more posterior caudals, suggesting a gradual decrease in width of the centra posteriorly along the series. Early neodiapsids typically show a transition from a medial ridge to a sagittal canal framed by a pair of longitudinal ridges (Carroll, 1981; Currie, 1981a), but the preservation of the caudals prevents such an observation in *Coelurosauravus*. As seen in the lectotype, the transverse processes rapidly shorten along the proximal portion of the tail, as do the neural spines (Figs. 1, 2). Both appear to be absent from the fifth or sixth caudal posteriorly. The transverse processes are straight, extending at right angle from the neural arch on the lectotype. This contrasts with the posteriorly curved transverse processes of araeoscelidians (Reisz, 1981). The caudal neural spines are all low and triangular, shorter than the centrum and positioned at level with the postzygapophyses (Figs. 1, 2, 9C, 9D). As seen in MNHN.F.MAP327a, b, the zygapophyses remain well-developed throughout the preserved portion of the tail and articulate with those of the neighboring caudals (Figs. 9E, 9F), as in the

Eppelton and Ellrich specimens (Evans, 1982; Pritchard et al., 2021). We found no trace of an autotomic septum in any of the vertebrae of MNHN.F.MAP327a or the lectotype.

Haemal arches are preserved in lateral view in the lectotype and MNHN.F.MAP327a, b and appear to have been present throughout most of the preserved portion of the tail, although small intercentra are present between the anterior-most caudals instead (Figs. 9C–9D). The proximal portion of each haemal arch articulates between succeeding centra, as in most early diapsids, but in contrast to drepanosauromorphs, where the haemal arches are fused to the centra (Renesto et al., 2010). The first haemal arches are visible in the lectotype, showing a slight posteroventral curvature and a shallowly convex ventral margin (Figs. 1, 2). The haemal arches associated with caudals 13 to 29 are preserved in MNHN.F.MAP327b. They differ from those preserved in the lectotype in their proximal portion, which bears an anterior acuminate process (Figs. 9E, 9F). The transition thus occurs between the ninth and thirteenth caudals, but this region is poorly preserved on all *Coelurosauravus* specimens. All haemal arches gradually taper in width in lateral aspect. This morphology is consistent with that described for the Eppelton and Ellrich specimens (Evans, 1982; Pritchard et al., 2021).

Gastralia

Thin splint-like bones are visible in the abdominal region of all *Coelurosauravus* specimens, but are best preserved in MNHN.F.MAP327a (Figs. 5, 6, 10, S1). Based on their morphology, anatomical position and arrangement described below, we confidently identify these bones as gastralia.

The organization of the gastral basket is unclear because the trunk of MNHN.F.MAP327a is only visible in lateral view and has undergone slight diagenetic compression (Figs. 5, 6). However, the anterior region is better preserved and shows that the

gastralia were organized into a series of transverse rows, the first two of which are visible on the specimen (Fig. 10A). Each row consists of at least two thin splint-like elements, which will be numbered from medial to lateral. In contrast, only a single long curved element was described in the Ellrich specimen (Pritchard et al., 2021). Similarly, we were unable to identify more than one gastralium per row in the gastral basket of the Eppelton and Wolfsberg specimens, although this may be due to preservation (TWCMS B5937, cast SMNK-PAL 34910, VB, pers. obs.).

Gastralium 1 is the thinnest and is almost straight (Fig. 10). Its median portion is obscured in all visible gastral rows on MNHN.F.MAP327a. Therefore, it remains unclear if it corresponds to a pair of medial gastralia fused into a chevron-like element, as is the case in early neodiapsids (Carroll, 1981; Currie, 1981a) and in the most anterior gastral row in later saurians (e.g. Claessens, 2004), or if it is indeed the medial-most element. Gastralium 1 bears an anterodorsal facet for gastralium 2 in its lateral portion. Gastralium 2 is nearly 1.5 times longer and shows a strong curvature (Fig. 10). Its lateral end is strongly expanded (about 1.5 times the breadth of the corpus) and forms a knob. This knob is closely associated with a patagial spar in several places of the trunk in MNHN.F.MAP327a, suggesting these elements were articulated.

The trunk of MNHN.F.MAP327a has collapsed due to diagenetic compression, so the orientation of the gastral rows is uncertain. As preserved, the anterior-most rows appear to be posterolaterally oriented (Fig. 10A), suggesting these rows were organized in a series of anteriorly oriented chevrons spanning the width of the abdomen (as described by Witzmann, 2007). This is the typical organization in reptiles (e.g. Carroll, 1981; Claessens, 2004). However, the mid-posterior gastralia, while isolated, are all oriented anterolaterally (Fig. 10B), suggesting the gastral rows formed wide posteriorly oriented chevrons (as described by Witzmann, 2007) in contrast to the more anterior ones. A similar difference in orientation is

seen in the Ellrich specimen (Pritchard et al., 2021). However, it is also possible that these gastralia formed roughly transverse rows as in the gastral basket of the Eppelton specimen (Evans, 1982) or the Wolfsberg specimen (SMNK cast, VB, pers. obs.; Schaumberg, 1976).

Pritchard et al. (2021) recently proposed that the patagial spars of weigeltisaurids could be modified gastralia, as is suggested by their close association with the gastralia in the Ellrich specimen, which is similar to that of MNHN.F.MAP327a. Under that interpretation, each transverse gastral row would comprise three elements in *Coelurosauravus*, which is the typical number in early diapsids (Carroll, 1981; Currie, 1981a). *Sphenodon* and extant crocodilians have a similar number (e.g. Günther, 1867; Howes and Swinnerton, 1901; Vickaryous and Hall, 2008) whereas dinosaurs and pterosaurs have at most two gastralia on either side (Claessens, 2004; Claessens et al., 2009).

While Pritchard et al.'s (2021) interpretation remains plausible, we stress that more data are needed to assess the homology between the patagials of weigeltisaurid and the lateral gastralia of other reptiles, such as histological thin-sections. Thus, we retain the patagial spars and gastralia as distinct, potentially non-homologous elements in the following description.

Patagial Spars

Patagial spars (hereafter "patagials", following Pritchard et al., 2021:47) forming the bony support of the patagium, have long been recognized as diagnostic of weigeltisaurids (Frey et al., 1997; Schaumberg et al., 2007; Pritchard et al., 2021). Isolated spars are visible on the lectotype and paralectotypes, but MNHN.F.MAP327a appears to show a complete patagial skeleton and will thus serve as the basis for the following description (Figs. 5, 6).

MNHN.F.MAP327a shows at least 29 spars on the right side, with patagials 13 to 16 lying rotated anteriorly (Figs. 5, 6). Pritchard et al. (2021) reported the same number in this

specimen and counted at least 24 patagials in the Ellrich specimen. The distal extremities of the patagials from the left side are visible in the specimen, but their proximal portions are obscured. As is visible on the right side, the patagials are roughly regularly spaced throughout the patagium (Figs. 5, 6). This is in stark contrast to the "bundles" described for the Ellrich specimen (Frey et al., 1997:1451), suggesting a different organization of the patagial support. The individual spars are long and thin in MNHN.F.MAP327a. They maintain a roughly constant width for at least half to two-thirds of their length before tapering distally. Each patagial bears a longitudinal groove in its proximal and middle portions, and they were likely biconcave in cross-section, as described by Schaumberg et al. (2007).

Patagials 1 to 9 rapidly increase in length, with patagial 9 being the longest in the patagium (Table 3). Patagials 10 to 14 are incomplete distally, but what is preserved suggests a gradual decrease in length along the series. Between patagials 15 and 22, only patagials 16 and 19 are sub-complete distally, but the preserved patagial portions suggest a slightly more rapid decrease in length as concluded from the thickness at the distal breaks. The proximal portions of the more posterior patagials are missing so their length cannot be assessed. Patagials 1 to 10 show an increase in thickness and the following ones become gradually thinner along the wing. All this conforms well with the patagial series of the Ellrich specimen (Pritchard et al., 2021).

Patagials 1 and 2, the shortest in the patagium (Table 3), are oriented anterolaterally so that their distal portion lies anterior to their proximal one when the wing is deployed (Figs. 5, 6). They are sigmoidal, curving anteriorly in their proximal half and posteriorly in their distal half. In contrast, the anterior patagials of the Ellrich specimen are nearly straight (Pritchard et al., 2021). Patagials 3 to 8 of MNHN.F.MAP327a do not show such a sigmoidal curvature, although patagials 1 through 4 and 8 are posteriorly curved distally (Figs. 5, 6). Except for

patagials 19, 23 and 24, none of the more posterior patagials show a complete distal end. Thus, it remains unclear whether or not they were curved distally.

Pectoral Gridle

The pectoral gridle is preserved in all *Coelurosauravus* specimens. It is visible in right lateral view in the lectotype but is badly weathered (Figs. 1, 2). The individual bones are slightly disarticulated in the paralectotypes, allowing for the description of the articular surfaces (Figs. 3, 4). The pectoral girdle is exquisitely preserved in MNHN.F.MAP327a. This specimen will thus serve as the basis for the following description (Figs. 5, 6, 11A). The elements are preserved in connection, and the pectoral girdle is slightly angled relative to the transverse plane in a way that the right side is visible in lateral view and the left in medial view (Fig. 11A).

The pectoral girdle of MNHN.F.MAP327a comprises both scapulocoracoids, clavicles and cleithra (Fig. 11A). There is no trace of the interclavicle (contra Evans and Haubold, 1987:fig. 14), which is also not visible in the paralectotypes despite all the other bones being present. Owing to the otherwise exquisite preservation of all other bones that remain roughly in anatomical position, we propose this element was reduced or missing in *Coelurosauravus*. In contrast, the interclavicle is prominent in all early diapsids (Carroll, 1975; 1981; Gow, 1975; Currie, 1981a). Among diapsid reptiles, the loss of the interclavicle was only reported in limbless squamates (Conrad, 2008; Gauthier et al., 2012) and dinosaurs (Nesbitt, 2011, but see Vickaryous and Hall, 2010; Tschopp and Mateus, 2013).

None of the *Coelurosauravus* specimens preserves an ossified sternum, which is otherwise present in *Araeoscelis* and common among ‘younginiforms’ and ‘paliguanids’ (Vaughn, 1955; Carroll, 1975; Currie, 1981a; Zanon, 1990). However, as indicated by Carroll

(1978), the empty space between the posterior margin of the scapulocoracoid and the anterior-most row of gastralia in MNHN.F.MAP327a suggests that a broad cartilaginous sternum was likely present in *Coelurosauravus* (Figs. 5, 6).

Scapulocoracoid—The scapula and coracoid are fused in MNHN.F.MAP327a without any discernable suture (Fig. 11), as is the case in the lectotype and paralectotype (Figs. 1–4). This has been proposed as indicating maturity in diapsid reptiles (Currie and Carroll, 1984; Griffin et al., 2021) and thus suggests a mature age of the *Coelurosauravus* specimens (see Buffa et al., 2021 for a more detailed assessment based on the skull).

The scapular blade extends vertically as a rectangular plate and is about three times as high as it is wide (Fig. 11). Dorsally, it extends roughly to the level of the vertebral column (Fig. 11) in contrast to the shorter scapular blades of *Claudiosaurus* and *Hovasaurus* (Carroll, 1981; Currie, 1981a) and the extremely tall and narrow blades of drepanosauromorphs (Renesto et al., 2010; Castiello et al., 2016). As is visible in medial view on the left side of MNHN.F.MAP327a, the scapular blade is reinforced anteriorly by a low scapular torus (sensu Pawley and Warren, 2006), and the blade becomes gradually thinner dorsally in longitudinal direction (Fig. 11). Its anterior margin is roughly vertical in contrast to the strongly convex anterodorsal margin of the scapular blade of araeoscelidians (Vaughn, 1955; Reisz, 1981), and the concave one of drepanosauromorphs (Renesto et al., 2010; Castiello et al., 2016) and several archosauromorphs (Dilkes, 1998; Spielmann et al., 2008; Nesbitt et al., 2015). The dorsal surface of the blade forms a rugose margin suggesting the presence of a cartilaginous suprascapula. The anterior margin of the scapular blade bears a thin articular surface for the cleithrum.

The scapular blade progressively becomes transversely and longitudinally broader just dorsal to the glenoid and its contact with the coracoid portion of the scapulocoracoid. The posterior margin of the scapular blade is prolonged by a low-but-robust lateral supraglenoid

ridge dorsal to the glenoid (Fig. 11). There is neither a supraglenoid buttress nor a supraglenoid foramen, as is typical in neodiapsids (deBraga and Rieppel, 1997) but in contrast to araeoscelidians (Vaughn, 1955; Reisz, 1981).

As is visible on MNHN.F.MAP327a and MNHN.F.MAP317a, b, the coracoid and scapular portions of the scapulocoracoid meet at slightly more than a right angle (Fig. 11). The coracoid plate extends medially to the sagittal plane of the animal. It does not protrude anterior to the scapular blade, and its posterior extent is not visible in any specimen. From what is preserved we conclude that it extended for a short distance posterior to the glenoid. The posteromedial portion coracoid of MNHN.F.MAP317b appears turned dorsally, although this is likely due to diagenetic compression (Figs. 3, 4).

The glenoid is poorly preserved in all specimens. Two triangular protrusions, the scapular and coracoidal contributions to the glenoid articulation, are exposed in the vicinity of the humeral head in the lectotype (Figs. 1, 2). The glenoid of *Coelurosauravus* had the 'screw-shaped' morphology typical of early tetrapods (Romer, 1956).

Cleithrum—Cleithra are visible in all specimens, but are best preserved in MNHN.F.MAP327a (Fig. 11). The bone comprises a slender cleithral shaft, extending ventrally from the dorsal region of the scapular blade to the level of the top of the lateral supraglenoid ridge. As visible in both MNHN.F.MAP327a and the lectotype, the bone fans slightly dorsally over the top of the scapular blade. The posterior margin of the cleithral shaft bears a long articular surface that meets the anterior margin of the scapular blade along most of its height.

Paired cleithra were described in araeoscelidians, *Acerosodontosaurus* and *Hovasaurus* (Currie, 1980, 1981a; Reisz, 1981) but were considered absent in most other stem-saurians. As the cleithrum is liable to be unpreserved or misinterpreted (e.g. as a cervical

rib, Romer and Price, 1940:114), we suggest that its absence in *Youngina* (Gow, 1975) is equivocal. On the contrary, as indicated by numerous specimens, we follow Carroll (1981) in considering this bone absent in *Claudiosaurus*.

Clavicles—The clavicles are visible in dorsal and lateral views on MNHN.F.MAP327a and MNHN.F.MAP317a and in posteroventral view in MNHN.F.MAP317b (Figs. 3, 4H). As seen in MNHN.F.MAP327a, the clavicles are composed of a dorsal portion that covered the cleithrum and a ventral one that articulates with the anterior margin of the scapular blade. Part of the ventral portion of the clavicle extends medially along the anterior margin of the coracoid plate (Fig. 11). Both portions merge smoothly into each other at an obtuse angle of about 120°.

The dorsal process of the clavicle gradually tapers towards its terminus. It is convex anteriorly, but its posterior surface bears an elongate articular surface for the cleithrum and scapulocoracoid, as is visible in MNHN.F.MAP317b (Fig. 2). On the contrary, the ventral process of the clavicle becomes gradually broader medially. At the same time, it gradually decreases in height medially and possibly forms an articular surface for the interclavicle, although we were unable to identify a corresponding sutural surface. The subtle, gradual expansion of the ventral process of the clavicle conforms well with that of other neodiapsids (e.g. Currie, 1981a), but lacks the broader expansion typical of early reptiles and araeoscelidians (Holmes, 1977; Reisz, 1981).

Forelimb

Elements of the forelimb are preserved in all specimens. The description of the long bones follows the terminology of Romer (1922) and considers that the humerus is oriented perpendicular to the sagittal plane of the animal, with the lower arm set at a right angle to the

humerus, pointing downwards. The orientation axes of the individual bones are thus consistent with previous studies on stem-saurian reptiles (e.g. Carroll, 1981; Currie, 1981a). The long bones are slightly disarticulated in the lectotype (Figs. 1, 2) but are mostly complete and lie in connection with each other on both sides in the paralectotypes (Figs. 3, 4). The right forelimb is exquisitely preserved in MNHN.F.MAP327a and lies in connection with the pectoral girdle (Figs. 5, 6, 11).

Humerus—The humerus is the longest bone in the forelimb (Fig. 11). It has the tetrahedral shape typical of all early tetrapods (Romer, 1922), with the epiphyses twisted almost at right angle to each other. As is seen in all specimens, the humerus of *Coelurosauravus* is gracile, with the epiphyses only slightly enlarged relative to the diaphysis. Among early diapsids, this morphology is typical for weigeltisaurids (Evans and Haubold, 1987; Bulanov and Sennikov, 2010; Pritchard et al., 2021), and araeoscelidians (Vaughn, 1955; Reisz, 1981; Reisz et al., 1984). In contrast, other early neodiapsids possess greatly enlarged humeral heads (Carroll, 1975, 1981; Currie, 1980, 1981a), as do most early archosauromorphs (Gottmann-Quesada and Sander, 2009; Nesbitt et al., 2015). As seen in all *Coelurosauravus* specimens, the humerus is nearly straight with both epiphyses aligned in the proximodistal axis of the bone (Fig. 11). This is also the case in the *Weigeltisaurus* holotype (Evans and Haubold, 1987), but contrasts with the strongly curved humerus of *Rautiania* (Bulanov and Sennikov, 2010).

The humerus is preserved either in dorsal or ventral view in all specimens (Figs. 1–4, 11). Thus, the proximal epiphysis is only partially visible. The proximal epiphysis of MNHN.F.MAP327a is partially visible in ventral view (Fig. 11B). It bears a robust deltopectoral crest extending ventrally from the proximal articulation over the length of the epiphysis. This crest delimits deep anteroproximal and posteroproximal concavities on the proximal epiphysis and is prolonged distally by a low longitudinal ridge separating the ventral

and posterior surfaces of the bone. The anteroproximal cavity is delimited ventrally by a sharp transverse ridge (transverse humeral line of Romer, 1922:555). The dimensions of this cavity suggest an extensive insertion for the M. scapulohumeralis. The posteroproximal cavity probably represents the broad proximal insertion pit of the M. coracobrachialis brevis (Holmes, 1977). MNHN.F.MAP317b exposes the proximal epiphyses of both humeri in dorsal view (Fig. 11C). The robust humeral head comprises of a smooth, ovate condyle. It is oriented dorsoventrally as in *Rautiania* (Bulanov and Sennikov, 2010). More distally, the proximal epiphysis bears a strong tuber on its dorsal surface, separated from the humeral head by an anteroposteriorly oriented groove. Based on its position relative to the articular head, this conforms well with the insertion of the M. subcoracoscapularis described for *Captorhinus* (Holmes, 1977). Kuehneosaurids also show a prominent insertion area for the M. subcoracoscapularis (Colbert, 1970).

All preserved humeri bear longitudinal grooves on their dorsal and ventral surfaces, likely due to slight diagenetic compression. This indicates that the bone structure was fragile, more so than that of the exceptionally preserved vertebrae, suggesting it was mostly hollow with thin cortical walls.

The distal epiphysis is about twice as wide as the diaphysis. As is seen in all specimens, the ectepicondyle is small and does not extend beyond the posterior margin of the diaphysis (Fig. 11). As is best seen in MNHN.F.MAP317a, the supinator process is slender and extends distally parallel to the main axis of the bone, forming the anterior wall of the ectepicondylar foramen (Figs. 3, 4). This foramen appears open in the lectotype and MNHN.F.MAP327a because the supinator process is obscured or broken distally (Fig. 11), but was presumably closed in these specimens prior to the fracture, as in the paralectotypes (Figs. 3, 4). An enclosed ectepicondylar foramen was also described for *Rautiania* (Bulanov

and Sennikov, 2010). In contrast, this foramen is not enclosed by the supinator process in the *Weigeltisaurus* holotype (Evans and Haubold, 1987).

As seen in all *Coelurosauravus* specimens, the entepicondyle extends slightly posteriorly beyond the distal margin of the diaphysis and distal to the trochlea (Fig. 11) as in *Rautiania* (Bulanov and Sennikov, 2010). The entepicondyle is roughly triangular, meeting the diaphysis at an obtuse angle (ca. 160°), unlike the robust and rectangular entepicondyle of *Hovasaurus* and *Thadeosaurus* (Carroll, 1981; Currie, 1981a). An entepicondylar foramen is visible in all *Coelurosauravus* specimens on the proximal portion of the entepicondyle as in *Rautiania* (Bulanov and Sennikov, 2010). The capitellum consists of a robust ovate condyle that articulated with the proximal epiphysis of the radius. The trochlea of the distal epiphysis is subtle and rounded distally. The capitellum and trochlea are well ossified and prominent in comparison to those of *Youngina* (BP/1/3859, VB, pers. obs.) or contemporaneous neodiapsids (Currie, 1980, 1981a; Carroll, 1981). Such a morphology is also present in *Rautiania* (Bulanov and Sennikov, 2010) and is reminiscent of early reptiles (Holmes, 1977; Reisz, 1981) or putative arboreal reptiles such as drepanosauromorphs (Pritchard et al., 2016). As best seen in MNHN.F.MAP327a, the ventral surface of the entepicondyle posterior to the trochlea forms a low crest, suggesting a strong origin point of the M. epitrochleoanconaeus (Fig. 11B; Holmes, 1977). This appears to be the case in *Rautiania* as well (Bulanov and Sennikov, 2010:fig. 4). The dorsal surface of the distal epiphysis is broken and weathered on both the lectotype and MNHN.F.MAP317b. What is preserved in MNHN.F.MAP317b suggests that there was a deep olecranon fossa framed on either side by low epicondylar ridges.

Radius—The radius is visible in all specimens but is best preserved in MNHN.F.MAP327a, where the bone is seen in posterior view. The radius is an elongate and gracile bone with a cylindrical shaft. The bone is slightly sigmoidal, and the distal epiphysis

appears to be inclined anterodistally (Fig. 11). There is no trace of the strong twisting observed in other neodiapsids (*Claudiosaurus*, *Hovasaurus*, Carroll, 1981; Currie, 1981a). The radius of other weigeltisaurids was described as straight in the *Weigeltisaurus* holotype and the Ellrich specimen (Pritchard et al., 2021), but we think that a slight inclination of the distal epiphysis may have been obliterated by diagenetic compression. Both epiphyses are only slightly expanded relative to the diaphysis.

The proximal epiphysis of the radius is best preserved in MNHN.F.MAP317a (Figs. 3, 4). Its proximal surface is strongly concave to accommodate the prominent capitellum of the humerus. As is best seen in the paralectotypes (Figs. 3, 4), the radius bears a slight lateral lip reminiscent of a tiny olecranon ("posterior lip" of Carroll, 1981:330). This structure is obscured by the ulna in MNHN.F.MAP327a (Fig. 11). This lip was otherwise recognized in *Hovasaurus* and *Thadeosaurus* (Carroll, 1981; Currie, 1981a). Pritchard et al. (2021) described a radioulnar articulation in the Ellrich specimen. However, we were unable to identify an articular facet on either bone in any *Coelurosauravus* specimen. Owing to the slight rotation of these bones, we think that the presence of this articulation is equivocal (see below). The proximal epiphysis becomes gradually more slender and continues into the diaphysis.

The distal epiphysis is best preserved in MNHN.F.MAP327a (Fig. 11B). Its distal surface is slightly concave and oriented anterodistally. It shows an anteroposterior constriction slightly lateral to the longitudinal axis of the bone, dividing the distal articular surface into a broad medial surface and a small lateral surface (Figs. 11C, 12). This lateral surface is roughly four times smaller than the medial one. It served for the articulation with the intermedium whereas the medial one served for the articulation with the radiale.

Ulna—The ulna is preserved in similar manner as the radius in the *Coelurosauravus* material. It is an elongate, gracile bone with a cylindrical shaft and is slightly sigmoidal in

posterior view. Both epiphyses are expanded relative to the diaphysis, reaching up to twice the width of the shaft in posterior aspect.

The proximal epiphysis bears a well-developed olecranon delimited medially by a deeply concave sigmoid notch (Fig. 11). This process is also seen in the *Weigeltisaurus* holotype and the Ellrich specimen (Evans and Haubold, 1987; Pritchard et al., 2021). As is seen in MNHN.F.MAP327a, the olecranon and sigmoid notch are reinforced by a prominent ridge running along the posterior surface of the bone. The posterior surface of the olecranon bears subtle pits, suggesting that the olecranon served as the insertion of a robust tendon for the M. triceps medialis (Holmes, 1977).

The distal epiphysis of the ulna is best preserved in posterior view in MNHN.F.MAP327a but is broken in two parts distally (Fig. 11A). According to the outline of the less well-preserved ulnae of the paralectotypes (Figs. 3, 4), the distal epiphysis of the ulna was slightly broader than the diaphysis and presumably articulated with both the intermedium and ulnare. It also articulated with the neighboring pisiform, as in all amniotes (Romer, 1956) but this articular surface is obscured in all specimens.

Manus

Elements of the manus are preserved in all specimens, although none of them are complete. The carpal elements are best preserved in MNHN.F.MAP327a, where they are seen in ventral view (Figs. 12, S2). This specimen will thus serve as the basis of the following description.

Our re-examination of the carpus resulted in a novel interpretation of the individual elements, which slightly differs from that of Carroll (1978:fig. 6) and Evans and Haubold (1987:fig. 15A). The carpus of *Coelurosauravus* comprises 11 bones, which is the standard

number in early amniotes (Romer, 1956), and includes the radiale, intermedium, ulnare, pisiform, two centralia and five distal carpals. Carpal elements are also present in the paralectotypes but are mostly obscured and hard to identify (Figs. 3, 4). Some are also completely disarticulated and unidentifiable on the lectotype (Figs. 1, 2).

None of the digits are preserved in the left manus, but preservation permits examination of the metacarpals (Fig. 12). The digits of the right hand of the paralectotype is slightly more complete (Figs. 3, 4). The digit that lies closest to the skull shows three phalanges in connection, none of which being the ungual. This digit likely represents digit V (see below). The manus has thus rotated relative to the forearm because this digit now lies medial to the others.

Radiale—The radiale is a small, rounded bone lying in proximoventral view close to the articular surface of the distal epiphysis of the radius (Fig. 12). The ventral surface of the bone bears a deep recess with a circular outline. Owing to its size and position relative to the other carpals, this bone likely articulated with the distomedial articular surface of the radius and the intermedium proximally, the medial centrale laterally and distal carpal 1 distally. It may have articulated with distal carpal 2 as well, although this cannot be ascertained because both bones are partially obscured and the individual elements slightly displaced. In araeoscelidians (Reisz, 1981) and early neodiapsids (Carroll, 1981; Currie, 1981a), the radiale is excluded from an articulation with distal carpal 1 by the medial centrale.

Intermedium—We identify a small bone lying just distal to the ulna as the intermedium, which is visible in proximoventral view (Fig. 12). Evans and Haubold (1987) only described the ventral surface of this element, and Carroll (1978) identified this element as the lateral centrale. According to its broad proximal surface, the bone likely articulated with the distolateral articular facet of the radius and distomedial portion of the ulna proximally. The long medial margin of the bone suggests that it articulated with the radiale

medially (see above). The lateral surface of the intermedium bears a low incisura, indicating its contribution to the perforating foramen. As in most early amniotes, the intermedium likely formed the median half of the perforating foramen and articulated with the medial margin of the ulnare. However, we failed to identify a corresponding incisura on the ulnare (see below). Based on its position and the size of the neighboring elements, the intermedium likely articulated with both centralia distally. This conforms with the contacts reconstructed by Evans and Haubold (1987).

Ulnare—As described by Carroll (1978) and Evans and Haubold (1987), the ulnare is a rectangular element, which is visible in ventral view, lying slightly distal to the intermedium and pisiform in MNHN.F.MAP327a (Fig. 12). The ventral surface of the bone is shallowly concave and bears a low ridge near its center. Owing to its slight displacement and the lack of an identifiable incisura for the perforating foramen, it is difficult to say whether or not the ulnare has rotated. Therefore, the reconstruction of its contacts with the neighboring bones is somewhat speculative. The shape of the carpal elements is compatible with the typical carpal articulation in early amniotes (Romer, 1956), suggesting the ulnare may have contacted the ulna, intermedium and pisiform proximally, the lateral centrale medially, and distal carpal 5 distally. Based on the size of the lateral centrale, it is possible that it articulated with distal carpal 4 as well, although this cannot be ascertained. This configuration would conform with the contacts proposed by Evans and Haubold (1987).

Pisiform—We follow Carroll (1978) and Evans and Haubold (1987) in their identification of the pisiform in MNHN.F.MAP327a, which is visible in proximoventral view (Fig. 12). This carpal lies distolateral to the ulna close to its anatomical position. Based on its position relative to the neighboring elements, it articulated with the ulna proximally and the ulnare medially, as is typical in early amniotes (Romer, 1956). A small sub-rectangular structure lies proximal to the pisiform, lateral to the distal head of the ulna. It may correspond

to a broken-off portion of the pisiform, although this remains tentative because the pisiform would then be unusually large compared to other amniotes (Romer, 1956).

Medial Centrale—The medial centrale is a small polygonal element visible in distoventral view in MNHN.F.MAP327a (Fig. 12). It is keystone-shaped, with its distal margin being wider than its proximal one. Based on its position and the articular surfaces on the neighboring elements, the medial centrale likely articulated with the radiale, intermedium and lateral centrale proximally, and distal carpals 1 and 2 distally. Whether or not it articulated with distal carpal 3 cannot be ascertained because of the disarticulation of the bones in MNHN.F.MAP327a. Contrary to Evans and Haubold (1987), we suggest no contact between the medial centrale and distal carpal 4. Both *Hovasaurus* and *Thadeosaurus* have a wide medial centrale that contacts distal carpal 4 (Carroll, 1981; Currie, 1981a).

Lateral Centrale—We follow Evans and Haubold (1987) in their identification of the lateral centrale of MNHN.F.MAP327a (Fig. 12). This rectangular element is seen in ventral aspect but is partially obscured by the ulnare and distal carpal 3. It is unclear whether or not this element has rotated, making the reconstruction of its articulations difficult. As the shape of the carpal elements is compatible with the typical carpal articulation in early amniotes (see ulnare above), the lateral centrale may have articulated with the intermedium and ulnare proximally, the medial centrale medially and distal carpal 4 distally.

Distal Carpals—All five distal carpals are preserved in MNHN.F.MAP327a (Fig. 12). Our interpretation follows that of Carroll (1978). Distal carpal 1 is seen in ventral view. It is a robust cylindrical bone that articulated with the radiale proximally, distal carpal 2 laterally and metacarpal I distally (Fig. 12). Because of its slender distal terminus, a distal contact with metacarpal II seems unlikely.

Following Carroll (1978), we consider a broad, mostly obscured element as distal carpal 2 (Fig. 12) and not as fused distal carpals 2 and 3 as reported by Evans and Haubold (1987). Distal carpal 2 articulated with the medial centrale proximally, distal carpals 1 medially, distal carpal 3 laterally and metacarpal II distally. Contacts with the radiale proximomedially and metacarpal III distolaterally are equivocal because these elements are slightly displaced and partially unpreserved. Distal carpal 2 was likely excluded from a contact with metacarpal III by the large distal carpal 3.

Evans and Haubold (1987) identified the large subcircular element lying lateral to metacarpal III as distal carpal 4 because of its large size as is typical in most early amniotes (Romer, 1956). However, we concur with Carroll (1978) in identifying this bone as distal carpal 3 instead based on its close location to distal carpal 2 and metacarpal III (Fig. 12). The size and robustness of distal carpal 3 conforms well with that of the less well-preserved carpus of the *Weigeltisaurus* holotype (SMNK cast of SSWG 113/7, VB, pers. obs.). This bone likely articulated with the lateral centrale proximally, distal carpals 2 medially, distal carpal 4 laterally and metacarpals III and IV distally. A contact between distal carpal 3 and the medial centrale is equivocal because these two bones are only partially preserved.

Distal carpal 4 is a relatively small subtriangular element compared to distal carpal 3 (Fig. 12), at most as large as distal carpal 3. In contrast, distal carpal 4 is typically the largest of the series in early amniotes (Romer, 1956). Based on the articular facets of the bone, distal carpal 4 articulated with the ulnare proximally, the lateral centrale proximomedially, distal carpals 3 medially, distal carpal 5 laterally, and metacarpal IV distally.

Distal carpal 5 is sub-rectangular and the smallest of the series. Distal carpal 5 thus articulated with the ulnare proximally, distal carpal 4 medially, and metacarpal V distally.

Metacarpals—The proximal portions of the metacarpals are preserved in MNHN.F.MAP327a, but the rest of the bones are not preserved in this specimen (Fig. 12). The right manus of the paralectotypes is the most complete of any specimen, but its metacarpal I is also partially preserved (Figs. 3, 4). Metacarpal III is the longest in the series, as is the case in the *Weigeltisaurus* holotype and *Rautiania* (Evans and Haubold, 1987; Bulanov and Sennikov, 2010). In contrast, the longest in the series is typically metacarpal IV in early amniotes (Romer, 1956). Owing to the preservation of the paralectotypes and MNHN.F.MAP327a, it remains unclear whether or not the metacarpals overlapped each other proximally. Such an overlap is described for the *Weigeltisaurus* holotype (Evans and Haubold, 1987).

As seen in MNHN.F.MAP327a, metacarpal I bears a slightly expanded proximal extremity relative to the shaft, which bears a shallowly concave articular facet for distal carpal 1 (Fig. 12). Metacarpals II and III are visible mostly in ventrolateral view (Fig. 12). Their proximal articular surfaces are slightly concave to accommodate the respective distal carpals. Metacarpal III is more robust than the other metacarpals, as seen on MNHN.F.MAP317a, b (Fig. 4). The head of metacarpal IV is 1.2 times wider than that of metacarpal I in MNHN.F.MAP327a (Fig. 12). As for metacarpals II and III, metacarpal V is mostly visible in ventrolateral view. It bears a prominent proximolateral process that frames the entire lateral margin of distal carpal 5.

Phalanges—All *Coelurosauravus* specimens preserve portions of the phalangeal series. The non-ungual phalanges are all long slender bones with slightly expanded extremities (Figs. 1–4). Digit V of the right manus of the paralectotypes is the only reasonably complete digit (Figs. 3, 4). It shows two phalanges in connection with the space for the missing first phalanx between this series and metacarpal V. The most distal phalanx is the longest, and identified as the penultimate by comparison with the long penultimate phalanx in

digit V of *Rautiania* (Bulanov and Sennikov, 2010). The ungual phalanx is missing, indicating that digit V of *Coelurosauravus* comprised four phalanges as in other weigeltisaurids (Evans and Haubold, 1987; Bulanov and Sennikov, 2010; Pritchard et al., 2021). In contrast, all Permo–Carboniferous diapsids have three phalanges in digit V (Romer, 1956).

Ungual phalanges are preserved in the lectotype and MNHN.F.MAP327b. They are all recurved and sharply pointed with the distal tip of the claw extending roughly to the level of the strong flexor tubercle. These bones all bear lateral longitudinal carinae.

Pelvic Girdle

The right pelvis is well-preserved in lateral view in MNHN.F.MAP327a (Figs. 9A, 9B). It is partially obscured by the femoral head so that only portions of the ilium and pubis are visible. The left puboischiatic plate is visible in medial view in the lectotype (Figs. 1, 2), as suggested by Carroll (1978) based on its shape and position relative to the sacral region. This plate is badly weathered with a triangular pubic portion pointing anteroventrally and a trapezoidal ischiatic portion pointing posteriorly (Figs. 1, 2). An even more weathered triangular structure expands dorsally from this puboischiatic plate, which might represent the ilium. However, this identification remains tentative. The pelvis is missing in the paralectotype (Figs. 3, 4).

Provided that our identification of the pelvic girdle of the lectotype is correct, the putative puboischiatic plate shows no trace of a thyroid fenestra (Figs. 1, 2). This fenestra is also absent in the puboischiadic plates of other weigeltisaurids (Evans, 1982).

Ilium—The outline of the ilium seems to be partially preserved on the lectotype, although this identification remains tentative (see above; Figs. 1, 2). The bone is otherwise

preserved in lateral view in MNHN.F.MAP327a (Figs. 9A, 9B). It is a thin dorsoventrally compressed bone. The pubic peduncle bears an anteroventrally oriented surface for the pubis as indicated by the low groove separating both bones. Nothing can be said about the ischiatic peduncle.

A robust, posterodorsally oriented supraacetabular buttress borders the acetabular cavity (Figs. 9A, 9B). A similarly robust supraacetabular buttress is present in *Claudiosaurus* and 'younginiforms' (Carroll, 1981; Currie, 1980, 1981a). This supraacetabular buttress is most massive in its middle portion, immediately dorsal to the acetabulum. Anteriorly, it merges into the pubic peduncle and is aligned with the preacetabular buttress of the pubis (Figs. 9A, 9B). More posteriorly, the supraacetabular buttress forms the posteroventral margin of the iliac blade and gradually decreases in transverse thickness, fading into the iliac blade posterodorsally.

The iliac blade is triangular in lateral aspect, flaring dorsally and with roughly symmetrical preacetabular and postacetabular processes, the latter being only slightly longer (Figs. 9A, 9B). The antero- and posteroventral margins of the iliac blade thus diverge anterodorsally and posterodorsally whereas its dorsal margin runs roughly horizontally. This morphology is similar to other weigeltisaurids (Evans, 1982; Pritchard et al., 2021), but we found no trace of the dorsal embayment reported by Pritchard et al. (2021) for the Ellrich specimen. In contrast, the iliac blade of other stem-saurians is typically lanceolate in lateral aspect and lacks a preacetabular process, as in *Hovasaurus* or *Thadeosaurus* (Carroll, 1981; Currie, 1981a), or only bears a small preacetabular tuber as in *Acerosodontosaurus* (Currie, 1980). However, a similar but smaller preacetabular process is present in several archosauromorphs (Nesbitt et al., 2015; Pritchard and Sues, 2019). Provided our interpretation of the pelvic girdle of the lectotype is correct, the postacetabular process did not extend posterior to the ischium in *Coelurosauravus* (Figs. 1, 2). This would contrast with the

situation in other stem-saurians, where the postacetabular process of the iliac blade extends beyond the posterior margin of the ischium (Currie, 1980, 1981a; Carroll, 1981). Fine striations radiate dorsally across the lateral surface of the iliac blade in MNHN.F.MAP327a (Figs. 9A, 9B). They presumably mark the attachment area of the thigh musculature (Romer, 1922).

Pubis—Little of the pubis is visible in MNHN.F.MAP327a (Figs. 9A, 9B). As described by Carroll (1978), the most conspicuous part of the bone is the prominent, anteroventrally oriented pubic tubercle, which ends with a concavity presumably housing the iliopubic ligament (Romer, 1922). A robust ridge extends from the preacetabular buttress of the pubis to this concavity. Anteriorly, the preacetabular buttress delimits a broad posteriorly facing surface for the contribution of the pubis to the acetabulum. In *Acerosodontosaurus*, *Hovasaurus* and *Thadeosaurus* the pubis barely contributes to the acetabulum, and none of these taxa have a preacetabular buttress (Currie, 1980, 1981a; Carroll, 1981). Lastly, the anterodorsal margin of the pubis of MNHN.F.MAP327a lacks the short flange present in 'younginiforms' (Currie, 1980, 1981a; Carroll, 1981).

Ischium—Provided our interpretation of the pelvic girdle of the lectotype is correct, the ischium is preserved in medial view (Figs. 1, 2). The bone is short and trapezoidal in lateral aspect, being slightly anteroposteriorly longer than the ischium. The medial surface of the ischium is shallowly concave.

Hindlimb

The lectotype preserves elements of both hindlimbs, with both femora lying perpendicular to the long axis of the body and the knees bent in a way that the forelegs and pes extend posteromedially along the vertebral column of the tail of the animal (Figs. 1, 2).

The left hindlimb underlies the broken-off trunk of the animal and is mostly obscured, but the right one is almost complete. Despite being weathered, the individual bones remain mostly in anatomical position. Elements of the hindlimbs in MNHN.F.MAP327a are more poorly preserved. They extend posteriorly from the pelvic region and are oriented posteroventrally with respect to the tail (Figs. 5, 6). There is no trace of the hindlimbs in the paralectotypes (Figs. 3, 4).

As for the forelimb, we follow the terminology of Romer (1922) for the description. For the sake of clarity, the femora are described as if oriented perpendicular to the sagittal plane, with the foreleg bent ventrally roughly at a right angle. This is consistent with previous descriptions of weigeltisaurids including *Coelurosauravus* (Carroll, 1978; Evans and Haubold, 1987).

Femur—The right femur is subcomplete and visible in anteroventral view on the lectotype (Fig. 13). The left one is also preserved in anteroventral view, but only its distal epiphysis is exposed (Figs. 1, 2). Both femora are also partially preserved in MNHN.F.MAP327a but overlie each other (Figs. 5, 6). The diaphysis of the left femur is seen between the broken-off epiphyses of the right one.

As is best visible in the lectotype, the femur is a long and slender bone, being slightly longer than the humerus (Figs. 1, 2, 13). It consists of a cylindrical diaphysis with epiphyses that are about twice as wide as the shaft. In anterior view, the bone shows a slight sigmoidal curvature (Fig. 13) as is typical for early diapsids (Benton, 1985).

The proximal epiphysis is diagenetically compressed in the lectotype (Fig. 13). The femoral head is rounded in anteroventral view. As described by Carroll (1978), the low internal trochanter is visible distoventral to the femoral head, framing a mostly obscured intertrochanteric fossa. It does not extend proximally to the level of the proximal articulation,

as in the Ellrich specimen (Pritchard et al., 2021). Nothing can be said about the poorly preserved proximal surface of the right femur of MNHN.F.MAP327a (Figs. 9A, 9B).

The diaphysis is best preserved in the lectotype (Fig. 13). It is cylindrical and shows a slightly larger diameter than the humeral shaft (Figs. 1, 2). There is no trace of a fourth trochanter or an adductor crest which are typically present in early reptiles (Holmes, 2003), or of the thin linea aspera described for araeoscelidians (Vaughn, 1955; Reisz, 1981).

The distal epiphysis is visible in anteroventral view in the lectotype (Fig. 13A). Based on the position of the hindlimb relative to the pelvis and our identification of the shallow intercondylar fossa, it is also visible in posterodorsal view in MNHN.F.MAP327a (Fig. 13B). The tibial condyle is preserved on both sides of the lectotype. It is rounded in outline and forms a low anteroventral crest slightly offset from the bone (Fig. 13). Dorsal to this crest, the tibial condyle bears a low, triangular tibial fossa on its posterior surface. The slightly concave popliteal area is partially visible in the lectotype (Fig. 13). The fibular condyle is mostly obscured by tarsal elements in MNHN.F.MAP327a, but its outline suggests that it is rounded (Fig. 13B). What is visible in this specimen suggests that the tibial and fibular condyles extended posteriorly to the same level. This is typical for early neodiapsids (Carroll, 1975, 1981; Gow, 1975; Currie, 1980, 1981a). In contrast, in early amniotes, including araeoscelidians, the fibular condyle extends distal to the tibial one (Reisz, 1981; Holmes, 2003). Pritchard et al. (2021), described the latter morphology in the more poorly preserved Ellrich specimen, contrasting with the femur of *Coelurosauravus*.

As is seen in MNHN.F.MAP327a, the posterior and dorsal surfaces of the distal epiphyses bear short longitudinal striations, which likely mark the insertions areas of the flexor and extensor musculature respectively.

Tibia—The tibia is exquisitely preserved in lateral view on the right side of MNHN.F.MAP327a (Fig. 13B). Both tibiae are also preserved in connection with the femur in the lectotype, where they are visible in medial view (Figs. 1, 2, 13). The tibia is a long and slender bone with a slender distal epiphysis but a highly expanded proximal one reaching up to three times the width of the shaft. As is best seen in the lectotype, the bone is slightly curved, with a shallowly concave posterior margin and a convex anterior one.

As is best seen in MNHN.F.MAP327a, the proximal epiphysis rapidly expands from the diaphysis (Fig. 13B). It bears a prominent cnemial crest anteriorly, which is separated from the proximal epiphysis by a deep cnemial trough (sensu Pawley and Warren, 2006). The anteroproximal portion of the cnemial crest is obscured by tarsal elements, so it is impossible to say whether or not a cnemial tuber was present (Fig. 13B). A prominent cnemial crest is typically present in early reptiles (Holmes, 2003), including araeoscelidians (Vaughn, 1955; Reisz, 1981), but this structure is generally considered absent in early neodiapsids (Ford and Benson, 2020: character 282), although it was also described in some early saurians (e.g., Nesbitt et al., 2015).

As is seen in MNHN.F.MAP327a, a low ridge runs along the anterior surface of the bone as a continuation of the cnemial crest (Fig. 13B). The diaphysis thus appears mediolaterally compressed. Most of the lateral surface of the bone bears short pits and scars, suggesting the insertion area of the extensor musculature of the tarsus. These scars extend distally to the base of the distal epiphysis (Fig. 13B).

The distal epiphysis is poorly preserved in both specimens. As is seen in the lectotype, it is only barely expanded relative to the diaphysis and rounded in medial view (Figs. 1, 2, 14). It articulates distally with the astragalus, but the distal surface of the bone is missing. It is thus unclear whether or not it showed a “stepped” outline, as described for the Ellrich specimen (Pritchard et al., 2021:44).

Fibula—The right fibula is visible in medial view in the lectotype. It is poorly preserved, with a mostly collapsed medial surface (Figs. 1, 2). Only the distal portion of the right fibula is seen in MNHN.F.MAP327a, lying among the tarsal elements (Fig. 13B).

As is visible in the lectotype, the distal anterior margin of the bone is weakly concave (Figs. 1, 2). However, because the proximal epiphysis of the bone is obscured, it remains unclear whether or not the bone was arcuate as in early reptiles (Holmes, 2003) or sigmoidal as in early neodiapsids (Carroll, 1981; Currie, 1981a). Little can be said about the medial surface of the diaphysis because it is compacted. The distal epiphysis is slightly expanded with respect to the diaphysis and accommodates the adjacent astragalus and calcaneus (Figs. 1, 2, 14).

Pes

The right pes is completely preserved in the lectotype and is visible in ventral view, including the proximal portions of several digits (Figs. 14, S3). Disarticulated tarsals, metatarsals and phalanges are also preserved in MNHN.F.MAP327a, although the individual bones are impossible to distinguish (Fig. 13B). Carroll (1978:fig. 2) and Evans and Haubold (1987:fig. 17A) proposed various interpretations of the tarsus of the lectotype, but both illustrated a proximolateral expansion of the astragalus. Careful examination of the cast and original specimen indeed shows a polygonal structure proximolateral to the astragalus (Fig. 14), but it is located too far from the latter to be a part of it. It remains unclear if this element is a portion of the calcaneus or just a concretion.

Astragalus—The astragalus of the lectotype lies distal to the tibia. It has slightly rotated from its anatomical orientation, and is now visible in lateral view (Fig. 14). The overall shape of the bone and its articular surface for the tibia thus remain unknown. In lateral

view, the bone shows a gradual increase in thickness, with its distal margin being twice as thick as its proximal one. The bone bears a short proximolaterally oriented articular facet for the fibula (Fig. 14).

The entire lateral surface of the astragalus served as an articular surface for the calcaneus (Fig. 14). However, this surface is interrupted near its mid-height by an incisura forming the medial wall of the foramen for the perforating artery. This foramen forms a ventrodistally running groove separating the calcaneal articulation into proximal and distal facets that are subequal in height. This morphology is typical in early neodiapsids (Brinkman, 1979; Carroll, 1981; Currie, 1981a). In contrast, the proximal facet is roughly twice as wide as the distal one in araeoscelidians (Vaughn, 1955; Reisz, 1981). The proximal calcaneal facet is slightly convex whereas the distal one is concave and oriented distolaterally, corresponding to the respective facets of the calcaneus (Fig. 14).

Because the astragalus of the lectotype is only visible in lateral view, its distal articulations with the other bones are hard to reconstruct. However, based on the very slight displacement of the bones and the morphology of distal tarsal 4 (see below), the astragalus of *Coelurosauravus* likely articulated with the navicular and distal tarsals 2 and 4 distally.

Calcaneus—The calcaneus is the least well-preserved tarsal, visible in ventral view in the lectotype (Fig. 14). Its ventral surface seems slightly concave, but this may be due to slight diagenetic compression. As stated above, the proximal extent of the bone is unclear due to a small, indeterminate structure just distal to the fibula that may be a fragment of the calcaneus.

The medial margin of the bone bears a shallow incisura, forming the lateral margin of the perforating foramen (Fig. 14). As for the astragalus, this foramen divides the astragalar contact in proximal and distal portions. Whereas the proximal extent of the bone remains

uncertain, the distal articular facet is slightly proximomedially oriented, which conforms well with the corresponding facet on the astragalus. The distal margin of the bone is transversely short relative to the preserved lateral extent of the bone. It articulated with distal carpals 4 and 5 along its entire length.

As is seen in ventral view, the calcaneus shows its greatest thickness at its medial margin, which is also indicated by the calcaneal facets of the astragalus (Fig. 14). The bone then gradually tapers laterally. Carroll (1978:fig. 2) recognized a large lateral expansion, which was not identified by Evans and Haubold (1987:fig. 17A). Although the lateral extent of the bone is unpreserved, it certainly extended beyond the level of its distal margin (Fig. 14).

Navicular—The navicular (following Piñeiro et al., 2016, the 'centrale' or 'lateral centrale' of other authors) lies distal to the medial portion of the astragalus in the lectotype (Fig. 14). It is an almost quadratic bone in ventral view. Owing to its shape, the bone bears subequal articular facets for the astragalus proximally, distal tarsal 2 laterally, and distal tarsal 1 distally. It thus overhangs distal tarsal 1 and is excluded from distal tarsal 3 by the contact between the astragalus and distal tarsal 2.

A bone of similar shape and position was identified as distal tarsal 1 in the *Weigeltisaurus* holotype by Evans and Haubold (1987:fig. 11). We suggest that this element corresponds to the navicular, with distal tarsal 1 missing (SMNK cast of SSWG 113/7, VB, pers. obs.). We interpret the element identified as the navicular by Evans and Haubold (1987:fig.11) as the distal calcaneal articular surface of the astragalus, which is here visible in medial view. This conforms well with the morphology of the astragalus of *Coelurosauravus*, which is preserved in a similar view (see above).

Distal Tarsals—All five distal tarsals are visible in ventral view in the lectotype (Fig. 14). Each one shows a strongly concave dorsal surface, although this may be due to diagenetic compression.

Distal tarsal 1 lies between the navicular and metatarsal II in the lectotype (Fig. 14). It is a proximodistally compressed bone, at least twice as wide as it is long. It is the widest of all distal tarsals. The bone articulated with metatarsal I, but it is unclear whether or not it also articulated with metatarsal II because the latter bone is missing.

Distal tarsal 2 is the transversely thinnest in the series (Fig. 14). It is rectangular in dorsal aspect and its distal portion is obscured by distal tarsal 3. As described above, it articulated with the astragalus proximally, thereby excluding distal tarsal 3 from the navicular. Owing to its width, distal tarsal 2 articulated with metatarsal II only.

Distal tarsal 3 is teardrop-shaped, with its tapered end pointing proximally (Fig. 14). It is overhung proximally by distal tarsal 4, which excludes the bone from the astragalus. Owing to the shape of the proximal surface of metatarsal IV, it appears that distal tarsal 3 articulated with both metacarpals III and IV.

Distal tarsal 4 is the proximodistally longest in the series (Fig. 14). It is very slender, being roughly twice as long as it is wide. The bone bears a strong proximomedial process that overhangs distal tarsal 3 and articulates with the astragalus. Lateral to the astragalar contact, the proximal margin of the bone articulates with the calcaneus. The lateral margin of the bone is slightly convex and provides the articulation for distal tarsal 5.

Distal tarsal 5 is the smallest of the series (Fig. 14). It is subtriangular in dorsal aspect, points proximomedially and has a short proximal contact with the calcaneus.

Owing to our interpretation of the navicular of the *Weigeltisaurus* holotype, the tarsals of *Coelurosauravus* and *Weigeltisaurus* conform well with one another.

Metatarsals—The metatarsal series is partially preserved in the lectotype (Fig. 14). As identified by Evans and Haubold (1987), the digits are slightly jumbled so that metatarsals I, IV and V are visible, while metatarsal II is missing and metatarsal III is partially visible between metatarsals I and IV. All preserved metatarsals have long and slender shafts with slightly expanded proximal and distal articular extremities.

Metatarsal I has an almost flat proximal articular surface for distal tarsal 1. Its distal terminus has a quadrangular extremity, framed proximally by a pair of contralateral ridges. Metatarsal IV is only slightly longer than metatarsal I. As described above, its wide proximal extremity likely articulated with distal tarsals 3 and 4. The distal end of the bone is convex in ventral view, lacking the quadrangular extremity and contralateral ridges of metatarsal I. Metatarsal V is subequal in length to metatarsal I, but its overall morphology is more similar to that of metatarsal IV. It is not hooked, in contrast to most saurian reptiles (Lee, 1997) and lacks the outer (poterolateral) process that is present in other early neodiapsids (Robinson, 1975; Brinkman, 1979; Borsuk-Bialynicka, 2018). The fifth metatarsal of the lectotype also bears a proximolateral tubercle, just distal to its proximal articulation.

Phalanges—The digits are only partially preserved in the lectotype, but preservation allows for a minimal count of the phalanges of each digit (Fig. 14). Elements of all digits are preserved. These include both phalanges of digit I, the second of which being the ungual, at least two of digit II, one of digit III, and two of digits IV and V respectively (Fig. 14). Several disarticulated phalanges are also visible in MNHN.F.MAP327a, although none can be assigned to a given digit (Fig. 13B).

The non-ungual phalanges of the pes are roughly identical in shape to those of the manus, consisting of slender shafts with slightly expanded extremities (Fig. 14). A disarticulated distal digit comprising four bones including the ungual suggests that the penultimate phalanx was substantially longer than the antepenultimate.

DISCUSSION

A reappraisal of the phylogenetic position of weigeltisaurids is currently under study by the authors, and is outside the scope of this paper. However, the detailed re-description of the postcranial skeleton of *Coelurosauravus elivensis* provided here allows for a discussion of the anatomy, functional morphology and paleoecology of these enigmatic gliding reptiles.

Skeletal Reconstruction

The material available for *Coelurosauravus* allows for an almost complete reconstruction of the skeleton of this reptile (Fig. 15). We focus here on the postcranial skeleton of *Coelurosauravus*, as the skull reconstruction has already been provided by Buffa et al. (2021). The mandible, poorly preserved in all *Coelurosauravus* specimens, is reconstructed following the proportions of that of the *Weigeltisaurus* holotype (Bulanov and Sennikov, 2015b).

The reconstruction of the presacral vertebral column is based on the complete series preserved in the paralectotypes (Figs. 3, 4, 8), whereas the outline of the trunk is based on the partial Eppleton specimen, which is preserved mostly in dorsal view (TWCMS B5937, VB, pers. obs.; Evans, 1982). The latter specimen was also used by Pritchard et al. (2021) for their reconstruction of the Ellrich specimen. The rest of the vertebral column is mostly based on MNHN.F.MAP327a, although the tail of this specimen is incomplete and includes only the first 29 vertebrae (Figs. 5–7). Given a vertebral count of 50 to 70 among early amniotes (Romer, 1956), the tail of *Coelurosauravus* was much longer than what is preserved. The

girdles and limbs are reconstructed based on all known specimens. The manual and pedal digits, which are fragmentary in all *Coelurosauravus* specimens, are reconstructed based on the complete series of the Ellrich specimen (Pritchard et al., 2021). Several patagials are incompletely preserved in MNHN.F.MAP327a. Their extent was reconstructed by following the outline of the wing reconstructed from the few complete elements (Fig. 15).

Carroll (1978) provided the first and only skeletal reconstruction of *Coelurosauravus elivensis* to date. However, this reconstruction assumes that the wing was supported by the trunk ribs as in the extant agamid *Draco* and the Late Triassic kuehneosaurids. For a long time, this was a commonly accepted interpretation (Evans, 1982; Evans and Haubold, 1987, but see Schaumberg, 1976, 1986). All of the more recent reconstructions are based on the German material, particularly the Ellrich specimen (Frey et al., 1997; Schaumberg et al., 2007; Pritchard et al., 2021), and do not reflect the anatomy of *Coelurosauravus* from Madagascar. We thus provide a revised reconstruction of this taxon in dorsal view, as well as the first skeletal reconstruction of a weigeltisaurid in lateral view (Fig. 15).

According to our reconstruction, *Coelurosauravus* is a gracile reptile of ca. 180 mm in snout-vent length, and at least 320 mm in total length including the preserved portion of the tail (Fig. 15). Based on the length of the longest patagials (Table 3) and the width of the trunk preserved at this level in the Eppelton specimen (TWCMS B5937, VB, pers. obs.), this animal had a wingspan of ca. 350 mm (Fig. 15). These values differ slightly from those provided by Evans (1982), but this probably reflects differences in the reconstruction and interpretation of the patagials. *Coelurosauravus* had a dorsoventrally compressed body. Both limbs are long and lender, with large autopodia. Based on our reconstruction, the forelimb is ca. 80 mm in length, with the manus being ca. 33 mm long. The hindlimb is slightly longer, measuring ca. 90 mm with a 40 mm long pes.

Our reconstruction broadly conforms to that of Pritchard et al. (2021) for the Ellrich specimen but with some significant differences, such as in the proportions of the skull, neck and trunk, or the arrangement of the patagials. Based on direct observation of those specimens, we interpret these differences as interspecific differences between *Coelurosauravus elivensis* and *Weigeltisaurus jaekeli* (or at least the Ellrich specimen) rather than differences in interpretation.

Remarks on the Homology of Patagials

As summarized by Pritchard et al. (2021), early workers interpreted the patagials as true ribs, and consequently reconstructed the wing as derived from the dorsal half of the trunk (Carroll, 1978; Evans, 1982). The interpretation of the patagials as dermal ossification by Schaumberg (1976, 1986) and Frey et al. (1997) invalidated these reconstructions although the anchoring of the patagials, and consequently of the wing skeleton, to the rest of the body remained unknown. Based mostly on the Ellrich specimen, Pritchard et al. (2021) recently suggested that the base of the patagials was closely associated with the gastral basket, and thus emerged from the ventral half of the flanks. Our observations of MNHN.F.MAP327a confirm this interpretation and indicate a possible articulation between each patagial and the lateral-most element of each transverse gastral row (Figs. 10, 15).

The exact nature of the patagial ossifications, however, remains unclear. Based on previous works, it may be proposed that the patagials are: (1) neomorph ossifications with no known homologue; (2) intramembranous ossification from the laterally expanded myosepta of the trunk wall musculature; (3) lateral gastralia. We concur with Pritchard et al.'s (2021) assessment that these structures may be homologues of lateral gastralia. This interpretation indeed conforms best with the putative articulation between patagials and gastralia described

above because similar articulations are present between adjacent gastralia in other reptiles (Claessens, 2004). Further studies are needed to confirm this hypothesis.

Paleoecology of Weigeltisaurids

Weigeltisaurids have long been considered as arboreal and gliding reptiles (Carroll, 1978; Evans, 1982; Evans and Haubold, 1987; Frey et al., 1997; Schaumberg et al., 2007; Bulanov and Sennikov, 2010; Buffa et al., 2021; Pritchard et al., 2021), an interpretation followed here. Yet, the exquisite preservation of the *Coelurosauravus* material re-described above provides an opportunity to further discuss the functional morphology of the postcranial skeleton and lifestyle of these enigmatic animals.

Inferring the function of a given structure in the fossil record and reconstructing the paleoecology of extinct organisms is notoriously difficult (e.g. Gould, 1974; Benton, 2010; Padian and Horner, 2011; Hone and Faulkes, 2014). This is particularly true for weigeltisaurids in light of the scarcity of specimens and their phylogenetical distance to recent analogues (Buffa et al., 2021). As a result, the interpretations discussed here must remain speculative.

Arboreality—Weigelt (1930) and Huene (1930) first identified the arboreal lifestyle of weigeltisaurids by analogy with extant chamaeleonids mainly based on cranial similarities. The patagial skeleton was only recognized in later studies. As all extant gliding tetrapods are exclusively arboreal (Dudley et al., 2007; Socha et al., 2015), every study since then has accepted an obligatory arboreal life style of weigeltisaurids. However, they hardly consider the presence of non-patagial features, which are indicative of arboreality. Only Bulanov and Sennikov (2010) discuss the forelimb of *Rautiania* in the context of climbing. This is particularly surprising, as the patagium of weigeltisaurids would severely hinder terrestrial

locomotion (Bulanov and Sennikov, 2010), making weigeltisaurids some of the earliest known amniotes with an obligatory arboreal lifestyle, and among the first ones to be described from the Paleozoic in the literature.

For quadrupedal animals, locomotion in an arboreal habitat is subject to various challenges that include (1) moving up and down on inclined, vertical or overhanging surfaces, (2) bridging distances between branches, and (3) moving in a three-dimensional environment on substrates of variable width and compliance (Cartmill, 1974, 1985).

(1) Moving on inclined or vertical and often narrow and irregular surfaces requires generating traction to counteract the weight of the animal and prevent pitching in order to minimize the risk of falling (Cartmill, 1974, 1985). Traction is generated at the contact points or surfaces between animal and substrate. In medium- to large-sized quadrupeds (> 100 mm), traction is generated by interlocking the claws into the surface irregularities of the substrate (clinging), or by encircling the substrate with supporting appendages or the entire body (grasping; Cartmill, 1974, 1985; Hildebrand and Goslow, 2001; Fröbisch and Reisz, 2009). A third mechanism (adhesion), implies the generation of capillary or van der Waals forces though adhesive surfaces (Cartmill, 1985; Labonte et al., 2016). This mechanism is common in small-sized animals (< 100 mm; Fröbisch and Reisz, 2009), and is represented in larger animals by gekkotans (up to 200 g; Russell et al., 2019). In the latter, the presence of large adhesive surfaces implies prominent specializations of the autopodia such as the dorsal flexion of the penultimate phalanges, eventual reduction of other phalanges including unguals, and presence of paraphalanges (summarized in Russell and Bauer, 2008). As there is no evidence for such specializations in the large-sized weigeltisaurids (> 250 g, Evans, 1982), it seems unlikely that these reptiles clung to trees through adhesion.

As identified by Fröbisch and Reisz (2009), claw-based clinging is characterized by an elongation of the penultimate phalanges, whereas autopodial grasping is characterized by an

elongation of the proximal ones. All known weigeltisaurid autopodia show conspicuous elongation of the penultimate phalanges (Figs. 3, 4, 14; Evans, 1982; Evans and Haubold, 1987; Bulanov and Sennikov, 2010; Pritchard et al., 2021), suggesting that as arboreal quadrupeds, weigeltisaurids likely used clinging to generate traction (Fig. 16). This is strongly supported by the sharp, laterally compressed and strongly recurved ungual phalanges of weigeltisaurids (Bulanov and Sennikov, 2010; Pritchard et al., 2021), which have long been considered typical of clinging arboreal taxa (Arnold, 1998; Zani, 2000; Tulli et al., 2009; D'Amore et al., 2018). Such claws are commonly used to infer an arboreal lifestyle in extinct and extant taxa (Feduccia, 1993; Spielmann et al., 2005, 2006; Fröbisch and Reisz, 2009; Birn-Jeffrey et al., 2012; Simões et al., 2015, 2017; Jenkins et al., 2020).

Among clinging arboreal quadrupeds, pitching during arboreal locomotion is avoided by keeping the body, and thus the center of gravity, close to the substrate (Cartmill, 1974, 1985; Higham and Jayne, 2004; Lammers and Zurcher, 2011; Schmidt and Fischer, 2011). These taxa thus typically show a dorsoventrally compressed body. Such a flat body outline is seen in many extant and extinct arboreal squamates (e.g. Arnold, 1998; Simões et al., 2017) such as the gliding agamid *Draco* (Hoffstetter and Gasc, 1969) and the putative arboreal varanopid *Ascendonanus* from the Middle Permian of Germany (Spindler et al., 2018). The dorsoventrally compressed body of *Coelurosauravus* (Fig. 15) could allow for a locomotion on inclined surfaces and is thus suggestive of an arboreal lifestyle (Fig. 16).

Extant arboreal limbed squamates, further counterbalance pitching through active stiffening of the trunk (Grinham and Norman, 2020). These taxa typically exhibit an elongate preacetabular process of the ilium compared to closely related terrestrial forms (e.g. Tinius et al., 2018). This process serves as the origin of the M. quadratus lumborum (Russell and Bauer, 2008), a dorsoflexor muscle that stiffens the posterior part of the trunk and thus provides bracing against gravitational forces during arboreal or bipedal locomotion (Borsuk-

Białynicka, 2008; Grinham and Norman, 2020; Paparella et al., 2020). Provided weigeltisaurids had a similar muscular arrangement, their prominent preacetabular process suggests a similar active pitching control during arboreal locomotion.

In addition, arboreal quadrupeds typically use their forelimbs to generate traction during locomotion (Arnold, 1998). In such taxa, the forelimbs approximate the hindlimbs in length. This is seen in various squamates (Arnold, 1998), including extinct taxa (Evans and Barbadillo, 1998; Simões et al., 2015, 2017), and the Permian varanopid *Ascendonanus* (Spindler et al., 2018). This morphology would provide more symmetrical attachment points anterior and posterior to the center of gravity, which would further help in keeping the body of the animal close to the substrate (Arnold, 1998; Alexander, 2013), and would increase reach to bridge gaps. In weigeltisaurids, the forelimb is ca. 90% the length of the hindlimb, which is consistent with those taxa that use the forelimbs significantly during arboreal locomotion (Fig. 16).

Lastly, most of the propulsion is generated during the retraction phase of the hindlimb in quadrupedal climbers (Zaaf et al., 1999; Anzai et al., 2014). These taxa thus typically show a larger area of origin for the hindlimb retractor muscles than for the protractor muscles (Tinius et al., 2018). In contrast, the large preacetabular process of the ilium in weigeltisaurids could have served as a broad origin area for the hindlimb protractors, suggesting a faster and more powerful protraction during locomotion (Hutchinson, 2001; Russell and Bauer, 2008). As noted by Tinius et al. (2018), an increase in hindlimb protractor origin area could be linked to frequent controlled arboreal head-down descent in extant squamates, suggesting a similar behavior for weigeltisaurids. However, given that gliding is a rather energically cheap locomotion (e.g. Socha et al., 2015), it may have been cheaper than frequent arboreal descent. It is thus likely that the protractor muscles were involved during other movements, possibly allowing for a faster arboreal ascent, or were also active during gliding (see below).

(2) In an arboreal habitat, the substrate is discontinuous (Cartmill, 1985). To compensate such discontinuities, extant arboreal tetrapods show a variety of gap-crossing behaviors such as swinging (exclusively in graspers), jumping, gliding or flying (Cartmill, 1974, 1985; Graham and Socha, 2020). Evidently, the patagia of weigeltisaurids would have allowed them to cross large gaps by gliding similar to extant arboreal gliders (Graham and Socha, 2020). As argued by Pritchard et al. (2021), the patagia of weigeltisaurids are inserted more ventrally than in *Draco* and are thus likely attached below the center of gravity of the animal (Fig. 15). This low-wing configuration would offer maneuverability but less stability (Frey et al., 2003). However, the large wingspan of weigeltisaurids could have allowed for a dihedral position of the patagia, which would have stabilized flight and thus effectively counterbalanced this trade-off (Frey et al., 2003). Such a wing conformation would have provided both a stable long-distance flight combined with optional maneuverability when necessary.

Lastly, the tail has been identified as a key component of locomotion in arboreal habitats (Gillis and Higham, 2016). Indeed, numerous extant arboreal quadrupeds, namely reptiles, use their tail for balance while climbing (Jusufi et al., 2008; Fleming and Bateman, 2012), turning or crossing gaps (Higham et al., 2001; Larson and Stern, 2006), jumping (Gillis et al., 2009; Kuo et al., 2012; Libby et al., 2012) or falling (Jusufi et al., 2008, 2010, 2011). In the case of *Draco*, tail stiffness is muscularly controlled and serves to direct the gliding course (John, 1971; Clark et al., 2021). The tail of weigeltisaurids is long and slender with short neural and haemal spines (Fig. 9; Evans, 1982). As argued for coelurosaurian dinosaurs, which show a similar morphology of the tail skeleton, this may indicate a reduction of the caudofemoral musculature and suggest a decoupling of the tail and hindlimb. This decoupling would allow the tail to act as a stabilizer (Persons and Currie, 2012; Persons et al., 2013; Pittman et al., 2013).

(3) There is little to no evidence to support a discussion regarding the diameter and compliance of the substrates favored by weigeltisaurids, or to assess the density of foliage or branches in the late Permian forest ecosystems where these reptiles lived. Most extant arboreal squamates have slender bodies enabling them to walk on narrow substrates and move around obstructions (Arnold, 1998). While the dorsoventrally compressed body of weigeltisaurids seems consistent with such environments, one must account for the patagia of these animals. Their large span, especially compared to *Draco*, would physically have hindered locomotion with lateral body undulations, even when folded back (Fig. 16).

Gliding—The gliding locomotion of weigeltisaurids has long been consensual (Schaumberg, 1976, 1986; Carroll, 1978; Evans, 1982; Evans and Haubold, 1987; Frey et al., 1997), and is not challenged here. However, little is known on the gliding performance of these animals. McGuire and Dudley (2011) suggested that weigeltisaurids were too big to be efficient gliders by comparison with the extant agamid *Draco*. However, the patagia of weigeltisaurids is unique in terms of shape and high aspect ratio (Fig. 15; Evans, 1982), low-wing configuration with the option for a dihedral configuration during flight (Fig. 15; Pritchard et al., 2021), and supporting structures (Schaumberg, 1976, 1986; Frey et al., 1997; Schaumberg et al., 2007; Pritchard et al., 2021). All of these factors may have increased the gliding capacity of weigeltisaurids although this cannot be ascertained without studying the aerodynamic performance of these animals.

At present, it is unclear how the wing of weigeltisaurids was extended during flight. Schaumberg et al. (2007), based on their reconstruction of the patagium very close to the forelimb, suggested a tendinous connection between the scapula and anterior-most patagial. According to that interpretation, the wing could be extended by a sharp protraction of the forelimb and could be further stabilized by filling the lungs with air to inflate the ribcage (Schaumberg et al., 2007). While there is no basis to discuss the benefits of inspiration during

gliding in the available material, it is apparent that the anterior margin of the patagium is positioned at a distance to the forelimb in MNHN.F.MAP327a, likely due to the presence of a cartilaginous sternum (Figs. 5, 6). Such a gap would have been difficult to bridge by a tendon while maintaining an efficient angle of attack. Furthermore, extension of the patagia through protraction of the forelimb is unlikely because it would cause accidental openings of the patagia during limb-based locomotion.

In *Draco*, the patagia are first extended by the contraction of the iliocostal and intercostal musculature (Colbert, 1967; John, 1970; Russell and Dijkstra, 2001) and can be further expanded by interlocking the claws in the scales on the anterior dorsal surface of the patagia (Dehling, 2017). This is permitted by the long arms of this squamate and by a postaxial abduction of the manus. As indicated by Dehling (2017), such an abduction appears possible in weigeltisaurids as well, as shown by the position of the right manus of the Ellrich specimen (Pritchard et al., 2021). Furthermore, as exemplified by *Coelurosauravus* (Fig. 15), the forelimb could likely extend across the proximal half of the leading edge of the wing. Provided our reconstruction of the digits is correct, they could reach the level of the fifth patagial, which incidentally corresponds to the first patagial without distal curvature (Fig. 15). In *Draco*, the aspect ratio of the patagia is much lower than in weigeltisaurids. Thus, the forelimb spans the entire leading edge, and grasps the almost straight first rib, forming the transverse leading edge of the wing. Based on the similarities between *Draco* and *Coelurosauravus*, we suggest that weigeltisaurids were able to grasp, extend, hold, and to a certain degree manipulate the patagia during gliding flight, even if they could not reach the distal end of the leading edge (Fig. 16).

Interestingly, weigeltisaurids have an additional phalanx in manual digit V, as reported in *Rautiania*, *Weigeltisaurus* (Bulanov and Sennikov, 2010; Pritchard et al., 2021), and now in *Coelurosauravus* (Figs. 3, 4, 15). Their manual phalangeal formula is thus 2/3/4/5/4 instead

of the plesiomorphic 2/3/4/5/3 formula of amniotes (Romer, 1956). This is surprising in light of the extreme rarity of such occurrences of hyperphalangy in terrestrial amniotes (Greer, 1992; Russell and Bauer, 2008). Similar cases of hyperphalangy have been reported in a few gekkotan genera (Russell and Bauer, 1990, 2008), and a similar morphology can be attained in anurans by the addition of an intercalary bone between the penultimate and ungual phalanges (Greene, 1981; Paukstis and Brown, 1990; Manzano et al., 2007). However, in both cases, such hyperphalangy evolved in the context of an increase in adhesive surface, which is unlikely to have been the case in weigeltisaurids because of their larger size (see above).

However, the digit morphology of weigletisaurids follows the pattern known in extant tetrapods in adding a phalanx to digit V, the lateral-most digit (Greer, 1992; Fedak and Hall, 2004). This additional phalanx would increase the reach of the hand significantly in weigeltisaurids (Greer, 1992), which Bulanov and Sennikov (2010) interpreted as an adaptation to arboreal lifestyle that would have a negative effect on terrestrial locomotion.

We further suggest that the increase in reach by the lateral-most manual digit could facilitate the grasping of the leading edge of the wing and thus could have helped in controlling the expansion, tension, orientation and camber of the large patagia of weigeltisaurids. According to this interpretation, weigeltisaurids would represent the first known tetrapods to have evolved hyperphalangy in the context of aerial locomotion (Fedak and Hall, 2004).

The hindlimbs are involved during gliding in most extant gliding reptiles. They are often abducted, positioned at or slightly below the coronal plane of the animal, and bent at the knees so that the forelegs are oriented posteromedially (Emerson and Koehl, 1990; McGuire, 2003; Dehling, 2017). This posture has been proposed to increase stability (Emerson and Koehl, 1990). A similar behavior has been inferred for extinct paravians, which may have employed a biplane gliding apparatus (Longrich, 2006; Catterjee and Tremplin, 2007, but see

Padian and Dial, 2005; Dececchi and Larsson, 2011). As seen in MNHN.F.MAP327a, weigeltisaurids appear to have been capable of an extensive hind limb abduction (Figs. 5, 6). This is further supported by the triangular iliac blade of these animals, which would have provided a large origin area for the iliofemoral abductor muscle (Hutchinson, 2001; Russell and Bauer, 2008). The hind limbs of the *Coelurosauravus* lectotype also show a bended posture similar to that employed by extant gliders (Figs. 1, 2; Emerson and Koehl, 1990). Weigeltisaurids thus likely employed a gliding posture similar to that of the extant agamid *Draco* (Fig. 16).

Lastly, evidence from in situ forests suggests that late Pennsylvanian forests, while taxonomically and vertically heterogenous, had rather open canopy strata with spatially separated arborescent taxa resulting in little crown overlap (reviewed in DiMichele and Falcon-Lang, 2011, but see Opluštil et al., 2009, 2014). In contrast, Cisularian forests show evidence of denser communities, suggestive of more continuous canopy strata (Gulbranson et al., 2012; Wang et al., 2012; Luthardt et al., 2016), although less dense forests also occurred (Gulbranson et al., 2012; Opluštil et al., 2021). It could thus be argued that selective pressure for an aerial locomotion in a continuous canopy was minimal prior to the Cisularian, but this assumption requires further paleoecological studies, especially with respect to canopy density and continuity. However, such change in forest structure could explain why no gliders have been reported prior to weigeltisaurids although several arboreal or scansorial amniotes have been described from Pennsylvanian and Cisularian deposits (Spindler et al., 2018; Mann et al. 2021).

CONCLUSION

The detailed re-description of the postcranial skeleton of all known specimens of *Coelurosauravus elivensis* reveals hitherto unknown anatomical details. *C. elivensis* has a shorter neck and longer trunk than the weigeltisaurids from Western Europe (at least the Ellrich specimen). The re-examination of the osteology of these specimens yields new information for future phylogenetic and biomechanical analyses of weigeltisaurids. Weigeltisaurids have long been considered as arboreal, mostly in relation to their assumed gliding capacities, but this has only barely been discussed with respect to the non-patagial postcranium. However, the long, gracile and dorsoventrally compressed body of weigeltisaurids, as well as their almost equally long fore- and hindlimbs with elongate autopodia strongly support a clinging arboreal lifestyle for these animals.

Additionally, we describe a fourth phalanx in the fifth manual digit of *C. elivensis*, making it the third weigeltisaurid taxon showing this apomorphy. This supernumerary phalanx has previously been interpreted as feature to increase reach during tree climbing. We further suggest that the longer reach of digit V of the weigeltisaurid manus aligned with an apparent abduction ability, would have allowed these animals to grasp the leading edge of their patagia at the midpoint of their leading edges. The extant agamid *Draco*, which controls the expansion, orientation and camber of its wing in part through such a grasp, supports this assumption. The likely derivation of the patagial spars from the gastralia basket resulting in an attachment of the patagium below the center of gravity would have increased the maneuverability by destabilizing the flight. Stable flight could have been brought about by the dihedral angling of the patagia with the help of the arms. Thus, we suggest that weigeltisaurids were both the first known gliding tetrapods with an adjustable flight apparatus and among the first with an anatomically supported obligatory arboreal lifestyle. Furthermore, weigeltisaurid appear to represent the only known animals to have evolved hyperphalangy in the context of both climbing and gliding.

ACKNOWLEDGMENTS

We thank N.-E. Jalil (MNNH) for access to the MNHN specimens and constructive discussions on weigeltisaurids and Permo–Triassic amniotes. Many thanks to C. Letenneur (MNHN) for her life reconstruction of *Coelurosauravus*. Thanks also to D. M. Henderson (TMP) for his help in the examination of *Wapitisaurus*. We thank O. Béthoux (MNHN) for his help in RTI methodology and loaning the necessary hardware to V.B., and P. Loubry (CNRS) and D. Germain (MNHN) for their help in photography. We also thank J. Falconnet (MNHN), A. Pritchard (VMNH) and H.-D. Sues (NMNH) for constructive discussions on weigeltisaurids and Permo–Triassic reptiles. Finally, we thank X. Jenkins and an anonymous reviewer for their constructing reviews of the manuscript, and G. Bever and L. Leuzinger for their editorial work. This work is supported by the French Ministry of Superior Education and Research (annual credits of the CR2P and Ph.D. grant to V.B.).

DATA AVAILABILITY

The data underlying this article are available in Zenodo, at http://doi.org/10.5281/zenodo.6078599.

LITERATURE CITED

Alexander, R. M. 2013. Principles of Animal Locomotion. Princeton University Press, Prinston, NJ, 384 pp.

Anzai, W., A. Omura, A. C. Diaz, M. Kawata, and H. Endo. 2014. Functional morphology and comparative anatomy of appendicular musculature in Cuban Anolis lizards with different locomotor habits. Zoological Science 31:454–463.

Arnold, E. N. 1998. Structural niche, limb morphology and locomotion in lacertid lizards (Squamata, Lacertidae); a preliminary survey. Bulletin of the Natural History Museum (Zoology Series) 64:63–89.

Benton, M. J. 1985. Classification and phylogeny of the diapsid reptiles. Zoological Journal of the Linnean Society 84:97–164.

Benton, M. J. 2010. Studying function and behavior in the fossil record. PLoS Biology 8:e1000321.

Béthoux, O., A. Llamosi, and S. Toussaint. 2016. Reinvestigation of *Protelytron permianum* (Insecta; Early Permian; USA) as an example for applying reflectance transformation imaging to insect imprint fossils. Fossil Record 20:1–7.

Birn-Jeffery, A. V., C. E. Miller, D. Naish, E. J. Rayfield, and D. W. E. Hone. 2012. Pedal claw curvature in birds, lizards and Mesozoic dinosaurs – complicated categories and compensating for mass-specific and phylogenetic control. PLoS ONE 7:e50555.

Borsuk-Białynicka, M. 2018. Diversity of diapsid fifth metatarsals from the Lower Triassic karst deposits of Czatkowice, southern Poland—functional and phylogenetic implications. Acta Palaeontologica Polonica 63.

Boule, M. 1910. Sur le Permien de Madagascar. Bulletin de la Société Géologique de France 10:314–316.

Brinkman, D. 1979. The structural and functional evolution of the diapsid tarsus. Ph.D. dissertation, McGill University, Montreal, 328 pp.

Brinkman, D. 1988. A weigeltisaurid reptile from the Lower Triassic of British Columbia. Palaeontology 31:951–956.

Buffa, V., E. Frey, J.-S. Steyer, and M. Laurin. 2021. A new cranial reconstruction of *Coelurosauravus elivensis* Piveteau, 1926 (Diapsida, Weigeltisauridae) and its implications on the paleoecology of the first gliding vertebrates. Journal of Vertebrate Paleontology 0:e1930020.

Bulanov, V. V., and A. G. Sennikov. 2006. The first gliding reptiles from the Upper Permian of Russia. Paleontological Journal 40:S567–S570.

Bulanov, V. V., and A. G. Sennikov. 2010. New data on the morphology of Permian gliding weigeltisaurid reptiles of Eastern Europe. Paleontological Journal 44:682–694.

Bulanov, V. V., and A. G. Sennikov. 2015a. New data on the morphology of the Late Permian gliding reptile *Coelurosauravus elivensis* Piveteau. Paleontological Journal 49:413–423.

Bulanov, V. V., and A. G. Sennikov. 2015b. *Glaurung schneideri* gen. et sp. nov., a new weigeltisaurid (Reptilia) from the Kupfershiefer (Upper Permian) of Germany. Paleontological Journal 49:1353–1364.

Bulanov, V. V., and A. G. Sennikov. 2015c. Substantiation of validity of the Late Permian genus *Weigeltisaurus* Kuhn, 1939 (Reptilia, Weigeltisauridae). Paleontological Journal 49:1101–1111.

Caldwell, M. W. 1995. Developmental constraints and limb evolution in Permian and extant lepidosauromorph diapsids. Journal of Vertebrate Paleontology 14:459–471.

Campione, N. E., and R. R. Reisz. 2011. Morphology and evolutionary significance of the atlas-axis complex in varanopid synapsids. Acta Palaeontologica Polonica 56:739–748.

Carroll, R. L. 1975. Permo–Triassic "lizards" from the Karroo. Paleontologia Africana 18:71–87.

Carroll, R. L. 1977. The origin of lizards; pp. 359–396 in S. M. Andrews, R. S. Miles, and A. D. Walker (eds.), Problems in Vertebrate Evolution. Academic Press, London.

Carroll, R. L. 1978. Permo–Triassic "lizards" from the Karoo System. Part II. A gliding reptile from the Upper Permian of Madagascar. Paleontologia Africana 21:143–159.

Carroll, R. L. 1981. Plesiosaur ancestors from the Upper Permian of Madagascar. Philosophical Transactions of the Royal Society of London. Series B, Biological Sciences 293:315–383.

Cartmill, M. 1974. Pads and claws in arboreal locomotion. Primate Locomotion 1:43–83.

Cartmill, M. 1985. Climbing; pp. 73–88 in M. Hildebrand, D. M. Bramble, K. F. Liem, and D. B. Wake (eds.), Functional Vertebrate Morphology. Harvard University Press, Cambridge, MS.

Castiello, M., S. Renesto, and S. C. Bennett. 2016. The role of the forelimb in prey capture in the Late Triassic reptile *Megalancosaurus* (Diapsida, Drepanosauromorpha). Historical Biology 28:1090–1100.

Chatterjee, S., and R. J. Templin. 2007. Biplane wing planform and flight performance of the feathered dinosaur *Microraptor gui*. Proceedings of the National Academy of Sciences 104:1576–1580.

Claessens, L. P. A. M. 2004. Dinosaur gastralia; origin, morphology, and function. Journal of Vertebrate Paleontology 24:89–106.

Claessens, L. P. A. M., P. M. O'Connor, and D. M. Unwin. 2009. Respiratory evolution facilitated the origin of pterosaur flight and aerial gigantism. PLoS ONE 4:e4497.

Clark, J., C. Clark, and T. E. Higham. 2021. Tail control enhances gliding in arboreal lizards: an integrative study using a 3D geometric model and numerical simulation. Integrative and Comparative Biology 61:579–588.

Colbert, E. H. 1967. Adaptations for gliding in the lizard *Draco*. American Museum Novitates 2283:1–20.

Colbert, E. H. 1970. The Triassic gliding reptile *Icarosaurus*. Bulletin of the American Museum of Natural History 143:87–142.

Conrad, J. L. 2008. Phylogeny and systematics of Squamata (Reptilia) based on morphology. Bulletin of the American Museum of Natural History 310:1–182.

Cui, Y., S. Toussaint, and O. Béthoux. 2018. The systematic position of the stonefly †*culonga* Sinitshenkova, 2011 (Plecoptera: Leuctrida) reassessed using Reflectance Transforming Imaging and cladistic analysis. Arthropod Systematics & Phylogeny 72:173–178.

Currie, P. J. 1980. A new younginid (Reptilia: Eosuchia) from the Upper Permian of Madagascar. Canadian Journal of Earth Sciences 17:500–511.

Currie, P. J. 1981a. *Hovasaurus boulei*, an aquatic eosuchian from the Upper Permian of Madagascar. Paleontologia Africana 24:99–168.

Currie, P. J. 1981b. The vertebrae of *Youngina* (Reptilia: Eosuchia). Canadian Journal of Earth Sciences 18:815–818.

Currie, P. J., and R. L. Carroll. 1984. Ontogenetic changes in the eosuchian reptile *Thadeosaurus*. Journal of Vertebrate Paleontology 4:68–84.

D'Amore, D. C., S. Clulow, J. S. Doody, D. Rhind, and C. R. McHenry. 2018. Claw morphometrics in monitor lizards: variable substrate and habitat use correlate to shape diversity within a predator guild. Ecology and Evolution 8:6766–6778.

deBraga, M. 2003. The postcranial skeleton, phylogenetic position, and probable lifestyle of the Early Triassic reptile *Procolophon trigoniceps*. Canadian Journal of Earth Sciences 40:527–556.

deBraga, M., and O. Rieppel. 1997. Reptile phylogeny and the interrelationships of turtles. Zoological Journal of the Linnean Society 120:281–354.

Dececchi, T. A., and H. C. E. Larsson. 2011. Assessing arboreal adaptations of bird antecedents: testing the ecological setting of the origin of the avian flight stroke. PLoS ONE 6:e22292.

Dehling, J. M. 2017. How lizards fly: a novel type of wing in animals. PLoS ONE 12:e0189573.

Dilkes, D. W. 1998. The early Triassic rhynchosaur *Mesosuchus browni* and the interrelationships of basal archosauromorph reptiles. Philosophical Transactions of the Royal Society of London. Series B, Biological Sciences 353:501–541.

DiMichele, W. A., and H. J. Falcon-Lang. 2011. Pennsylvanian 'fossil forests' in growth position (T0 assemblages): origin, taphonomic bias and palaeoecological insights. Journal of the Geological Society 168:585–605.

Dudley, R., G. Byrnes, S. P. Yanoviak, B. Borrell, R. M. Brown, and J. A. McGuire. 2007. Gliding and the functional origins of flight: biomechanical novelty or necessity? Annual Review of Ecology, Evolution, and Systematics 38:179–201.

Emerson, S. B., and M. a. R. Koehl. 1990. The interaction of behavioral and morphological change in the evolution of a novel locomotor type: "flying" frogs. Evolution 44:1931–1946.

Evans, S. E. 1982. The gliding reptiles of the Upper Permian. Zoological Journal of the Linnean Society 76:97–123.

Evans, S. E., and H. Haubold. 1987. A review of the Upper Permian genera *Coelurosauravus*, *Weigeltisaurus* and *Gracilisaurus* (Reptilia: Diapsida). Zoological Journal of the Linnean Society 90:275–303.

Evans, S. E., and L. J. Barbadillo. 1998. An unusual lizard (Reptilia: Squamata) from the Early Cretaceous of Las Hoyas, Spain. Zoological Journal of the Linnean Society 124:235–265.

Ezcurra, M. D., T. M. Scheyer, and R. J. Butler. 2014. The origin and early evolution of Sauria: reassessing the Permian saurian fossil record and the timing of the crocodile-lizard divergence. PLoS ONE 9:e89165.

Fedak, T. J., and B. K. Hall. 2004. Perspectives on hyperphalangy: patterns and processes. Journal of Anatomy 204:151–163.

Feduccia, A. 1993. Evidence from claw geometry indicating arboreal habits of *Archaeopteryx*. Science 259:790–793.

Fleming, P. A., and P. W. Bateman. 2012. Autotomy, tail regeneration and jumping ability in Cape dwarf geckos (*Lygodactylus capensis*) (Gekkonidae). African Zoology 47:55–59.

Ford, D. P., and R. B. J. Benson. 2020. The phylogeny of early amniotes and the affinities of Parareptilia and Varanopidae. Nature Ecology & Evolution 4:57–65.

Frey, E., H.-D. Sues, and W. Munk. 1997. Gliding mechanism in the Late Permian reptile *Coelurosauravus*. Science 275:1450–1452.

Frey, E., M.-C. Buchy, and D. M. Martill. 2003. Middle- and bottom-decker Cretaceous pterosaurs: unique designs in active flying vertebrates. Geological Society Special Publications 217:267–274.

Fröbisch, J., and R. R. Reisz. 2009. The Late Permian herbivore *Suminia* and the early evolution of arboreality in terrestrial vertebrate ecosystems. Proceedings of the Royal Society B: Biological Sciences 276:3611–3618.

Gauthier, J. A., M. Kearney, J. A. Maisano, O. Rieppel, and A. D. Behlke. 2012. Assembling the squamate Tree of Life: perspectives from the phenotype and the fossil record. Bulletin of the Peabody Museum of Natural History 53:3–308.

Gillis, G., and T. E. Higham. 2016. Consequences of lost endings: caudal autotomy as a lens for focusing attention on tail function during locomotion. Journal of Experimental Biology 219:2416–2422.

Gillis, G. B., L. A. Bonvini, and D. J. Irschick. 2009. Losing stability: tail loss and jumping in the arboreal lizard *Anolis carolinensis*. Journal of Experimental Biology 212:604–609.

Gottmann-Quesada, A., and P. M. Sander. 2009. A redescription of the early archosauromorph *Protorosaurus speneri* Meyer, 1832, and its phylogenetic relationships. Palaeontographica Abteilung A 287:123–220.

Gould, S. J. 1974. The origin and function of "bizarre" structures: antler size and skull size in the "Irish Elk," *Megaloceros giganteus*. Evolution 28:191–220.

Gow, C. E. 1972. The osteology and relationships of the Millerettidae (Reptilia: Cotylosauria). Journal of Zoology 167:219–264.

Gow, C. E. 1975. The morphology and relationships of *Youngina capensis* Broom and *Prolacerta broomi* Parrington. Paleontologia Africana 89–131.

Graham, M., and J. J. Socha. 2020. Going the distance: the biomechanics of gap-crossing behaviors. Journal of Experimental Zoology Part A: Ecological and Integrative Physiology 333:60–73.

Green, D. M. 1981. Adhesion and the toe-pads of treefrogs. Copeia 1981:790–796.

Greer, A. E. 1992. Hyperphalangy in squamates: insight on the reacquisition of primitive character states in limb-reduced lineages. Journal of Herpetology 26:327–329.

Griffin, C. T., M. R. Stocker, C. Colleary, C. M. Stefanic, E. J. Lessner, M. Riegler, K. Formoso, K. Koeller, and S. J. Nesbitt. 2021. Assessing ontogenetic maturity in extinct saurian reptiles. Biological Reviews 96:470–525.

Griffiths, E. F., D. P. Ford, R. B. J. Benson, and S. E. Evans. 2021. New information on the Jurassic lepidosauromorph *Marmoretta oxoniensis*. Papers in Palaeontology 7:2255–2278.

Grinham, L. R., and D. B. Norman. 2020. The pelvis as an anatomical indicator for facultative bipedality and substrate use in lepidosaurs. Biological Journal of the Linnean Society 129:398–413.

Gulbranson, E. L., J. L. Isbell, E. L. Taylor, P. E. Ryberg, T. N. Taylor, and P. P. Flaig. 2012. Permian polar forests: deciduousness and environmental variation. Geobiology 10:479–495.

Günther, A. 1867. Contribution to the anatomy of *Hatteria* (*Rhynchocephalus*, Owen). Philosophical Transactions of the Royal Society of London 157:595–629.

Hammer, Ø., S. Bengtson, T. Malzbender, and D. Gelb. 2002. Imaging fossils using reflectance transforation and interactive manipulation of virtual light sources. Palaeontologia Electronica 5:1–9.

Hankel, O. 1994. Early Permian to Middle Jurassic rifting and sedimentation in East Africa and Madagascar. Geologische Rundschau 83:703–710.

Higham, T. E., and B. C. Jayne. 2004. Locomotion of lizards on inclines and perches: hindlimb kinematics of an arboreal specialist and a terrestrial generalist. Journal of Experimental Biology 207:233–248.

Higham, T. E., M. S. Davenport, and B. C. Jayne. 2001. Maneuvering in an arboreal habitat: the effects of turning angle on the locomotion of three sympatric ecomorphs of *Anolis* lizards. Journal of Experimental Biology 204:4141–4155.

Hildebrand, M., and G. E. Goslow. 2001. Analysis of Vertebrate Structure, 5th ed. John Wiley & Sons, New York, NY, 656 pp.

Hoffstetter, R., and J.-P. Gasc. 1969. Vertebrae and ribs of modern reptiles; pp. 201–310 in C. Gans, A. d'A. Bellairs, and T. S. Parsons (eds.), Biology of the Reptilia. Volume 1. Morphology A. Academic Press, New York, NY.

Holmes, R. 1977. The osteology and musculature of the pectoral limb of small captorhinids. Journal of Morphology 152:101–140.

Holmes, R. B. 2003. The hind limb of *Captorhinus aguti* and the step cycle of basal amniotes. Canadian Journal of Earth Sciences 40:515–526.

Hone, D. W. E., and C. G. Faulkes. 2014. A proposed framework for establishing and evaluating hypotheses about the behaviour of extinct organisms. Journal of Zoology 292:260–267.

Howes, G. B., and H. H. Swinnerton. 1901. On the development of the skeleton of the tuatara, *Sphenodon punctatus*; with remarks on the egg, on the hatching, and on the hatched young. Transactions of the Zoological Society of London 16:1–84.

Huene, F. R. von. 1930. *Palaeochameleo* und *Coelurosauravus*. Centralblatt für Geologie und Paläontologie (B) 440–441.

Huene, F. R. von. 1956. Paläontologie und Phylogenie der Niederen Tetrapoden. VEB Gustav Fischer Verlag, Jena, 716 pp.

Hutchinson, J. R. 2001. The evolution of pelvic osteology and soft tissues on the line to extant birds (Neornithes). Zoological Journal of the Linnean Society 131:123–168.

Jenkins, X. A., A. C. Pritchard, A. D. Marsh, B. T. Kligman, C. A. Sidor, and K. E. Reed. 2020. Using manual ungual morphology to predict substrate use in the Drepanosauromorpha and the description of a new species. Journal of Vertebrate Paleontology 40:e1810058.

John, K. O. 1970. On the 'patagial musculature' of the South Indian flying lizard *Draco dussumieri* Dum and Bib. British Journal of Herpetology 4:161–168.

John, K. O. 1971. Caudal musculature of the South Indian flying lizard *Draco dussumieri* Dum. and Bib. Acta Zoologica 52:249–255.

Jusufi, A., D. I. Goldman, S. Revzen, and R. J. Full. 2008. Active tails enhance arboreal acrobatics in geckos. Proceedings of the National Academy of Sciences 105:4215–4219.

Jusufi, A., D. T. Kawano, T. Libby, and R. J. Full. 2010. Righting and turning in mid-air using appendage inertia: reptile tails, analytical models and bio-inspired robots. Bioinspiration & Biomimetics 5:045001.

Jusufi, A., Y. Zeng, R. J. Full, and R. Dudley. 2011. Aerial righting reflexes in flightless animals. Integrative and Comparative Biology 51:937–943.

Kuhn, O. 1939. Schädelbau und systematische Stellung von *Weigeltisaurus*. Paläontologische Zeitschrift 21:163–167.

Kuo, C.-Y., G. B. Gillis, and D. J. Irschick. 2012. Take this broken tail and learn to jump: the ability to recover from reduced in-air stability in tailless green anole lizards [*Anolis*

carolinensis (Squamata: Dactyloidae)]. Biological Journal of the Linnean Society 107:583–592.

Labonte, D., C. J. Clemente, A. Dittrich, C.-Y. Kuo, A. J. Crosby, D. J. Irschick, and W. Federle. 2016. Extreme positive allometry of animal adhesive pads and the size limits of adhesion-based climbing. Proceedings of the National Academy of Sciences 113:1297–1302.

Lammers, A., and U. Zurcher. 2011. Stability During Arboreal Locomotion; pp. 319–334 in V. Klika (ed.), Theoretical Biomechanics. IntechOpen Limited, London.

Larson, S. G., and J. T. Stern. 2006. Maintenance of above-branch balance during primate arboreal quadrupedalism: Coordinated use of forearm rotators and tail motion. American Journal of Physical Anthropology 129:71–81.

Laurin, M. 1991. The osteology of a Lower Permian eosuchian from Texas and a review of diapsid phylogeny. Zoological Journal of the Linnean Society 101:59–95.

Libby, T., T. Y. Moore, E. Chang-Siu, D. Li, D. J. Cohen, A. Jusufi, and R. J. Full. 2012. Tail-assisted pitch control in lizards, robots and dinosaurs. Nature 481:181–184.

Longrich, N. 2006. Structure and function of hindlimb feathers in *Archaeopteryx lithographica*. Paleobiology 32:417–431.

Lucas, S. G. 2017. Permian tetrapod biochronology, correlation and evolutionary events. Geological Society, London, Special Publications 450:405–444.

Luthardt, L., R. Rößler, and J. W. Schneider. 2016. Palaeoclimatic and site-specific conditions in the early Permian fossil forest of Chemnitz—sedimentological, geochemical and palaeobotanical evidence. Palaeogeography, Palaeoclimatology, Palaeoecology 441:627–652.

Mann, A., T. W. Dudgeon, A. C. Henrici, D. S. Berman, and S. E. Pierce. 2021. Digit and ungual morphology suggest adaptations for scansoriality in the Late Carboniferous eureptile *Anthracodromeus longipes*. Frontiers in Earth Science 9:675337.

Manzano, A. S., M. Fabrezi, and M. Vences. 2007. Intercalary elements, treefrogs, and the early differentiation of a complex system in the Neobatrachia. The Anatomical Record 290:1551–1567.

McGuire, J. A. 2003. Allometric prediction of locomotor performance: an example from Southeast Asian flying lizards. The American Naturalist 161:337–349.

McGuire, J. A., and R. Dudley. 2011. The Biology of Gliding in Flying Lizards (Genus *Draco*) and their Fossil and Extant Analogs. Integrative and Comparative Biology 51:983–990.

Merck, J. 2003. An arboreal radiation of non-saurian diapsids. Journal of Vertebrate Paleontology 23:78A.

Miedema, F., S. N. F. Spiekman, V. Fernandez, J. W. F. Reumer, and T. M. Scheyer. 2020. Cranial morphology of the tanystropheid *Macrocnemus bassanii* unveiled using synchrotron microtomography. Scientific Reports 10:12412.

Müller, J. 2004. The relationships among diapsid reptiles and the influence of taxon selection; pp. 379–408 in M. V. H. Arratia and R. Cloutier (eds.), Recent Advances in the Origin and Early Radiation of Vertebrates. Dr. Friedrich Pfeil, München.

Müller, J., T. M. Scheyer, J. J. Head, P. M. Barrett, I. Werneburg, P. G. P. Ericson, D. Pol, and M. R. Sánchez-Villagra. 2010. Homeotic effects, somitogenesis and the evolution of vertebral numbers in recent and fossil amniotes. Proceedings of the National Academy of Sciences 107:2118–2123.

Nesbitt, S. J. 2011. The early evolution of archosaurs: relationships and the origin of major clades. Bulletin of the American Museum of Natural History 352:1–292.

Nesbitt, S. J., J. J. Flynn, A. C. Pritchard, J. M. Parrish, L. Ranivoharimanana, and A. R. Wyss. 2015. Postcranial osteology of *Azendohsaurus madagaskarensis* (?Middle to Upper Triassic, Isalo Group, Madagascar) and its systematic position among stem archosaur reptiles. Bulletin of the American Museum of Natural History 398:1–126.

Nosotti, S. 2007. *Tanystropheus Longobardicus* (Reptilia, Protorosauria): re-interpretations of the anatomy based on new specimens from the Middle Triassic of Besano (Lombardy, Northern Italy). Memorie Della Società Italiana Di Scienze Naturali e Del Museo Civico Di Storia Naturale Di Milano 35:1–88.

O'Brien, A., D. I. Whiteside, and J. E. A. Marshall. 2018. Anatomical study of two previously undescribed specimens of *Clevosaurus hudsoni* (Lepidosauria: Rhynchocephalia) from Cromhall Quarry, UK, aided by computed tomography, yields additional information on the skeleton and hitherto undescribed bones. Zoological Journal of the Linnean Society 183:163–195.

Opluštil, S., J. Pšenička, J. Bek, J. Wang, Z. Feng, M. Libertín, Z. Šimůnek, J. Bureš, and J. Drábková. 2014. T0 peat-forming plant assemblage preserved in growth position by volcanic ash-fall: a case study from the Middle Pennsylvanian of the Czech Republic. Bulletin of Geosciences 89.

Opluštil, S., J. Pšenička, M. Libertín, A. R. Bashforth, Z. Šimůnek, J. Drábková, and J. Dašková. 2009. A Middle Pennsylvanian (Bolsovian) peat-forming forest preserved in situ in volcanic ash of the Whetstone Horizon in the Radnice Basin, Czech Republic. Review of Palaeobotany and Palynology 155:234–274.

Opluštil, S., J. Wang, H. W. Pfefferkorn, J. Pšenička, J. Bek, M. Libertín, J. Wang, M. Wan, X. He, M. Yan, H. Wei, and J. Votočková Frojdová. 2021. T0 Early Permian coal-forest preserved in situ in volcanic ash bed in the Wuda Coalfield, Inner Mongolia, China. Review of Palaeobotany and Palynology 294:104347.

Padian, K., and K. P. Dial. 2005. Could 'four-winged' dinosaurs fly? Nature 438:E3–E3.

Padian, K., and J. R. Horner. 2011. The evolution of 'bizarre structures' in dinosaurs: biomechanics, sexual selection, social selection or species recognition? Journal of Zoology 283:3–17.

Paparella, I., A. R. H. LeBlanc, M. R. Doschak, and M. W. Caldwell. 2020. The iliosacral joint in lizards: an osteological and histological analysis. Journal of Anatomy 236:668–687.

Paukstis, G. L., and L. E. Brown. 1990. Evolutionary trends in the morphology of the intercalary phalanx of anuran amphibians. Canadian Journal of Zoology 69:1297–1301.

Pawley, K. A. T., and A. Warren. 2006. The appendicular skeleton of *Eryops megacephalus* Cope, 1877 (Temnospondyli: Eryopoidea) from the lower Permian of North America. Journal of Paleontology 80:561–580.

Peabody, F. E. 1952. *Petrolacosaurus kansensis* Lane, a Pennsylvanian reptile from Kansas. University of Kansas Paleontological Contributions, Vertebrata 1:1–41.

Persons, S. W. IV., and P. J. Currie. 2012. Dragon tails: convergent caudal morphology in winged archosaurs. Acta Geologica Sinica (English Edition) 86:1402–1412.

Persons, S. W. IV., P. J. Currie, and M. A. Norell. 2013. Oviraptorosaur tail forms and functions. Acta Palaeontologica Polonica 59:553–567.

Piñeiro, G., P. Núñez Demarco, and M. D. Meneghel. 2016. The ontogenetic transformation of the mesosaurid tarsus: a contribution to the origin of the primitive amniotic astragalus. PeerJ 4:e2036.

Pittman, M., S. M. Gatesy, P. Upchurch, A. Goswami, and J. R. Hutchinson. 2013. Shake a tail feather: the evolution of the theropod tail into a stiff aerodynamic surface. PLoS ONE 8:e63115.

Piveteau, J. 1926. Paléontologie de Madagascar: XII. amphibiens et reptiles Permiens. Annales de Paléontologie 1–151.

Pritchard, A. C., and H.-D. Sues. 2019. Postcranial remains of *Teraterpeton hrynewichorum* (Reptilia: Archosauromorpha) and the mosaic evolution of the saurian postcranial skeleton. Journal of Systematic Palaeontology 17:1745–1765.

Pritchard, A. C., H.-D. Sues, D. Scott, and R. R. Reisz. 2021. Osteology, relationships and functional morphology of *Weigeltisaurus jaekeli* (Diapsida, Weigeltisauridae) based on a complete skeleton from the Upper Permian Kupferschiefer of Germany. PeerJ 9:e11413.

Pritchard, A. C., A. H. Turner, S. J. Nesbitt, R. B. Irmis, and N. D. Smith. 2015. Late Triassic tanystropheids (Reptilia, Archosauromorpha) from northern New Mexico (Petrified Forest Member, Chinle Formation) and the biogeography, functional morphology, and evolution of Tanystropheidae. Journal of Vertebrate Paleontology 35:e911186.

Pritchard, A. C., A. H. Turner, R. B. Irmis, S. J. Nesbitt, and N. D. Smith. 2016. Extreme modification of the tetrapod forelimb in a Triassic diapsid reptile. Current Biology 26:2779–2786.

Reisz, R. R. 1981. A diapsid reptile from the Pennsylvanian of Kansas. Special Publication of the Museum of Natural History, University of Kansas 7:1–74.

Reisz, R. R., D. S. Berman, and D. Scott. 1984. The anatomy and relationships of the Lower Permian reptile *Araeoscelis*. Journal of Vertebrate Paleontology 4:57–67.

Reisz, R. R., S. P. Modesto, and D. M. Scott. 2011a. A new Early Permian reptile and its significance in early diapsid evolution. Proceedings of the Royal Society B: Biological Sciences 278:3731–3737.

Reisz, R. R., H. C. Maddin, J. Fröbisch, and J. Falconnet. 2011b. A new large caseid (Synapsida, Caseasauria) from the Permian of Rodez (France), including a reappraisal of "*Casea*" *rutena* Sigogneau-Russell & Russell, 1974. Geodiversitas 33:227–246.

Renesto, S., and N. C. Fraser. 2003. Drepanosaurid (Reptilia: Diapsida) remains from a Late Triassic fissure infilling at Cromhall Quarry (Avon, Great Britain). Journal of Vertebrate Paleontology 23:703–705.

Renesto, S., J. A. Spielmann, S. G. Lucas, and G. T. Spagnoli. 2010. The taxonomy and paleobiology of the Late Triassic (Carnian–Norian: Adamanian–Apachean) drepanosaurs

(Diapsida: Archosauromorpha: Drepanosauromorpha). New Mexico Museum of Natural History and Science Bulletin 46:1–81.

Romer, A. S. 1922. The locomotor apparatus of certain primitive and mammal-like reptiles. Bulletin of the American Museum of Natural History 40:517–606.

Romer, A. S. 1956. Osteology of the Reptiles, 3rd ed. University of Chicago Press, Chicago, IL, 772 pp.

Romer, A. S., and L. I. Price. 1940. Review of the Pelycosauria. Geological Society of America, Special Papers 28:1–538.

Russell, A. P., and A. M. Bauer. 1990. Digit I in pad-bearing gekkonine geckos: alternate designs and the potential constraints of phalangeal number. Memoirs of the Queensland Museum 29:453–472.

Russell, A. P., and A. M. Bauer. 2008. The appendicular locomotor apparatus of *Sphenodon* and Normal-limbed Squamates; pp. 1–465 in C. Gans, A. S. Gaunt, and K. Adler (eds.), Biology of the Reptilia, Volume 21, Morphology I. The Skull and Appendicular Locomotor Apparatus of Lepidosauria. Society for the Study of Amphibians and Reptiles, Ithaca, New York.

Russell, A. P., and L. D. Dijkstra. 2001. Patagial morphology of *Draco volans* (Reptilia: Agamidae) and the origin of glissant locomotion in flying dragons. Journal of Zoology 253:457–471.

Russell, A. P., A. Y. Stark, and T. E. Higham. 2019. The integrative biology of gecko adhesion: historical review, current understanding, and grand challenges. Integrative and Comparative Biology 59:101–116.

Schaumberg, G. 1976. Zwei Reptilneufunde (*Weigeltisaurus* Kuhn [?], Lepidosauria [?], Reptilia) aus dem Kupferschiefer von Richelsdorf (Perm, Hessen). Philippia 3:3–8. [German 3–8; English 3]

Schaumberg, G. 1986. Bemerkungen zu einem Neufund von *Weigeltisaurus jaekeli* (Weigelt) im nordhessischen Kupferschiefer. Paläontologische Zeitschrift 60:319–327. [German 319–327; English 319]

Schaumberg, G., D. M. Unwin, and S. Brandt. 2007. New information on the anatomy of the Late Permian gliding reptile *Coelurosauravus*. Paläontologische Zeitschrift 81:160–173.

Schmidt, A., and M. S. Fischer. 2011. The kinematic consequences of locomotion on sloped arboreal substrates in a generalized (*Rattus norvegicus*) and a specialized (*Sciurus vulgaris*) rodent. Journal of Experimental Biology 214:2544–2559.

Schoch, R. R., and H.-D. Sues. 2018. Osteology of the Middle Triassic stem-turtle *Pappochelys rosinae* and the early evolution of the turtle skeleton. Journal of Systematic Palaeontology 16:927–965.

Sennikov, A. G., and V. K. Golubev. 2017. Sequence of Permian tetrapod faunas of Eastern Europe and the Permian–Triassic ecological crisis. Paleontological Journal 51:600–611.

Senter, P. 2004. Phylogeny of Drepanosauridae (Reptilia: Diapsida). Journal of Systematic Palaeontology 2:257–268.

Simões, T. R., M. W. Caldwell, and A. W. A. Kellner. 2015. A new Early Cretaceous lizard species from Brazil, and the phylogenetic position of the oldest known South American squamates. Journal of Systematic Palaeontology 13:601–614.

Simões, T. R., M. W. Caldwell, R. L. Nydam, and P. Jiménez-Huidobro. 2017. Osteology, phylogeny, and functional morphology of two Jurassic lizard species and the early evolution of scansoriality in geckoes. Zoological Journal of the Linnean Society 180:216–241.

Smith, R. M. H. 2020. Biostratigraphy of the *Cistecephalus* Assemblage Zone (Beaufort Group, Karoo Supergroup), South Africa. South African Journal of Geology 123:181–190.

Smith, R. M. H., and S. E. Evans. 1996. New material of *Youngina*: evidence of juvenile aggregation in Permian diapsid reptiles. Palaeontology 39:289–304.

Sobral, G., T. R. Simões, and R. R. Schoch. 2020. A tiny new Middle Triassic stem-lepidosauromorph from Germany: implications for the early evolution of lepidosauromorphs and the Vellberg fauna. Scientific Reports 10:2273.

Socha, J. J., F. Jafari, Y. Munk, and G. Byrnes. 2015. How animals glide: from trajectory to morphology. Canadian Journal of Zoology 93:901–924.

Spielmann, J. A., A. B. Heckert, and S. G. Lucas. 2005. The Late Triassic archosauromorph *Trilophosaurus* as an arboreal climber. Rivista Italiana Di Paleontologia e Stratigrafia 111:395–412.

Spielmann, J. A., S. Renesto, and S. G. Lucas. 2006. The utility of claw curvature in assessing the arboreality of fossil reptiles. New Mexico Museum of Natural History and Science Bulletin 37:365–368.

Spielmann, J. A., S. G. Lucas, L. F. Rhinehart, and A. B. Heckert. 2008. The Late Triassic archosauromorph *Trilophosaurus*. New Mexico Museum of Natural History and Science Bulletin 43:1–177.

Spindler, F., R. Werneburg, J. W. Schneider, L. Luthardt, V. Annacker, and R. Rößler. 2018. First arboreal "pelycosaurs" (Synapsida: Varanopidae) from the early Permian Chemnitz Fossil Lagerstätte, SE Germany, with a review of varanopid phylogeny. PalZ 92:315–364.

Sues, H.-D. 2019. The Rise of Reptiles: 320 Million Years of Evolution. Johns Hopkins University Press, Baltimore, MD, 401 pp.

Sumida, S. S. 1990. Vertebral morphology, alternation of neural spine height, and structure in Permo–Carboniferous tetrapods, and a reappraisal of primitive modes of terrestrial locomotion. University of California Publications, Zoology 122:1–129.

Sumida, S. S., and S. Modesto. 2001. A phylogenetic perspective on locomotory strategies in early amniotes. Integrative and Comparative Biology 41:586–597.

Sumida, S. S., R. E. Lombard, and D. S. Berman. 1992. Morphology of the atlas-axis complex of the late Palaeozoic tetrapod suborders Diadectomorpha and Seymouriamorpha. Philosophical Transactions of the Royal Society of London. Series B, Biological Sciences 336:259–273.

Tinius, A., A. P. Russell, H. A. Jamniczky, and J. S. Anderson. 2018. What is bred in the bone: ecomorphological associations of pelvic girdle form in greater Antillean *Anolis* lizards. Journal of Morphology 279:1016–1030.

Tschopp, E., and O. Mateus. 2013. Clavicles, interclavicles, gastralia, and sternal ribs in sauropod dinosaurs: new reports from Diplodocidae and their morphological, functional and evolutionary implications. Journal of Anatomy 222:321–340.

Tulli, M. J., F. B. Cruz, A. Herrel, B. Vanhooydonck, and V. Abdala. 2009. The interplay between claw morphology and microhabitat use in neotropical iguanian lizards. Zoology 112:379–392.

Vaughn, P. P. 1955. The Permian reptile *Araeoscelis* restudied. Bulletin of the Museum of Comparative Zoology 113:1–467.

Vickaryous, M. K., and B. K. Hall. 2008. Development of the dermal skeleton in *Alligator mississippiensis* (Archosauria, Crocodylia) with comments on the homology of osteoderms. Journal of Morphology 269:398–422.

Vickaryous, M. K., and B. K. Hall. 2010. Comparative development of the crocodylian interclavicle and avian furcula, with comments on the homology of dermal elements in the pectoral apparatus. Journal of Experimental Zoology Part B: Molecular and Developmental Evolution 314B:196–207.

Wang, J., H. W. Pfefferkorn, Y. Zhang, and Z. Feng. 2012. Permian vegetational Pompeii from Inner Mongolia and its implications for landscape paleoecology and paleobiogeography of Cathaysia. Proceedings of the National Academy of Sciences 109:4927–4932.

Weigelt, J. 1930. *Palaeochamaeleo jaekeli* nov. gen. nov. sp. Ein neuer Rhynchocephale aus dem Mansfelder Kupfer schiefer. Leopoldina 6:625–642.

Wilson, J. A. 1999. A nomenclature for vertebral laminae in sauropods and other saurischian dinosaurs. Journal of Vertebrate Paleontology 19:639–653.

Witzmann, F. 2007. The evolution of the scalation pattern in temnospondyl amphibians. Zoological Journal of the Linnean Society 150:815–834.

Zaaf, A., A. Herrel, P. Aerts, and F. De Vree. 1999. Morphology and morphometrics of the appendicular musculature in geckoes with different locomotor habits (Lepidosauria). Zoomorphology 119:9–22.

Zani, P. A. 2000. The comparative evolution of lizard claw and toe morphology and clinging performance. Journal of Evolutionary Biology 13:316–325.

Zanon, R. T. 1990. The sternum of *Araeoscelis* and its implications for basal diapsid phylogeny. Journal of Vertebrate Paleontology 10:51A.

Submitted February 15, 2022; revisions received Month DD, YYYY; accepted Month DD, YYYY. [dates left blank, to be completed by the editors]

FIGURE CAPTIONS

FIGURE 1. *Coelurosauravus elivensis* Piveteau, 1926 (Madagascar, late? Permian), lectotype MNHN.F.MAP325a. **A**, dorsal surface of individual preserved as a natural external mold; **B**, silicone cast of A. Scale bar equals 5 cm. [planned for page width]

FIGURE 2. *Coelurosauravus elivensis* Piveteau, 1926 (Madagascar, late? Permian), lectotype MNHN.F.MAP325a. Interpretative drawing of dorsal surface of individual preserved as a natural external mold. **Abbreviations**: **carp**, carpal elements; **ch**, chevron; **cv**, cervical vertebra; **ct**, cleithrum; **dv**, dorsal vertebra; **ect.f**, ectepicondylar foramen; **ent.f**, entepicondylar foramen; **fe**, femur; **fi**, fibula; **gas**, gastralia; **gl**, glenoid; **hu**, humerus; **il**, ilium; **is**, ischium; **Mtt**, metatarsus; **pata**, patagial spar; **ph**, phalanx; **pub**, pubis; **ra**, radius; **scc**, scapulocoracoid; **sk**, skull; **tars**, tarsal elements; **ti**, tibia; **ul**, ulna. Scale bar equals 5 cm. [planned for column]

FIGURE 3. *Coelurosauravus elivensis* Piveteau, 1926 (Madagascar, late? Permian), paralectotypes MNHN.F.MAP317a, b. **A**, MNHN.F.MAP317b, dorsal surface of individual preserved as a natural mold; **B**, silicone cast of A; **C**, MNHN.F.MAP317a, ventral surface of individual preserved as a natural mold; **D**, silicone cast of C. Scale bar equals 5 cm. [planned for page width]

FIGURE 4. *Coelurosauravus elivensis* Piveteau, 1926 (Madagascar, late? Permian), paralectotypes MNHN.F.MAP317a, b. **A**, interpretative drawing of MNHN.F.MAP317b, dorsal surface of individual preserved as a natural mold; **B**, interpretative drawing of MNHN.F.MAP317b, dorsal surface of individual preserved as a natural mold. **Abbreviations**: **carp**, carpal elements; **cl**, clavicle; **ct**, cleithrum; **cv**, cervical vertebra; **dv**, dorsal vertebra; **ect.f**, ectepicondylar foramen; **ent.f**, entepicondylar foramen; **gas**, gastralia;

hu, humerus; **Mtc**, metacarpal; **ol**, olecranon process of ulna; **pata**, patagial spar; **ph**, phalanx (digit number in brackets when known); **ra**, radius; **scc**, scapulocoracoid; **sk**, skull; **ul**, ulna. Scale bar equals 5 cm. [planned for page width]

FIGURE 5. *Coelurosauravus elivensis* Piveteau, 1926 (Madagascar, late? Permian) MNHN.F.MAP327a. **A**, right lateral surface of individual preserved as a natural external mold; **B**, silicone cast of A. Scale bar equals 10 cm. [planned for page width]

FIGURE 6. *Coelurosauravus elivensis* Piveteau, 1926 (Madagascar, late? Permian) MNHN.F.MAP327a. Interpretative drawing of right lateral surface of individual preserved as a natural external mold. **Abbreviations**: **carp**, carpal elements; **cdv**, caudal vertebra; **cl**, clavicle; **ct**, cleithrum; **cv**, cervical vertebra; **dv**, dorsal vertebra; **fe**, femur; **gas**, gastralia; **hu**, humerus; **il**, ilium; **Mtc**, metacarpus; **pa**, parietal; **pata**, patagial spar; **ph**, phalanx; **pob**, postorbital; **pub**, pubis; **ra**, radius; **scc**, scapulocoracoid; **sk**, skull elements; **sq**, squamosal; **sv**, sacral vertebra; **tars**, tarsal elements; **ti**, tibia; **tvp**, transverse process of dorsal vertebra; **ul**, ulna. Scale bar equals 10 cm. [planned for page width]

FIGURE 7. *Coelurosauravus elivensis* Piveteau, 1926 (Madagascar, late? Permian) MNHN.F.MAP327b. **A**, left lateral surface of individual preserved as a natural external mold; **B**, silicone cast of A. **Abbreviations**: **cdv**, caudal vertebra; **pata**, patagial spar; **sk**, skull elements. Scale bar equals 10 cm. [planned for page width]

FIGURE 8. *Coelurosauravus elivensis* Piveteau, 1926 (Madagascar, late? Permian), presacral vertebrae. **A**, **B**, last cervicals and first dorsals of MNHN.F.MAP327a in right lateral view, silicone cast (A) and interpretative drawing (B) of individual preserved as a natural external mold; **C**–**E**, atlas-axis complex of paralectotype MNHN.F.MAP317a in right lateral view, silicone cast (C), interpretative drawing (D) and reconstruction (E) of individual preserved as a natural external mold; **F**–**K**, presacral vertebrae of paralectotype MNHN.F.MAP317a in

right lateral view, silicone cast and interpretative drawing of cervical 3 (F) and dorsals 2 and 3 (G), 6 (H), 10 (I), 16 (J), 18 (K). **Abbreviations**: **atc**, atlantal centrum; **ati**, atlantal intercentrum; **atn**, atlantal neural arch; **axi**, axial intercentrum; **axn**, axial neural spine; **axr**, axial rib; **ca**, capitulum; **cv**, cervical vertebra; **cvr**, cervical rib; **dia**, diapophysis; **dr**, dorsal rib; **dv**, dorsal vertebra; **exc**, excavation; **exo**, exoccipital; **nc**, notochordal canal; **ns**, neural spine; **para**, parapophysis; **pcdl**, posterior centrodiapophyseal lamina; **poa**, proatlas; **poz**, postzygapophysis; **ppdl**, paradiapophyseal lamina; **prdl**, prezygodiapophyseal lamina; **prz**, prezygodiapophysis; **sc.f**, subcentral foramen; **tu**, tuberculum; **tvp**, transverse process. Arrows indicate anterior direction. Scale bars equal 5 mm (A–E) and 2 mm (F–K). [planned for page width]

FIGURE 9. *Coelurosauravus elivensis* Piveteau, 1926 (Madagascar, late? Permian), MNHN.F.MAP327a, b, right pelvis, sacral and caudal vertebrae in right lateral view, individual preserved as a natural external mold. **A**, **B**, sacrum and right pelvis of MNHN.F.MAP327a, right lateral view; **C**, **D**, caudals 1 to 5 of MNHN.F.MAP327a, right lateral view; **E**, **F**, caudals 13 to 15 of MNHN.FMAP327b, left lateral view. Silicone casts (A, C, E) and interpretive drawings (B, D, F). **Abbreviations**: **ac**, acetabulum; **cdv**, caudal vertebra; **ch**, chevron; **ch.ap**, anterior process of chevron; **dia**, diapophysis; **dr**, dorsal rib; **fe**, femur; **ic**, intercentrum; **il**, ilium; **nc**, notochordal canal; **ns**, neural spine; **para**, parapophysis; **pata**, patagial spar; **poap**, postacetabular process of iliac blade; **poz**, postzygapophysis; **ppdl**, paradiapophyseal lamina; **prab**, preacetabular buttress; **prap**, preacetabular process of iliac blade; **prz**, prezygapophysis; **pu.tb**, pubic tubercle; **sab**, supraacetabular buttress; **sr**, sacral rib; **sv**, sacral vertebra; **vmr**, ventromedian ridge. Arrows indicate anterior direction. Dashed areas indicate breaks. Scale bars equal 5 mm. [planned for mage width]

FIGURE 10. *Coelurosauravus elivensis* Piveteau, 1926 (Madagascar, late? Permian), MNHN.F.MAP327a, b, gastralia, silicone cast individual preserved as a natural external mold.

A, gastalial rows 1 and 2 in right anterolateral view; **B**, mid-posterior gastralial row in right lateral view. **Abbreviations**: **brk**, break; **gas**, gastralia; **pata**, patagium. Scale bars equal 5 mm. [planned for column]

FIGURE 11. *Coelurosauravus elivensis* Piveteau, 1926 (Madagascar, late? Permian), forelimb, silicone casts of individuals preserved as natural external molds. **A**, pectoral girdle and right forelimb of MNHN.F.MAP in right lateral view; **B**, humerus of A in ventral view; **C**, humerus of paralectotype MNHN.F.MAP317b in dorsal view. **Abbreviations**: **bo**, basioccipital; **cap**, capitulum; **carp**, carpal elements; **cbb.c**, cavity for M. coracobrachialis brevis; **cl**, clavicle; **co**, coracoid plate; **ct**, cleithrum; **hu**, humerus; **delt**, deltopectoral crest; **ect**, ectepicondyle; **ect.f**, ectepicondylar foramen; **ent**, entepicondyle; **ent.f**, entepicondylar foramen; **epitr**, crest for M. epitrochleoanconaeus; **gv**, groove; **lsr**, lateral scapular ridge; **Mtc**, metacarpal; **ol**, olecranon process of ulna; **ol.f**, olecranon fossa; **pas**, proximal articular surface; **pbs**, parabasisphenoid; **ra**, radius; **rid**, ridge; **sca**, scapular blade; **scsc**, crest for M. subcoracoscapularis; **sctor**, scapular torus; **sh.c**, cavity for M. scapulohumeralis; **ul**, ulna; **trcl**, trochlea; **tvl**, transverse humeral line; **ve**, vertebra. Scale bars equal 1 cm (A) and 5 mm (B–C). [planned for page width]

FIGURE 12. *Coelurosauravus elivensis* Piveteau, 1926 (Madagascar, late? Permian), MNHN.F.MAP327a, carpus, ventral view. **A**, silicone cast of individual preserved as a natural external mold; **B**, interpretative drawing of A. **Abbreviations**: **dc**, distal carpal; **in**, intermedium; **lc**, lateral centrale; **mc**, medial centrale; **Mtc**, metacarpal; **pbs**, parabasisphenoid; **pf.f**, perforating foramen; **pi**, pisiform; **ra**, radius; **rae**, radiale; **ul**, ulna; **ule**, ulnare. Scale bars equal 2 mm. [planned for page width]

FIGURE 13. *Coelurosauravus elivensis* Piveteau, 1926 (Madagascar, late? Permian), hindlimb, silicone casts of individuals preserved as natural external molds. **A**, right femur of lectotype MNHN.F.MAP325a in anteroventral view; **B**, right tibia and partial fibula and

tarsus of MNHN.F.MAP327a in posterodorsal view. **Abbreviations**: **cn**, cnemial crest; **cnt**, cnemial trough; **fi**, fibula; **fic**, fibular condyle; **ic.fo**, intercondylar fossa; **intr**, internal trochanter; **intr.fo**, intertrochanteric fossa; **pas**, proximal articular surface; **ph**, phalanx; **popa**, popliteal area; **rid**, ridge; **tars**, tarsal elements; **ti**, tibia; **tic**, tibial condyle; **tif**, tibial fossa. Scale bars equal 5 mm. [planned for column]

FIGURE 14. *Coelurosauravus elivensis* Piveteau, 1926 (Madagascar, late? Permian), lectotype MNHN.F.MAP325a, right foot, dorsal view, individual preserved as a natural external mold. **A**, silicone cast; **B**, interpretative drawing of A. **Abbreviations**: **ast**, astragalus; **cal**, calcaneus; **clr**, contralateral ridge; **dcaf**, distal calcaneal facet of astragalus; **dt**, distal tarsal; **fi**, fibula; **fi.f**, fibular facet; **Mtt**, metatarsal; **nav**, navicular; **pcaf**, proximal calcaneal facet of astragalus; **pf.f**, perforating foramen; **ph**, phalanx (digit number in brackets); **phu**, ungual phalanx (digit number in brackets); **tb**, tubercle; **ti**, tibia. Scale bars equal 5 mm. [planned for page width]

FIGURE 15. *Coelurosauravus elivensis* Piveteau, 1926 (Madagascar, late? Permian), skeletal reconstruction in dorsal (**A**) and right lateral (**B**) view based on all referred specimens. Poorly known or unpreserved elements outlined by dashed lines and reconstructed from the Ellrich specimen (Pritchard et al., 2021). Skull reconstruction based on Buffa et al. (2021); outline of trunk in dorsal view based in part on the Eppelton specimen (TWCMS B5937, VB, pers. obs.); elements from the left side not figured; gastral basket too incomplete to be accurately reconstructed (see text). Scale bar equals 10 cm. [planned for page width]

FIGURE 16. *Coelurosauravus elivensis* Piveteau, 1926 (Madagascar, late? Permian), life reconstruction. Individuals clinging to *Glossopteris* trunk (*Glossopteris* leaves are associated with *C. elivensis* in the fossil assemblage) (Left), and gliding while grasping its wing (Right). The colors are based on the extant agamid *Draco* and chamaeleonid squamates. Illustration by Charlène Letenneur (MNHN). [planned for page width]

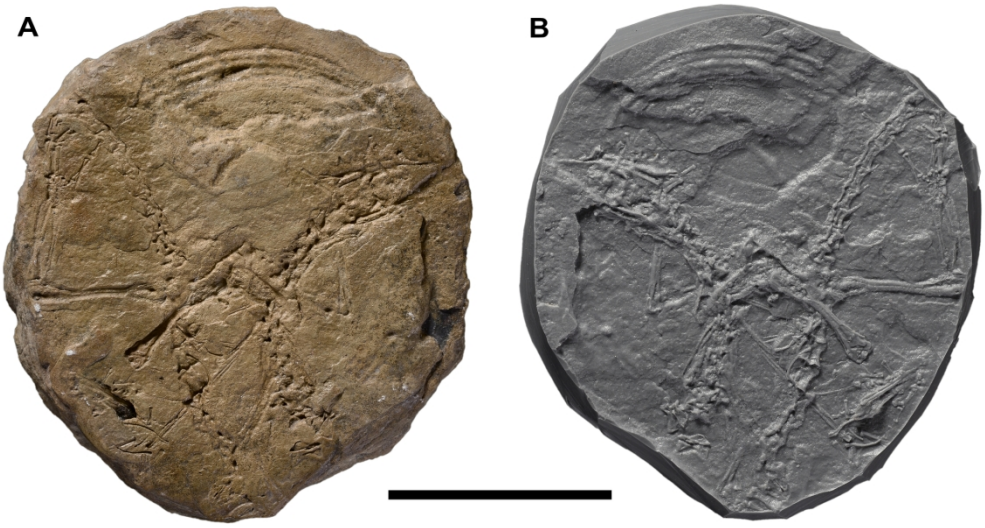

FIGURE 1. *Coelurosauravus elivensis* Piveteau, 1926 (Madagascar, late? Permian), lectotype MNHN.F.MAP325a. **A**, dorsal surface of individual preserved as a natural external mold; **B**, silicone cast of A. Scale bar equals 5 cm.

182x94mm (300 x 300 DPI)

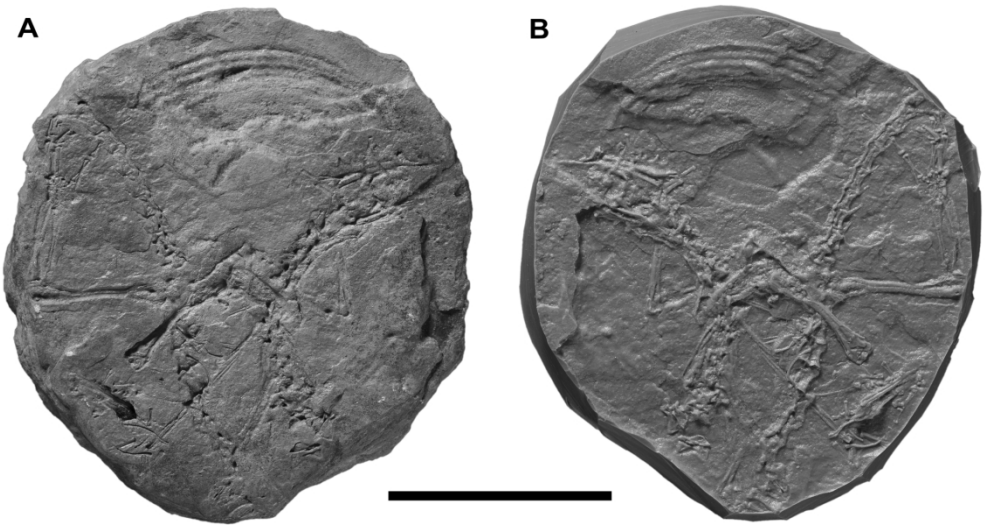

FIGURE 1. *Coelurosauravus elivensis* Piveteau, 1926 (Madagascar, late? Permian), lectotype MNHN.F.MAP325a. **A**, dorsal surface of individual preserved as a natural external mold; **B**, silicone cast of A. Scale bar equals 5 cm.

182x94mm (300 x 300 DPI)

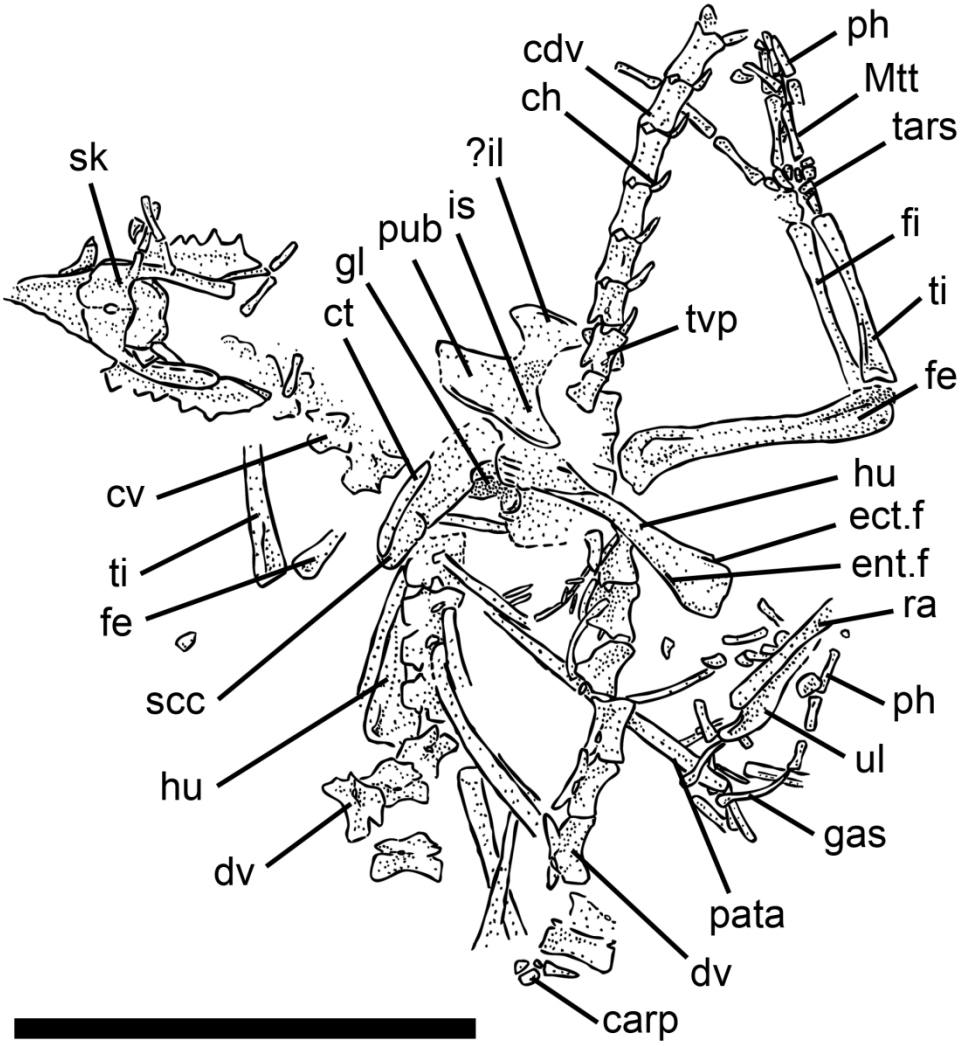

FIGURE 2. *Coelurosauravus elivensis* Piveteau, 1926 (Madagascar, late? Permian), lectotype MNHN.F.MAP325a. Interpretative drawing of dorsal surface of individual preserved as a natural external mold. **Abbreviations**: **carp**, carpal elements; **ch**, chevron; **cv**, cervical vertebra; **ct**, cleithrum; **dv**, dorsal vertebra; **ect.f**, ectepicondylar foramen; **ent.f**, entepicondylar foramen; **fe**, femur; **fi**, fibula; **gas**, gastralia; **gl**, glenoid; **hu**, humerus; **il**, ilium; **is**, ischium; **Mtt**, metatarsus; **pata**, patagial spar; **ph**, phalanx; **pub**, pubis; **ra**, radius; **scc**, scapulocoracoid; **sk**, skull; **tars**, tarsal elements; **ti**, tibia; **ul**, ulna. Scale bar equals 5 cm.

FIGURE 3. *Coelurosauravus elivensis* Piveteau, 1926 (Madagascar, late? Permian), paralectotypes MNHN.F.MAP317a, b. **A**, MNHN.F.MAP317b, dorsal surface of individual preserved as a natural mold; **B**, silicone cast of A; **C**, MNHN.F.MAP317a, ventral surface of individual preserved as a natural mold; **D**, silicone cast of C. Scale bar equals 5 cm.

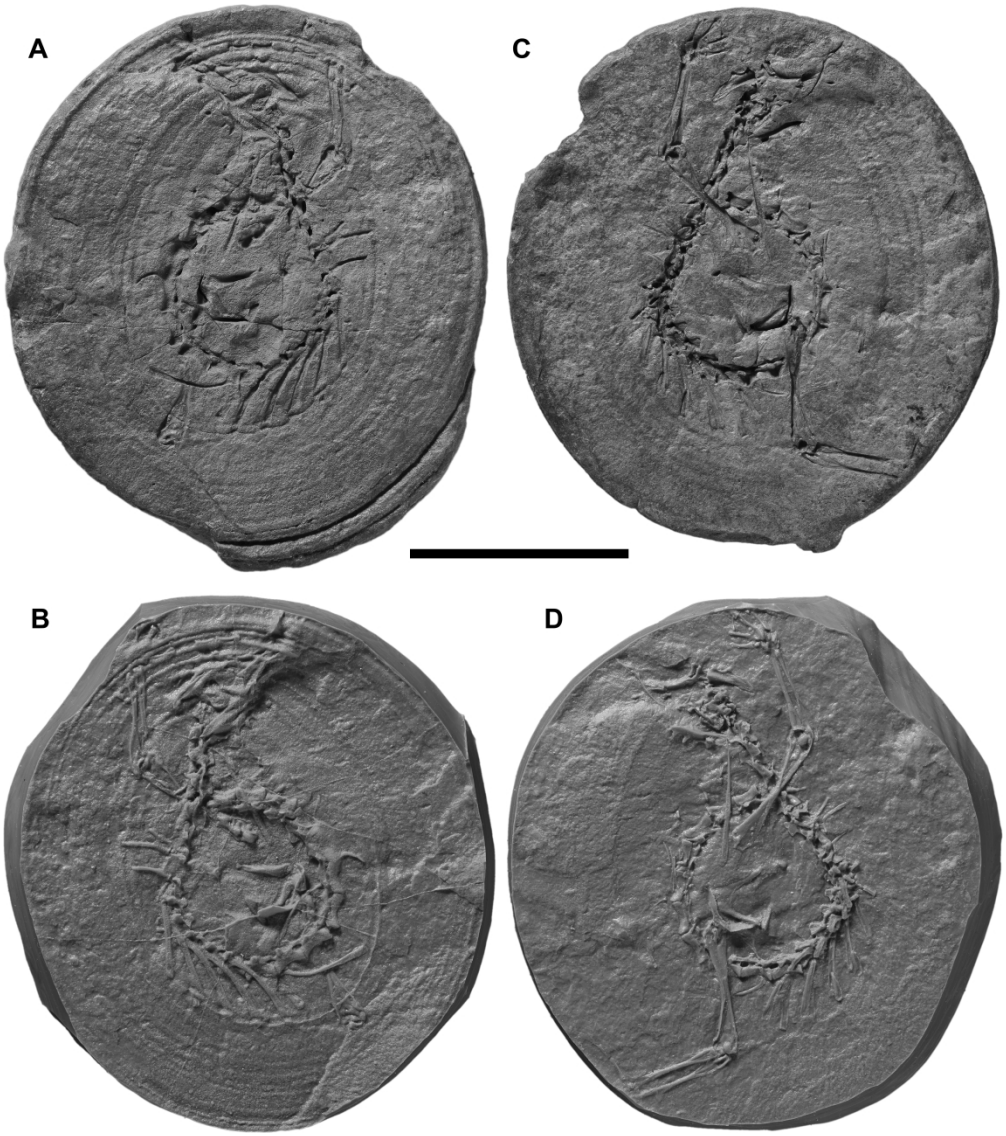

FIGURE 3. *Coelurosauravus elivensis* Piveteau, 1926 (Madagascar, late? Permian), paralectotypes MNHN.F.MAP317a, b. **A**, MNHN.F.MAP317b, dorsal surface of individual preserved as a natural mold; **B**, silicone cast of A; **C**, MNHN.F.MAP317a, ventral surface of individual preserved as a natural mold; **D**, silicone cast of C. Scale bar equals 5 cm.

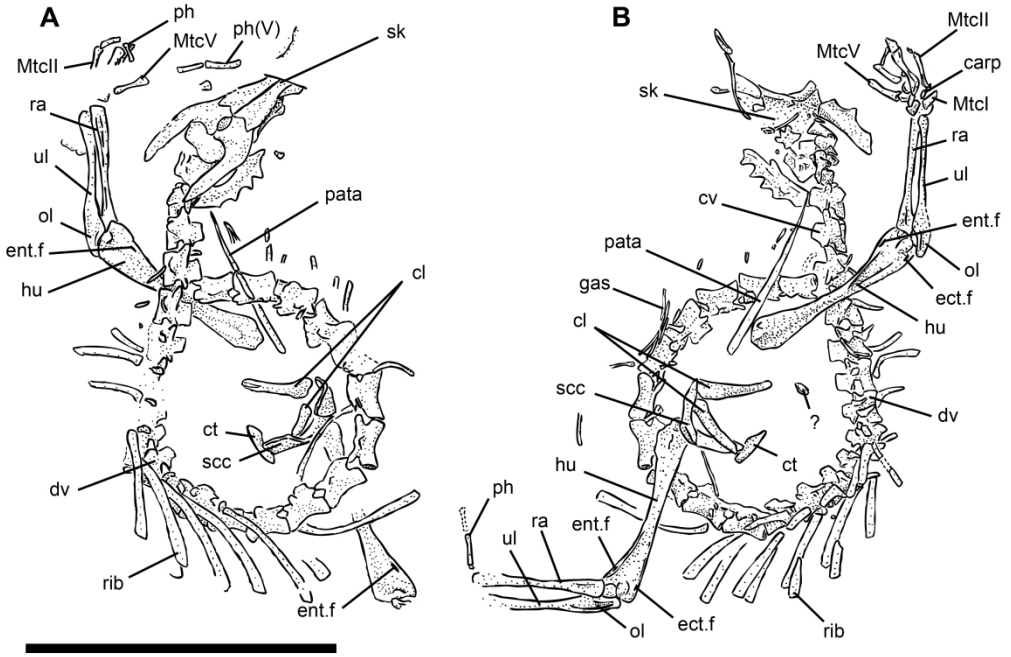

FIGURE 4. *Coelurosauravus elivensis* Piveteau, 1926 (Madagascar, late? Permian), paralectotypes MNHN.F.MAP317a, b. **A**, interpretative drawing of MNHN.F.MAP317b, dorsal surface of individual preserved as a natural mold; **B**, interpretative drawing of MNHN.F.MAP317b, dorsal surface of individual preserved as a natural mold. **Abbreviations**: **carp**, carpal elements; **cl**, clavicle; **ct**, cleithrum; **cv**, cervical vertebra; **dv**, dorsal vertebra; **ect.f**, ectepicondylar foramen; **ent.f**, entepicondylar foramen; **gas**, gastralia; **hu**, humerus; **Mtc**, metacarpal; **ol**, olecranon process of ulna; **pata**, patagial spar; **ph**, phalanx (digit number in brackets when known); **ra**, radius; **scc**, scapulocoracoid; **sk**, skull; **ul**, ulna. Scale bar equals 5 cm.

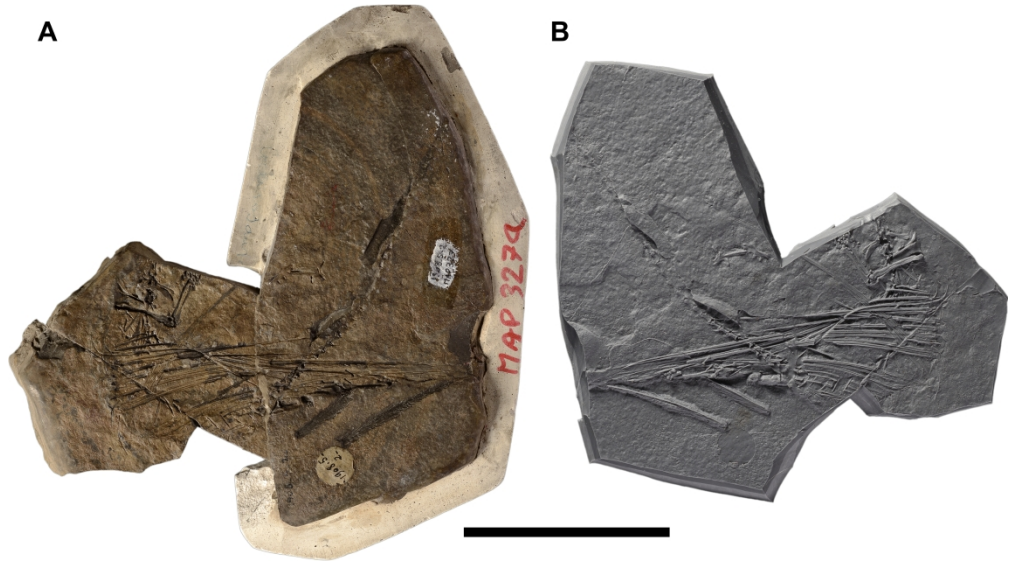

FIGURE 5. *Coelurosauravus elivensis* Piveteau, 1926 (Madagascar, late? Permian) MNHN.F.MAP327a. **A**, right lateral surface of individual preserved as a natural external mold; **B**, silicone cast of A. Scale bar equals 10 cm.

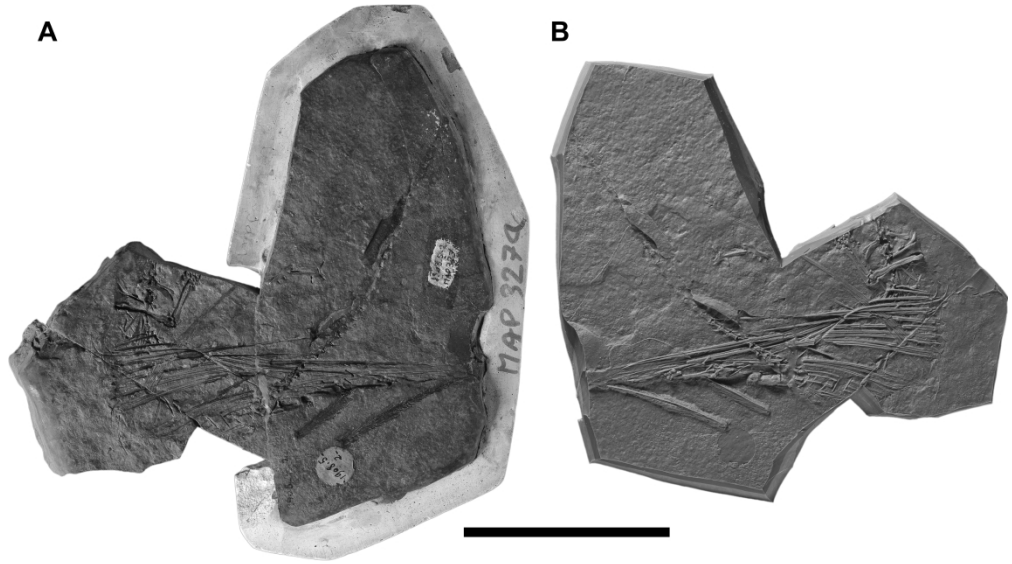

FIGURE 5. *Coelurosauravus elivensis* Piveteau, 1926 (Madagascar, late? Permian) MNHN.F.MAP327a. **A**, right lateral surface of individual preserved as a natural external mold; **B**, silicone cast of A. Scale bar equals 10 cm.

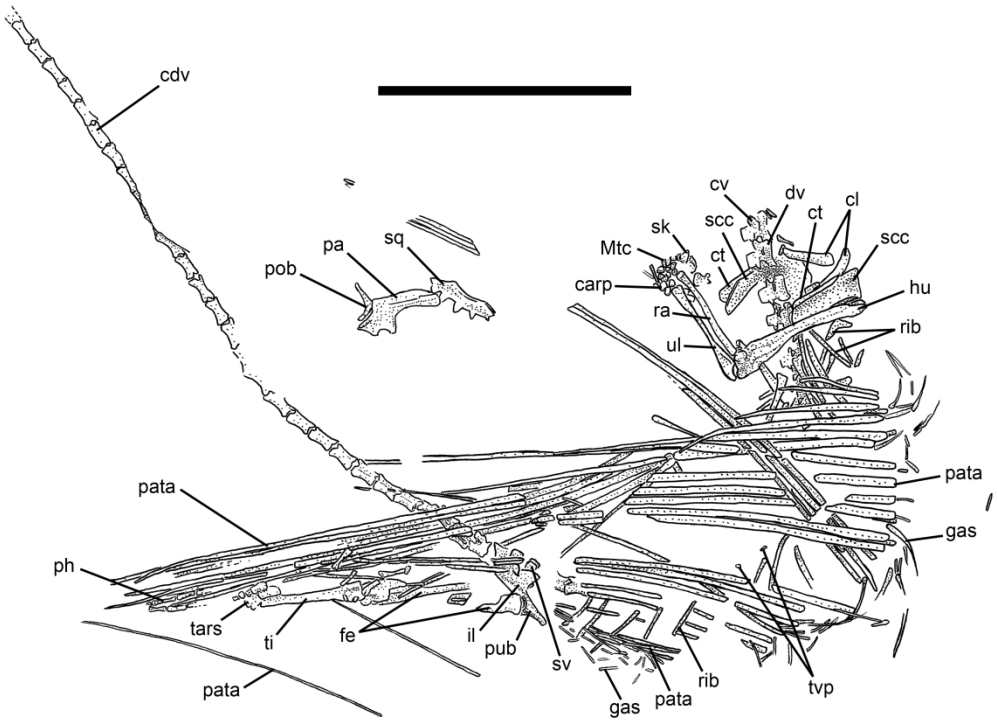

FIGURE 6. *Coelurosauravus elivensis* Piveteau, 1926 (Madagascar, late? Permian) MNHN.F.MAP327a. Interpretative drawing of right lateral surface of individual preserved as a natural external mold. **Abbreviations**: **carp**, carpal elements; **cdv**, caudal vertebra; **cl**, clavicle; **ct**, cleithrum; **cv**, cervical vertebra; **dv**, dorsal vertebra; **fe**, femur; **gas**, gastralia; **hu**, humerus; **il**, ilium; **Mtc**, metacarpus; **pa**, parietal; **pata**, patagial spar; **ph**, phalanx; **pob**, postorbital; **pub**, pubis; **ra**, radius; **scc**, scapulocoracoid; **sk**, skull elements; **sq**, squamosal; **sv**, sacral vertebra; **tars**, tarsal elements; **ti**, tibia; **tvp**, transverse process of dorsal vertebra; **ul**, ulna. Scale bar equals 10 cm.

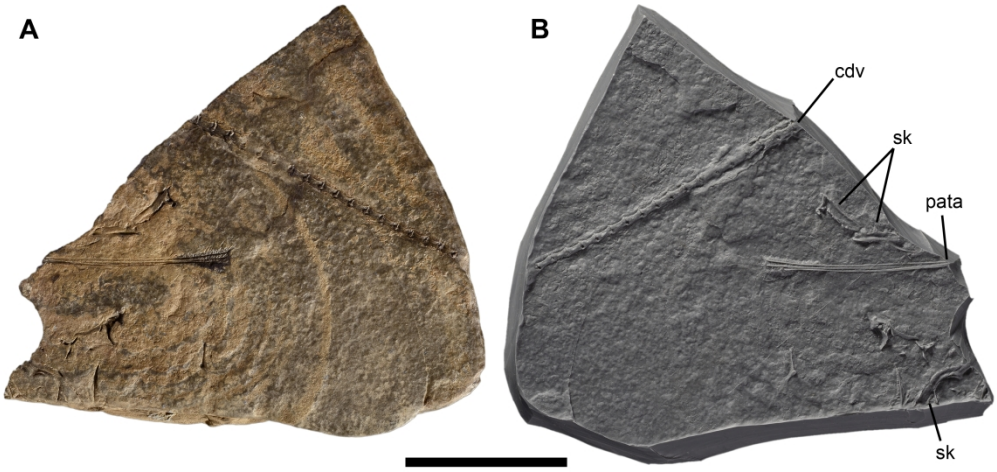

FIGURE 7. *Coelurosauravus elivensis* Piveteau, 1926 (Madagascar, late? Permian) MNHN.F.MAP327b. **A**, left lateral surface of individual preserved as a natural external mold; **B**, silicone cast of A. **Abbreviations**: **cdv**, caudal vertebra; **pata**, patagial spar; **sk**, skull elements. Scale bar equals 10 cm.

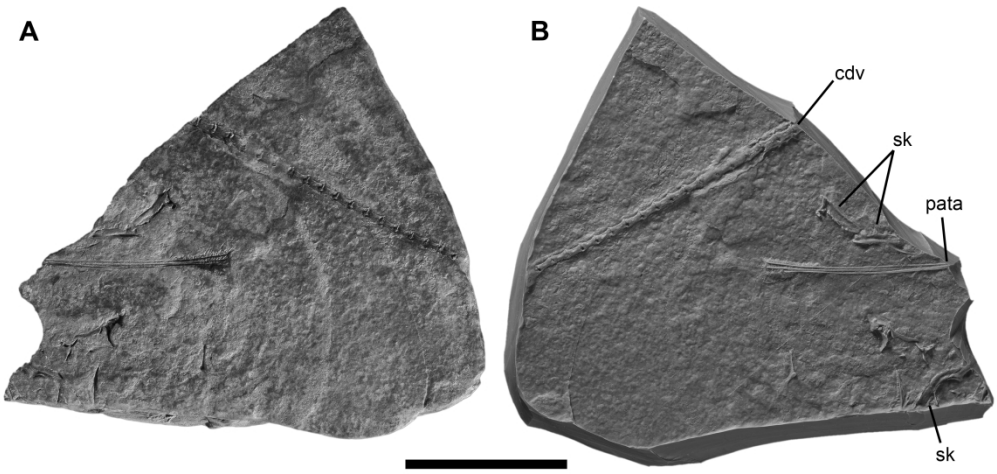

FIGURE 7. *Coelurosauravus elivensis* Piveteau, 1926 (Madagascar, late? Permian) MNHN.F.MAP327b. **A**, left lateral surface of individual preserved as a natural external mold; **B**, silicone cast of A. **Abbreviations**: **cdv**, caudal vertebra; **pata**, patagial spar; **sk**, skull elements. Scale bar equals 10 cm.

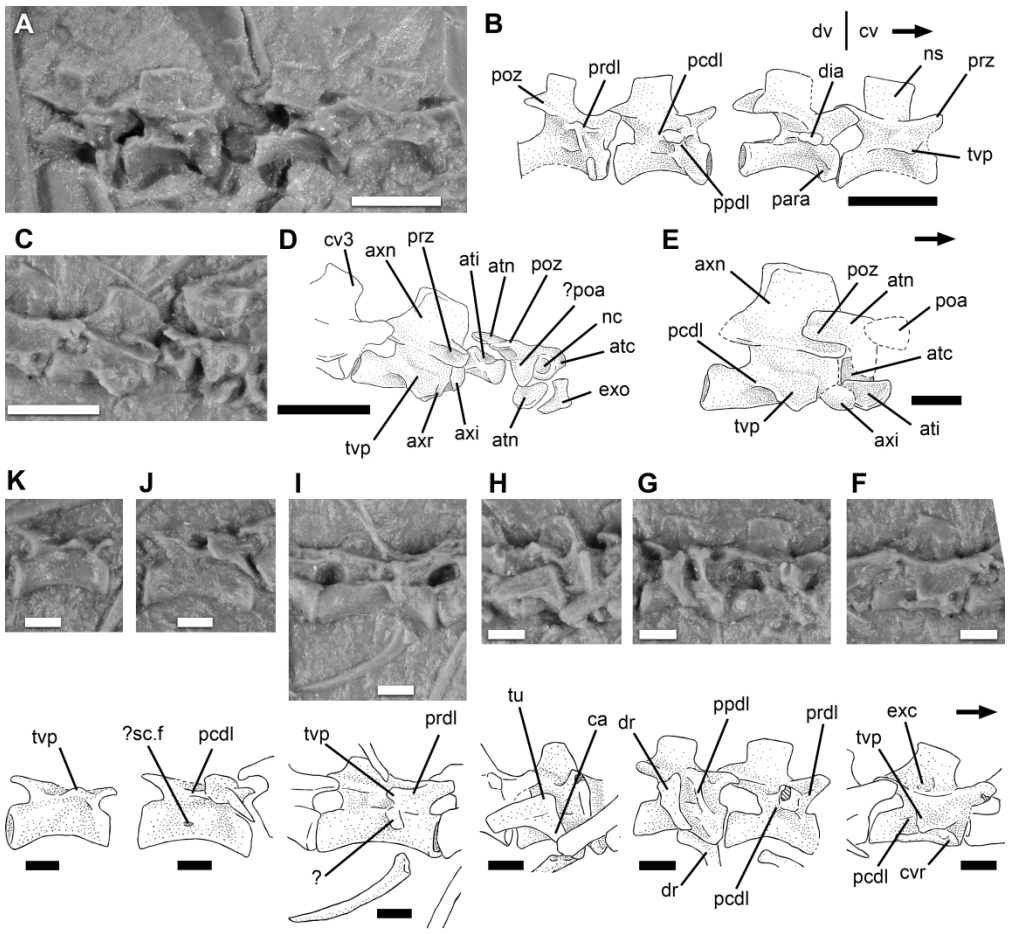

FIGURE 8. *Coelurosauravus elivensis* Piveteau, 1926 (Madagascar, late? Permian), presacral vertebrae. **A**, **B**, last cervicals and first dorsals of MNHN.F.MAP327a in right lateral view, silicone cast (A) and interpretative drawing (B) of individual preserved as a natural external mold; **C**–**E**, atlas-axis complex of paralectotype MNHN.F.MAP317a in right lateral view, silicone cast (C), interpretative drawing (D) and reconstruction (E) of individual preserved as a natural external mold; **F**–**K**, presacral vertebrae of paralectotype MNHN.F.MAP317a in right lateral view, silicone cast and interpretative drawing of cervical 3 (F) and dorsals 2 and 3 (G), 6 (H), 10 (I), 16 (J), 18 (K). **Abbreviations**: **atc**, atlantal centrum; **ati**, atlantal intercentrum; **atn**, atlantal neural arch; **axi**, axial intercentrum; **axn**, axial neural spine; **axr**, axial rib; **ca**, capitulum; **cv**, cervical vertebra; **cvr**, cervical rib; **dia**, diapophysis; **dr**, dorsal rib; **dv**, dorsal vertebra; **exc**, excavation; **exo**, exoccipital; **nc**, notochordal canal; **ns**, neural spine; **para**, parapophysis; **pcdl**, posterior centrodiapophyseal lamina; **poa**, proatlas; **poz**, postzygapophysis; **ppdl**, paradiapophyseal lamina; **prdl**, prezygodiapophyseal lamina; **prz**, prezygodiapophysis; **sc.f**, subcentral foramen; **tu**, tuberculum; **tvp**, transverse process. Arrows indicate anterior direction. Scale bars equal 5 mm (A–E) and 2 mm (F–K).

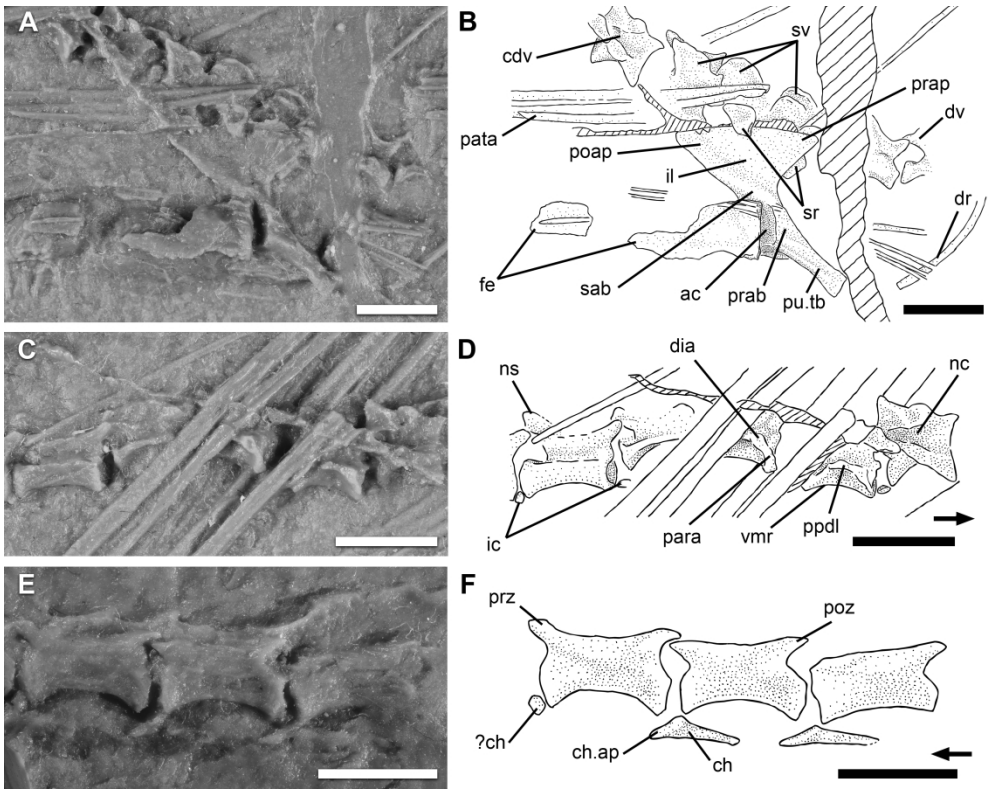

FIGURE 9. *Coelurosauravus elivensis* Piveteau, 1926 (Madagascar, late? Permian), MNHN.F.MAP327a, b, right pelvis, sacral and caudal vertebrae in right lateral view, individual preserved as a natural external mold. **A**, **B**, sacrum and right pelvis of MNHN.F.MAP327a, right lateral view; **C**, **D**, caudals 1 to 5 of MNHN.F.MAP327a, right lateral view; **E**, **F**, caudals 13 to 15 of MNHN.FMAP327b, left lateral view. Silicone casts (A, C, E) and interpretive drawings (B, D, F). **Abbreviations**: **ac**, acetabulum; **cdv**, caudal vertebra; **ch**, chevron; **ch.ap**, anterior process of chevron; **dia**, diapophysis; **dr**, dorsal rib; **fe**, femur; **ic**, intercentrum; **il**, ilium; **nc**, notochordal canal; **ns**, neural spine; **para**, parapophysis; **pata**, patagial spar; **poap**, postacetabular process of iliac blade; **poz**, postzygapophysis; **ppdl**, paradiapophyseal lamina; **prab**, preacetabular buttress; **prap**, preacetabular process of iliac blade; **prz**, prezygapophysis; **pu.tb**, pubic tubercle; **sab**, supraacetabular buttress; **sr**, sacral rib; **sv**, sacral vertebra; **vmr**, ventromedian ridge. Arrows indicate anterior direction. Dashed areas indicate breaks. Scale bars equal 5 mm.

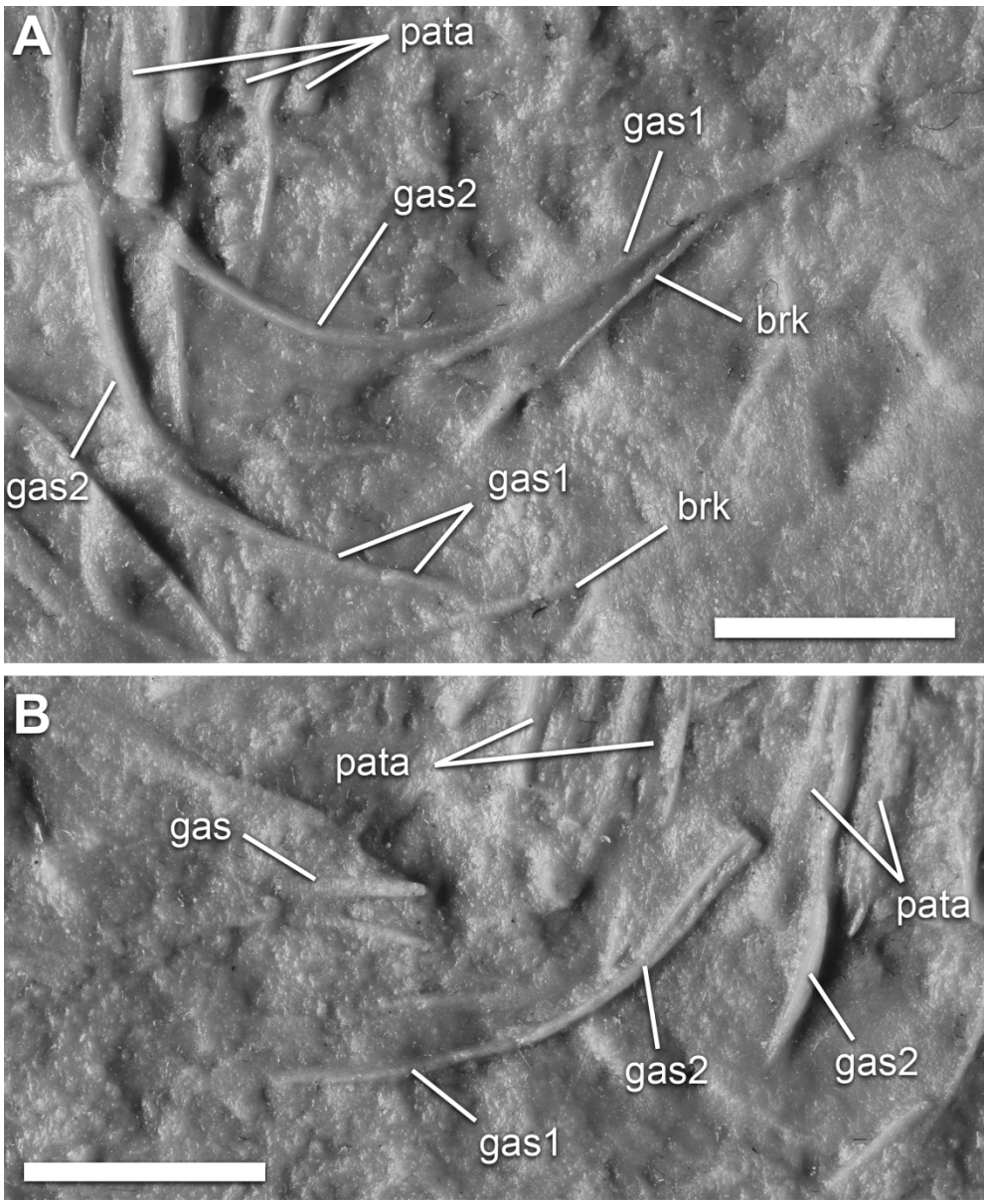

FIGURE 10. *Coelurosauravus elivensis* Piveteau, 1926 (Madagascar, late? Permian), MNHN.F.MAP327a, b, gastralia, silicone cast individual preserved as a natural external mold. **A**, gastalial rows 1 and 2 in right anterolateral view; **B**, mid-posterior gastralial row in right lateral view. **Abbreviations**: **brk**, break; **gas**, gastralia; **pata**, patagium. Scale bars equal 5 mm.

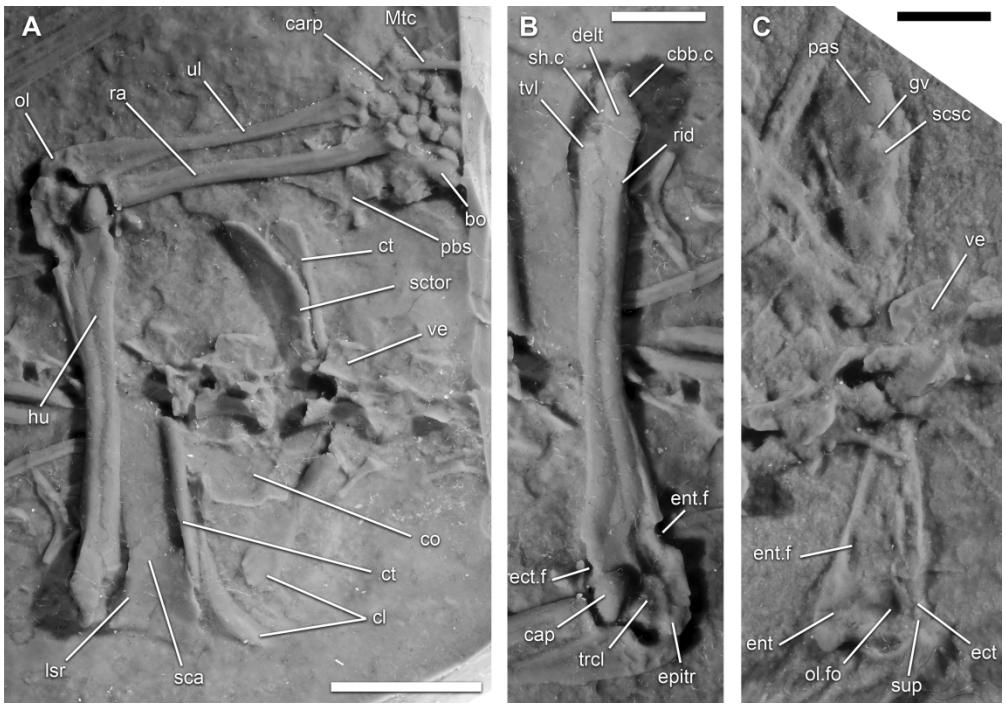

FIGURE 11. *Coelurosauravus elivensis* Piveteau, 1926 (Madagascar, late? Permian), forelimb, silicone casts of individuals preserved as natural external molds. **A**, pectoral girdle and right forelimb of MNHN.F.MAP in right lateral view; **B**, humerus of A in ventral view; **C**, humerus of paralectotype MNHN.F.MAP317b in dorsal view. **Abbreviations**: **bo**, basioccipital; **cap**, capitulum; **carp**, carpal elements; **cbb.c**, cavity for M. coracobrachialis brevis; **cl**, clavicle; **co**, coracoid plate; **ct**, cleithrum; **hu**, humerus; **delt**, deltopectoral crest; **ect**, ectepicondyle; **ect.f**, ectepicondylar foramen; **ent**, entepicondyle; **ent.f**, entepicondylar foramen; **epitr**, crest for M. epitrochleoanconaeus; **gv**, groove; **lsr**, lateral scapular ridge; **Mtc**, metacarpal; **ol**, olecranon process of ulna; **ol.f**, olecranon fossa; **pas**, proximal articular surface; **pbs**, parabasisphenoid; **ra**, radius; **rid**, ridge; **sca**, scapular blade; **scsc**, crest for M. subcoracoscapularis; **sctor**, scapular torus; **sh.c**, cavity for M. scapulohumeralis; **ul**, ulna; **trcl**, trochlea; **tvl**, transverse humeral line; **ve**, vertebra. Scale bars equal 1 cm (A) and 5 mm (B–C).

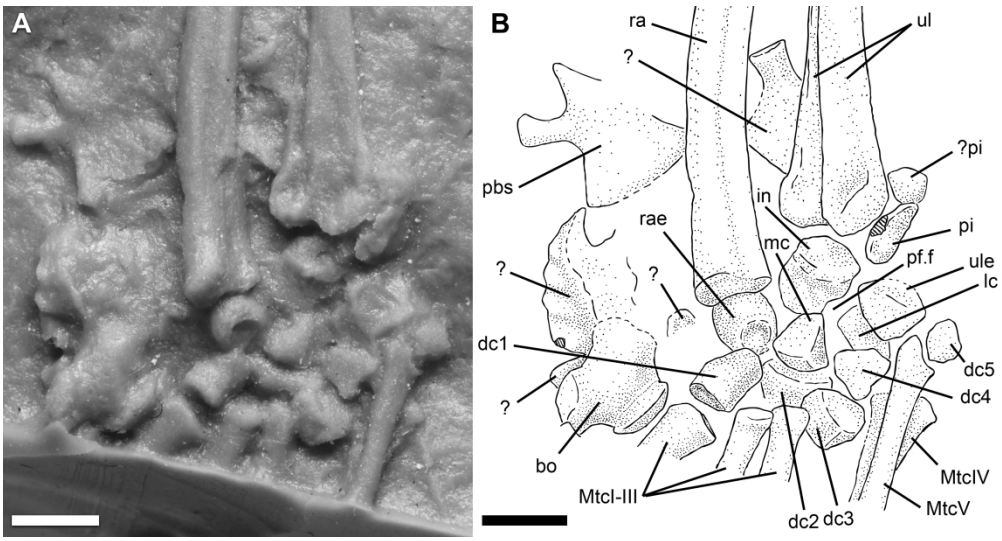

FIGURE 12. *Coelurosauravus elivensis* Piveteau, 1926 (Madagascar, late? Permian), MNHN.F.MAP327a, carpus, ventral view. **A**, silicone cast of individual preserved as a natural external mold; **B**, interpretative drawing of A. **Abbreviations**: **dc**, distal carpal; **in**, intermedium; **lc**, lateral centrale; **mc**, medial centrale; **Mtc**, metacarpal; **pbs**, parabasisphenoid; **pf.f**, perforating foramen; **pi**, pisiform; **ra**, radius; **rae**, radiale; **ul**, ulna; **ule**, ulnare. Scale bars equal 2 mm.

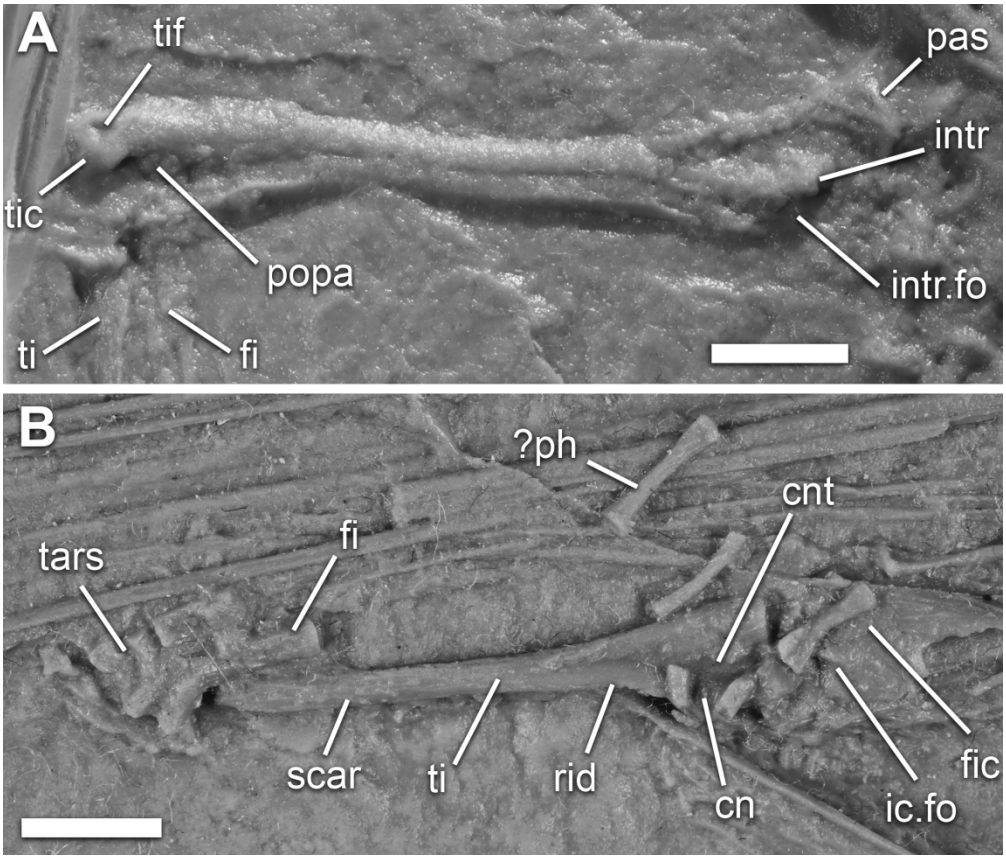

FIGURE 13. *Coelurosauravus elivensis* Piveteau, 1926 (Madagascar, late? Permian), hindlimb, silicone casts of individuals preserved as natural external molds. **A**, right femur of lectotype MNHN.F.MAP325a in anteroventral view; B, right tibia and partial fibula and tarsus of MNHN.F.MAP327a in posterodorsal view. **Abbreviations**: **cn**, cnemial crest; **cnt**, cnemial trough; **fi**, fibula; **fic**, fibular condyle; **ic.fo**, intercondylar fossa; **intr**, internal trochanter; **intr.fo**, intertrochanteric fossa; **pas**, proximal articular surface; **ph**, phalanx; **popa**, popliteal area; **rid**, ridge; **tars**, tarsal elements; **ti**, tibia; **tic**, tibial condyle; **tif**, tibial fossa. Scale bars equal 5 mm.

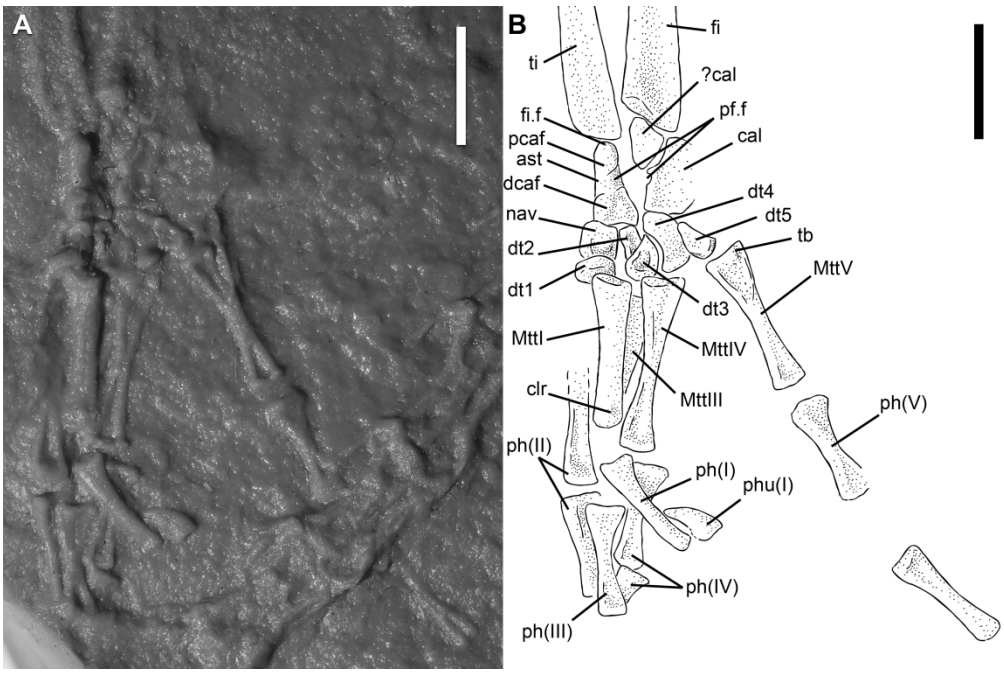

FIGURE 14. *Coelurosauravus elivensis* Piveteau, 1926 (Madagascar, late? Permian), lectotype MNHN.F.MAP325a, right foot, dorsal view, individual preserved as a natural external mold. **A**, silicone cast; **B**, interpretative drawing of A. **Abbreviations**: **ast**, astragalus; **cal**, calcaneus; **clr**, contralateral ridge; **dcaf**, distal calcaneal facet of astragalus; **dt**, distal tarsal; **fi**, fibula; **fi.f**, fibular facet; **Mtt**, metatarsal; **nav**, navicular; **pcaf**, proximal calcaneal facet of astragalus; **pf.f**, perforating foramen; **ph**, phalanx (digit number in brackets); **phu**, ungual phalanx (digit number in brackets); **tb**, tubercle; **ti**, tibia. Scale bars equal 5 mm.

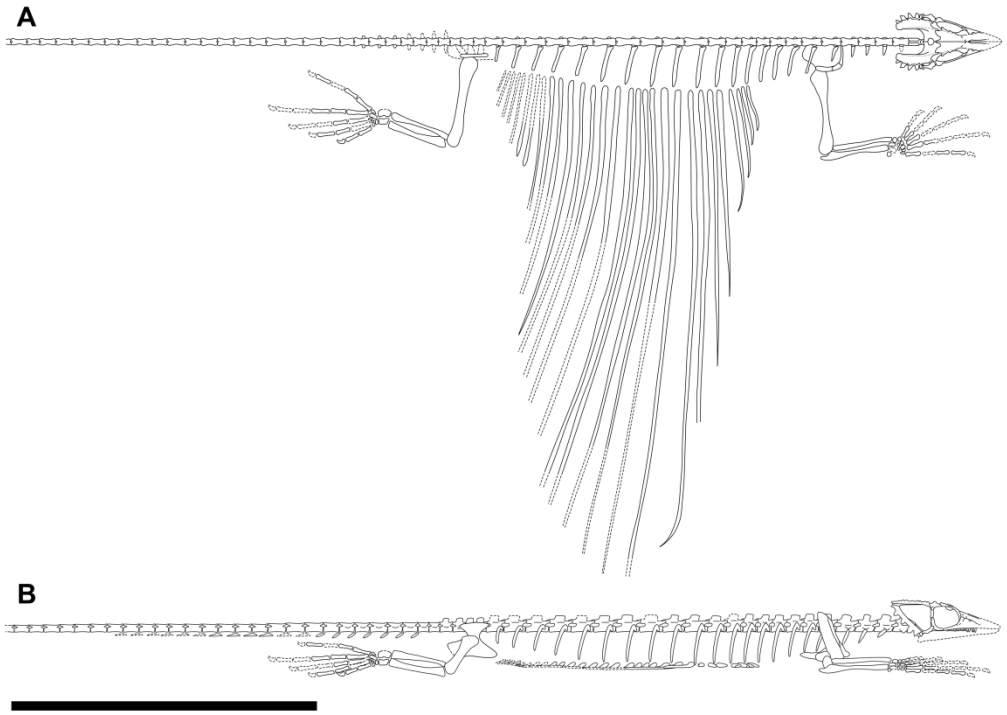

FIGURE 15. *Coelurosauravus elivensis* Piveteau, 1926 (Madagascar, late? Permian), skeletal reconstruction in dorsal (**A**) and right lateral (**B**) view based on all referred specimens. Poorly known or unpreserved elements outlined by dashed lines and reconstructed from the Ellrich specimen (Pritchard et al., 2021). Skull reconstruction based on Buffa et al. (2021); outline of trunk in dorsal view based in part on the Eppelton specimen (TWCMS B5937, VB, pers. obs.); elements from the left side not figured; gastral basket too incomplete to be accurately reconstructed (see text). Scale bar equals 10 cm.

FIGURE 16. *Coelurosauravus elivensis* Piveteau, 1926 (Madagascar, late? Permian), life reconstruction. Individuals clinging to *Glossopteris* trunk (*Glossopteris* leaves are associated with *C. elivensis* in the fossil assemblage) (Left), and gliding while grasping its wing (Right). The colors are based on the extant agamid *Draco* and chamaeleonid squamates. Illustration by Charlène Letenneur (MNHN).

182x136mm (300 x 300 DPI)

FIGURE 16. *Coelurosauravus elivensis* Piveteau, 1926 (Madagascar, late? Permian), life reconstruction. Individuals clinging to *Glossopteris* trunk (*Glossopteris* leaves are associated with *C. elivensis* in the fossil assemblage) (Left), and gliding while grasping its wing (Right). The colors are based on the extant agamid *Draco* and chamaeleonid squamates. Illustration by Charlène Letenneur (MNHN).

182x136mm (300 x 300 DPI)

TABLE 1. Denominations and identifications of previously published specimens referred to the genera *Coelurosauravus* and *Weigeltisaurus*.

Specimen denomination	Identification	Material examined	Remarks
MNHN.F.MAP325a	*Coelurosauravus elivensis* (Lectotype)	MNHN.F.MAP325a	Patrimonial number 1908-11-21a
MNHN.F.MAP317a & b	*Coelurosauravus elivensis* (Paralectotype)	MNHN.F.MAP317a-b	Patrimonial number 1908-11-22a & b
MNHN.F.MAP327a & b	*Coelurosaravus elivensis*	MNHN.F.MAP327a-b	Patrimonial number 1908-5-2

TABLE 1. (Continued)

Specimen denomination	Identification	Material examined	Remarks
SSWG 113/7	*Weigeltisaurus jaekeli* (Holotype)	SMNK-PAL 34899a (cast)	-
Ellrich specimen	*Weigeltisaurus* sp.	SMNK-PAL 2882	Counterpart in unknown private collection
GM 1462	*Weigeltisaurus* sp.	SMNK-PAL 34899b (cast)	-
Bodental specimen	*Weigeltisaurus* sp.	SMNK-PAL 34866 (cast) & 34866b (original)	Main slab in Bürger private collection
Wolfsberg specimen	*Weigeltisaurus* sp.	SMNK-PAL 34910 (cast)	Specimens in Munk private collection, currently being transferred to the Naturkundemuseum im Ottoneum, Kassel
Bahaus specimen	*Weigeltisaurus* sp.	-	Specimen in Simon private collection
Eppelton specimen	?*Weigeltisaurus* sp.	TWCMS B5937 (photographs)	-

TABLE 2. Presacral centrum length of paralectotype MNHN.F.MAP317a, b. '*' indicates approximate measurements due to incomplete preservation.

Presacral vertebra	Centrum length (mm)
Cervical 1 (= atlas)	0.80*
Cervical 2 (= axis)	5.31
Cervical 3	5.52
Cervical 4	5.62
Cervical 5	5.98
Dorsal 1	5.50
Dorsal 2	5.17
Dorsal 3	5.23
Dorsal 4	5.63
Dorsal 5	5.43*
Dorsal 6	5.01
Dorsal 7	5.41
Dorsal 8	5.60
Dorsal 9	6.84
Dorsal 10	7.15
Dorsal 11	7.47
Dorsal 12	7.50
Dorsal 13	7.30
Dorsal 14	7.19
Dorsal 15	7.07
Dorsal 16	7.04
Dorsal 17	6.69
Dorsal 18	5.99

TABLE 3. Selected measurements of MNHN.F.MAP327a, b. '*' indicates approximate measurements due to incomplete preservation. Chord length is measured along the line linking the proximal and distal ends of each patagial, and is thus independent from the curvature of each element.

Caudal vertebra	Centrum length (mm)	Patagial	Absolute length (mm)	Chord length (mm)
Caudal 1	3.39*	Patagial 1	15.80	15.47
Caudal 2	3.51	Patagial 2	20.26	19.41
Caudal 3	3.35*	Patagial 3	28.97	28.81
Caudal 4	3.85*	Patagial 4	42.40	41.74
Caudal 5	4.20	Patagial 5	60.83	60.71
Caudal 6	4.61	Patagial 6	86.53	86.20
Caudal 7	4.90	Patagial 7	105.97*	105.76*
Caudal 8	5.10	Patagial 8	153.405	152.32
Caudal 9	5.24	Patagial 9	163.755*	162.84*
Caudal 10	5.03	Patagial 10	> 53.37	> 53.32
Caudal 11	5.03	Patagial 11	119.51*	118.21*
Caudal 12	4.99	Patagial 12	118.77*	117.56*
Caudal 13	5.20	Patagial 13	130.91*	129.84*
Caudal 14	5.15	Patagial 14	135.73*	133.74*
Caudal 15	5.11	Patagial 15	> 16.53	> 16.53
Caudal 16	4.99	Patagial 16	131.64*	130.11*
Caudal 17	5.14	Patagial 17	> 56.73	> 56.36
Caudal 18	5.20	Patagial 18	> 49.86	> 49.56
Caudal 19	4.99	Patagial 19	73.38	73.20
Caudal 20	5.02	Patagial 20	> 39.99	> 39.66
Caudal 21	5.20	Patagial 21	> 37.38	> 37.22
Caudal 22	5.02	Patagial 22	> 50.59	> 50.15

TABLE 3. (Continued)

Caudal vertebra	Centrum length (mm)	Patagial	Absolute length (mm)	Chord length (mm)
Caudal 23	5.04	Patagial 23	> 12.95	> 12.95
Caudal 24	5.13	Patagial 24	> 12.93	> 12.93
Caudal 25	4.93	Patagial 25	> 11.15	> 11.15
Caudal 26	4.80	Patagial 26	> 10.97	> 10.97
Caudal 27	4.74	Patagial 27	> 11.60	> 11.60
Caudal 28	4.87	Patagial 28	> 15.709	> 15.709
Caudal 29	-	Patagial 29	> 6.162	> 6.162

SUPPLEMENTAL DATA

Journal of Vertebrate Paleontology

The postcranial skeleton of the gliding reptile *Coelurosauravus elivensis* Piveteau, 1926 (Diapsida, Weigeltisauridae) from the late Permian of Madagascar

VALENTIN BUFFA,[*,1] EBERHARD FREY,[2] J.-SÉBASTIEN STEYER,[1] and MICHEL LAURIN[1]

[1]Centre de Recherche en Paléontologie – Paris, UMR 7207 CNRS-MNHN-SU, Muséum national d'Histoire naturelle, CP38, 8 rue Buffon, 75005 Paris, France, valentin.buffa@edu.mnhn.fr;

[2]Abteilung Geowissenschaften, Staatliches Museum für Naturkunde Karlsruhe, Germany

[*] Corresponding author

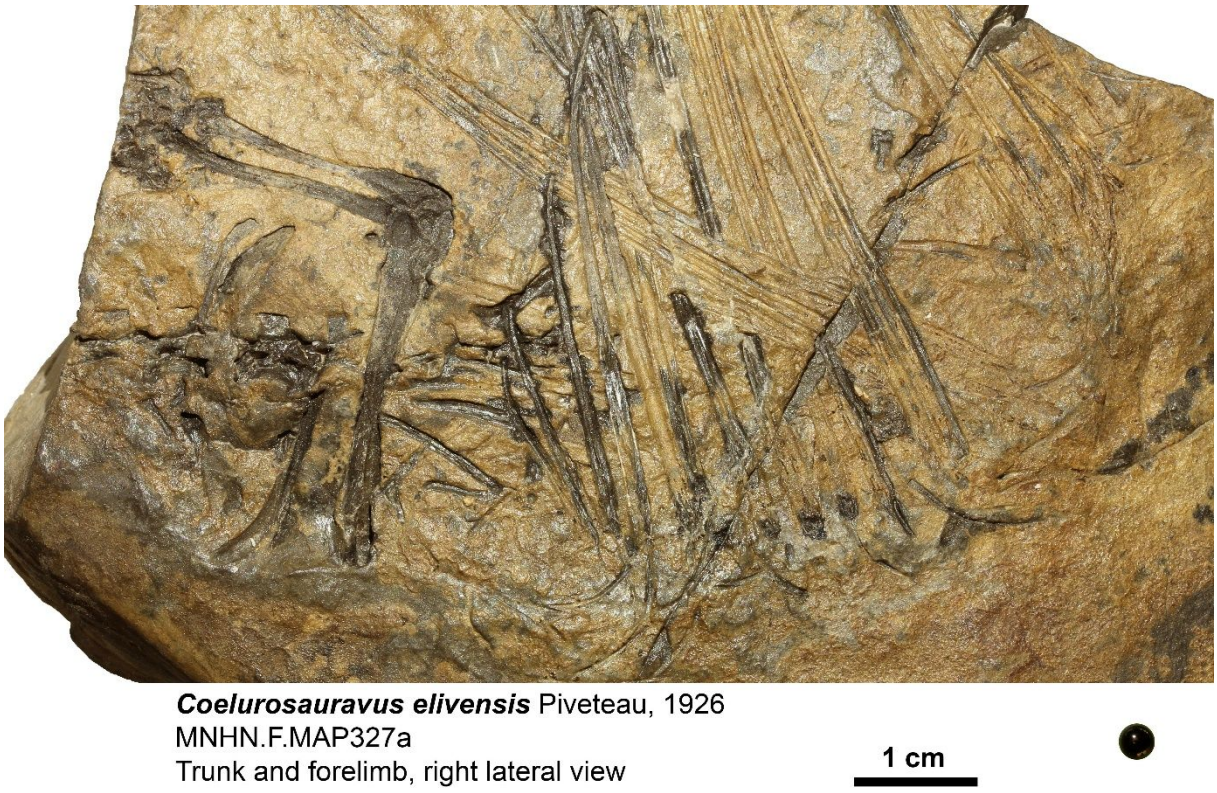

FIGURE S1. *Coelurosauravus elivensis* Piveteau, 1926 (Madagascar, late? Permian), MNHN.F.MAP327a, trunk and forelimb in right lateral view. Individual preserved as a natural external mold. Extract from RTI file available in Zenodo, at http://doi.org/10.5281/zenodo.6078599.

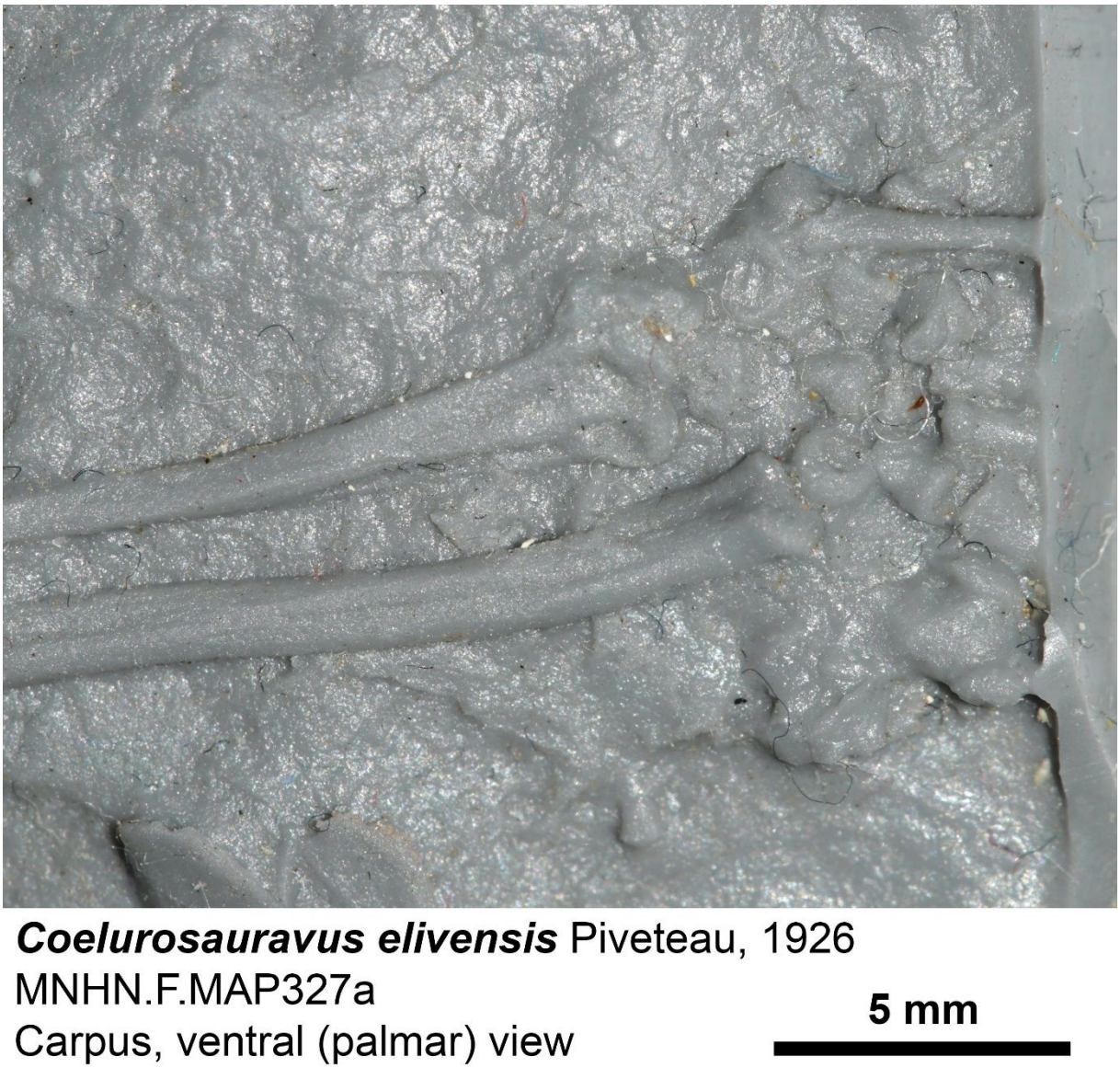

FIGURE S2. *Coelurosauravus elivensis* Piveteau, 1926 (Madagascar, late? Permian), MNHN.F.MAP327a, carpus, ventral (palmar) view. Silicone cast of individual preserved as a natural external mold. Extract from RTI file available in Zenodo, at http://doi.org/10.5281/zenodo.6078599.

FIGURE S3. *Coelurosauravus elivensis* Piveteau, 1926 (Madagascar, late? Permian), lectotype MNHN.F.MAP325a, pes in ventral (plantar) view. Silicone cast of individual preserved as a natural external mold. Extract from RTI file available in Zenodo, at http://doi.org/10.5281/zenodo.6078599.